Machine Learning-Based Prediction of Interfacial Tension in CO_2-Water and CO_2-Oil Systems.

by

Temirkhan Zhanabilev

THESIS SUPERVISOR

Masoud Riazi

THESIS CO-SUPERVISOR

Ainash Shabdirova

Thesis submitted to the School of Mining and Geosciences of Nazarbayev University in Partial Fulfillment of the Requirements for the Degree of **Master of Science in Petroleum Engineering**

Nazarbayev University

April, 2025

ORIGINALITY STATEMENT

I, Temirkhan Zhanabilev, hereby declare that this submission is my own work and to the best of my knowledge it contains no materials previously published or written by another person, or substantial proportions of material which have been accepted for the award of any other degree or diploma at Nazarbayev University or any other educational institution, except where due acknowledgement is made in the thesis.

Any contribution made to the research by others, with whom I have worked at NU or elsewhere is explicitly acknowledged in the thesis.

I also declare that the intellectual content of this thesis is the product of my own work, except to the extent that assistance from others in the project's design and conception or in style, presentation and linguistic expression is acknowledged.

Signed on April, 2025

_____

ABSTRACT

Accurate IFT prediction in CO_2–water and CO_2–oil systems play an important role in enhancing the performance of carbon sequestration, enhanced oil recovery (EOR) and subsurface fluid modeling. The accurate experimental procedures require extended periods of time along with restricted system investigation parameters (Zhang et al., 2023). This research utilizes seven machine learning models to predict IFT at different thermodynamic and compositional conditions: Artificial Neural Networks (ANN), Symbolic Regression–Genetic Programming (SR-GP), Decision Trees (DT), Random Forest (RF), Gradient Boosting Regression (GBR), Support Vector Regression (SVR) and XGBoost.

The methodology highlighted the development of predictive models that can accommodate the complexity of interfacial phenomena. Carefully curated datasets were used to train and test machine learning algorithms sensitive to the intricate relationship that governs CO_2–water and CO_2–oil systems. The ability of each model to handle non-linear and complex interactions was exhaustively examined to identify the best IFT prediction approach.

Model training and testing involved extensive datasets consisting of CO_2–water and CO_2–oil systems defused by various parameters including pressure, temperature, salinity, salt types, oil API gravity and impurities. Standard performance metrics consisting of RMSE, MSE, R^2, MAPE, AIC and BIC determined the assessment of model accuracy. GBR together with XGBoost and RF proved to be the most accurate ensemble models since they achieved R^2 (coefficient of determination) values greater than 0.97 while delivering superior predictive capabilities in the evaluation of both systems. The predictive capabilities of ANN models increased remarkably when optimized parameters were applied to the hidden layer structure.

The experimental data was verified through KDE plots alongside scatter diagrams which showed excellent correlation between predicted results. The results of sensitivity analyses demonstrated that pressure and temperature highly affect the IFT while salt types and impurities had notable effects. The presented work demonstrates that ML techniques can substitute experimental IFT measurement by providing dependable high-speed scalable options that benefit reservoir modeling and process optimization.

ACKNOWLEDGMENT

The most heartfelt thanks go first to my supervisor **Dr. Masoud Riazi**, who offered essential guidance during this research project together with his continuous support and encouragement. His knowledge alongside his perceptive guidance played a crucial role in developing both the direction and quality of this research.

My co-supervisor, **Dr. Ainash Shabdirova** deserves my equal thanks for supplying continuous backing together with helpful advice and patient guidance throughout the process. Her precise approach together with her wholehearted commitment led to the successful achievement of this thesis.

My appreciation extends to **Dr. Shams Kalam** because of his academic backing as well as the profound discussions which deepened my comprehension and built the foundation for this research.

The department's faculty members together with the staff deserve recognition for establishing an optimal research environment and I express my thanks to my family and friends for their ongoing encouragement throughout this project.

TABLE OF CONTENTS

LIST OF FIGURES

LIST OF TABLES

1. INTRODUCTION

1.1.Problem Statement

The ability to accurately predict the IFT of CO_2-oil and CO_2-water systems is a significant problem in many Enhanced Oil Recovery, CO_2 sequestration and reservoir engineering applications. IFT is known to be very important in decision making of efficiency of processes in relation to phase behavior, wettability and fluid flow in porous media (Al-Yaseri et al., 2022). Nevertheless, it is quite challenging to model IFT effectively owing to the integrated effect of several parameters such as pressure, temperature, and fluid characteristics and their composition. (Zhang et al., 2023). All these factors present nonlinear characteristics of the system that cannot be best described by simple empirical and analytical models.

Previous methods in predictive analysis are based on assumptions and the use of suboptimal data sets do not consider the interdependency of CO_2, water and oil under various reservoir conditions. This results in large discrepancies and especially when these data is transported high pressure, high temperature environment or when the chemical composition of the fluid is different such as brine salinity or heavy oil components (Maleki et al., 2024). In addition, it could be postulated that many of the existing models neglect important factors such as oil specific gravity, gas impurities which are necessary for reflect the interfacial tension behavior accurately. This omission is the major limitation that reduces their general reliability, as the insufficient portrayal of interfacial processes limits the models' use in different systems and environments (Mouallem et al., 2024).

In recent decades, machine learning approaches have become valuable methods for analyzing and modeling nonlinear systems in various scientific and engineering disciplines. Using predictive modeling, most ML methods allow to analyze large amounts of data and find relationships that are well hidden, but nevertheless are predictive, without having to rely on physical models. (Zhang et al., 2020). This feature is especially valuable for predicting IFT in CO_2-water systems, since IFT depends on many factors such as temperature, pressure and composition.

Several prior investigations have attempted to develop predictive models for IFT based on existing empirical and theoretical models for IFT prediction, and these models' capabilities are typically restricted by a lack of model adjustability and by failure to meet assumptions in various contexts (Tovakolian et al., 2024). In contrast, machine learning gives a more flexible approach that allows integration of various type of data and results in the capacity to predict over a wide range of thermodynamic conditions. Advancements in the ML algorithms combined with the increased quality of the experimental data that are currently available indicate a possibility of the improvement of the IFT models' predictive performance.

1.2.Objectives of the thesis

The objective of this study is to build and test the machine learning models for reliable IFT prediction in CO_2-water and CO_2-oil systems depending on thermodynamic state conditions. Using experimental data and machine learning techniques, the research will explore how values of critical variables including temperature, pressure, and fluid composition affect interfacial tension. Further, the current research aims at developing a reliable and accurate predictive model, which will reduce the number of experimental measurements required in these systems especially for the processes involved in enhanced oil recovery, carbon capture and storage and the modeling of subsurface fluid dynamics using accurate IFT predictions.

2. LITERATURE REVIEW

2.1. Understanding Interfacial Dynamics in CO_2-Water and CO_2-Oil Systems

The interfacial tension (IFT) between CO_2 and water/oil directly impacts subsurface processes in CCS and EOR. IFT behavior is important to comprehend since it impacts on the distribution of fluids, wettability and phase characteristics throughout the porous media and subsequently influences storage capacity and recovery factors (Chiquet et al., 2007).

Multiple conditions dominate the interfacial tension (IFT) as well as mass transfer behavior at the CO_2-water boundary. The thermophysical characteristics of supercritical CO_2 present unique properties because pressure and temperature control its density and viscosity levels. Scientific research indicates pressure-induced reductions in CO_2-water interfacial tension particularly near the critical point of CO_2 (Li et al., 2012; Chalbaud et al., 2009). The lowered interfacial tension

helps fluid extraction from porous spaces to improve CO_2 solution rates. Experimental research and molecular simulation studies demonstrate that hydrogen bonds and the dissimilar polarities at CO_2-water contact points matter significantly (Duan & Sun, 2003). The salinity levels of aqueous phases modify interfacial characteristics by influencing ion arrangement and interface structuring mechanisms at the interface where CO_2 solubility and wettability face alteration (Bachu & Bennion , 2009).

The CO_2-oil interface shows complex behavior patterns because crude oil contains various components with diverse compositions. CO_2 shows high solubility in various hydrocarbon phases thus enabling oil swelling as well as reduced viscosity and possible miscibility under specific combinations of pressure and temperature (Yang et al., 2005). The interaction dynamics between CO_2 and oil occur based on parameters such as the oil chemical composition and its components along with CO_2 partial pressure levels and temperature variations. Laboratory tests demonstrated that the CO_2 molecule diminishes oil-CO_2 interface tension thereby improving oil production from reservoirs (Gajbhiye et al., 2025). Research indicates that gas injection programs for EOR require consideration of immiscible to miscible displacement transitions as well as other critical parameters. The formation of interfacial films through surfactants and naturally occurring amphiphilic molecules in oil affects interface stability based on system conditions (Kamal et al., 2015).

2.2. Experimental Methods for Measuring Interfacial Tension (IFT).

IFT is considered as a vital variable in various applications in the industries including EOR and CO_2 sequestration. IFT determination of CO_2-water / CO_2-oil interfaces are critical in interpreting capillary pressures and fluid response prediction in sub-surface reservoirs. Numerous experimental methods are employed for evaluating IFT, which have certain benefits with regard to the precision of results, sensitivity, and ability to reproduce measurements at the required temperature and pressure, as well as compatibility with the investigated fluids. Major experimental techniques are pendant drop, assymetric drop shape analysis and capillary rise methods.

- Pendant Drop Method

The pendant drop method is accurate since it provides many potential effective readings with great accuracy of measurement regardless of the temperature and pressure conditions prevailing. A

pendant drop is created when a needle is used to drop a denser fluid into a light fluid environment (Sarmadivaleh et al., 2015). Analysis of the shape of interface between the two fluids (Fig. 1) under certain conditions at which the gravitational and surface forces balanced one other leads to its form (Arashiro and Demarquette, 1999).

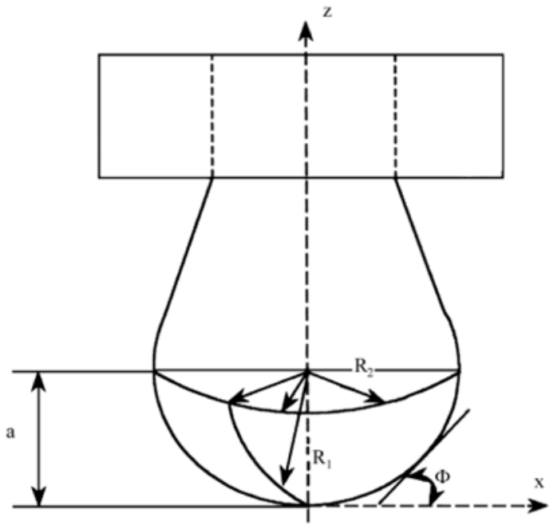

Figure 1. The pendant drop geometry (Arashiro et al., 1999)

The Young-Laplace equation (1) in combination with gravitational forces (2) are applied for the determination of IFT (3) using the force equilibrium of the gravitational and interfacial forces acting on the drop (Fordham, 1948).

$$\Delta P_p = \gamma \left(\frac{1}{R_1} + \frac{1}{R_2} \right) \quad (1)$$

$$\Delta P_{apex} = -\Delta P_p = z \Delta \rho g \quad (2)$$

$$\gamma = \frac{\rho g}{(\beta k_{apex})} \quad (3)$$

where, R_1 and R_2 are curving radii of two orthogonalcurves over identical points on the droplets, β is shape constant and k_{apex} is curving at the apex point of the droplet (z=0). Chiquet et al. (2007) using the pendant drop technique studied the impact of pressure and temperature that may be experienced by CO_2 – water system in geological storage. Similarly, this method was employed

by Al-Anssari et al. (2020) to investigate IFT of CO_2-oil system under high pressure and they showed that the method is accurate for a wide pressure range.

Better and more precise techniques to estimate interfacial tension (IFT) from pendant drop forms are being developed as a result of the advancements in computing capacity over the past few decades. Modern approaches analyze the entire drop profile with greater accuracy than traditional techniques which are based on specific drop dimension (Hoorfar et al., 2006).

The Axisymmetric Drop Shape Analysis (ADSA) is one of the most widely used method. The technique works in comparing experimental captured drop profile from a video image to a set of Laplacian curves known to correspond to well defined interfacial tensions. The objective function is minimized such that it can be seen as the sum of squared differences between the drop's detected edge (experimental profile) and theoretical curves. The interfacial tension value obtained from the best matching curve is the most accurate and it correlates with pendant drop's parameters (Rio et al., 1997).

This method has been developed by improved video image processing, advanced algorithms, and correction of optical distortion which have greatly increased the precision of this method (Neuman et al., 2010) . Moreover, interfacial tension values were studied as a function of aging effects by automated extraction and numerical analysis of drop profiles (Rio et al., 1997). It is well known that consistency and accuracy of IFT measurements are dependent on both image quality and drop elongation. A light filter then may be used to reduce chromatic distortions in drop images and therefore improve measurement reliability.

ADSA is a simple and accurate method for determining interfacial tension which has been widely applied in many systems. Literature reviews suggest that it is often employed to analyze reservoir fluids under high pressure conditions, especially with regard to water−gas (Georgiadis et al., 2010; Hebach et al., 2002) and of the water−hydrocarbon interfaces (Georgiadis et al., 2010).

- Capillary Rise method

The capillary rise method serves as a classical technique which uses the liquid height change in a capillary tube to determine surface and interfacial fluid tensions. A characteristic liquid column rise or depression occurs in this method because adhesive forces between liquid and tube balance with cohesive forces operating within the liquid (Pereira, 2016).

Surface tension measurement through the capillary rise method quantifies the height h of a liquid meniscus inside a cylindrical glass tube with the known radius r which appears in figure 2 (Drelich et al., 2002).

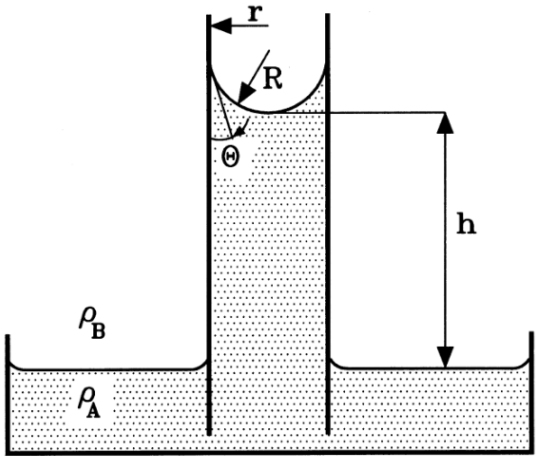

Figure 2. Illustration of capillary rise method (Drelich et al., 2002)

During the measurement of surface tension with narrow tubes where r<<h the meniscus adopts a spherical profile which enables calculation through a standard equation (4).

$$\gamma = \frac{\Delta\rho ghr}{2cos\theta} \qquad (4)$$

The glass tubes allow simple cleaning with acids and bases and organic solvents and full surface-wetting by liquids leading to routine simplification of the cosine term.

Experts view this approach as producing the most precise measurements for surface tension. The accurate determination of surface tension depends on achieving uniform manufacturing of capillary tubes and precise measurement of their internal diameter which cause technical problems. Also the measurement of interfacial tension between two liquid phases through this method proves to be less practical (Drelich et al., 2002).

2.3. CO2-water system

2.3.1. The role of IFT in CO2-water system

The estimation of IFT between the two phases is vital in CO_2 sequestration and aquifer storage because the flow characteristics of the fluids in such systems critically depend on the interfacial

tension at the CO_2–water interface. IFT has impact on processes such as, interfacial and phase behavior, wettability and the govern role on the stability and injectivity of CO_2 in the storage formations (Chiquet et al., 2007). For example, in CO_2 sequestration processes, low IFT, allows CO_2 to penetrate the previously unreachable pore space and increase storage capacity by reducing the possibility of leakage due to high competency of cap rock (Bachu & Bennion, 2009). However, excessively low IFT can also raise concerns about CO_2 aggregation and enhanced mobility, which may increase the risk of migration and leakage if caprock integrity is compromised.

Based on the current knowledge, the present study reveals that IFT in systems involving CO_2 and water is rather sensitive to several factors, such as temperature, pressure, and the salinity level. For instance, in deep geologic reservoirs at elevated pressures, we see a decrease in IFT which increases the spreading of CO_2 across the aqueous phase and may affect capillary trapping mechanisms (Park et al., 2005). Salinity also exerts a considerable influence for the rise of IFT due to high salt concenrations which enhances the hydrophobicity of CO_2 (Liu et al., 2015). Pressure, temperature, and salinity collectively govern the extent of CO_2 dissolution into the aqueous phase: higher pressures and lower temperatures enhance dissolution, while elevated salinity reduces it. Consequently, the quantification of these variables is critical to minimizing errors in the model's predictive accuracy of IFT across various storage facilities and conditions of subsurface heterogeneity.

2.3.2. Conventional approach of modeling IFT in CO2-water system

Previous approaches for predicting IFT in CO_2-water systems have mainly involved empirical as well as theoretical approaches, which have their own advantages and disadvantages. For instance, empirical models seek to reveal correlation between IFT and factors such as pressure, temperature and salinity by using data gathered from experimentation. However, like all models, they are useful for predicting IFT under strictly defined conditions, but may behave differently when faced with untested composition changes that are characteristic of dynamic reservoirs (Hebach et al., 2002).

Potential theoretic models with reference to thermodynamics theories, including the EOS, have also been used to estimate the IFT of CO_2-water through modeling the CO_2-water molecular enthalpy. However, such models do not consider dependent effects including effect of salinity and the presence of impurities in CO_2-fluid as shown by Isfehani et al. (2023). Consequently, whereas explicit mathematical formulations have offered great insights, their low reliability for a vast

number of conditions suggests the application of robust modeling techniques for capturing features in IFT data for high-pressure CO_2 sequestration (Mouallem et al., 2024).

2.3.3. Machine learning approaches for predicting IFT in CO2-water system

New achievements of ML suggest the possibility to avoid the mentioned obstacles of traditional IFT modeling methods by developing more precise and flexible models for CO_2-water systems. Due to the above capabilities, ML models lend themselves well to handling large datasets and thus form complex non-linearities with IFT and the factors such as temperature, pressure, and salinity and would give better accuracy than the empirical or theoretical methods (Zhang et al., 2020). In particular, supervised learning algorithms experimentally trained on big data can be trained based on a wide range of conditions that make it possible to predict conditions not reflected in the data, which is crucial for the variability of carbon dioxide storage sites (Hosseini et al., 2020).

Many papers have showed the advantages of ML in learning and predicting IFT in CO_2-water system. For instance, Mouallem et al., (2024) designed and trained the ML models that with high accuracy estimates the IFT in CO2-brine system specifying the input parameters as temperature, pressure, and salinity. Their models showed a clear fit with the actual results in a wide range of experiment settings, which make it an ideal device for CCS use. In the same way, Khan et al. (2024) implemented ML approaches to estimate IFT in CO_2-brine systems through accurate predictions to quantify the impacts of the change points of salinity and pressure on IFT. These studies have demonstrated that ML can be a good alternative to empirical modelling for CO_2-water systems relevant to CO_2 sequestration, where model accuracy is crucial, by confirming CO_2 granular modeling's ability to manage the ambiguity of IFT behavior.

The present work differ from previous studies since the previous models analyzed reservoir systems containing non-acidic impurities such as CH_4 and H_2 and N_2 yet this research expands to include acidic impurities. This research broadens the examination to analyze acidic impurities since they naturally occur in real reservoirs and produce substantial changes in CO_2 solubility together with interfacial tension and phase behavior patterns. The expanded data collection allows researchers to create better IFT prediction models that operate under real-world reservoir scenarios.

2.3.4. Key Data Sources for CO_2-Water IFT Modeling

In the study of Kvamme et al. (2007), interfacial tension (IFT) for CO_2-water systems was recorded at the reservoir conditions of varying pressure and temperature for CO_2 sequestration practices. The experiments were performed at various high pressures so that trends of IFT with pressure at predetermined temperature could be studied. However, in general, the IFT diminishes with an increase in pressure because of the increased solubility of CO_2 in water, which is important to identify the behavior of the fluid in reservoirs of a considerable depth (**Table 1**).

Table 1. Experimental and modelling results for water+CO_2 systems at 323K and various elevated pressures (Kvamme et al., 2007)

p (MPa)	T (K)	Density sat CO_2 (kg/m^3)	Density sat water (kg/m^3)	Cross-sim IFT (mN/m)	Sim IFT (mN/m)	IFT (mN/m)
1.1	322.8	18.8484	988.52	51.8	53.2	63.7
2.1	322.8	37.6033	990.71	48.0	50.1	57.1
4.18	322.9	83.397	995.07	48.6	46.7	47.5
6.22	322.9	143.052	997.94	43.8	44.5	44.1
8.26	322.8	235.565	1000.51	41.3	40.7	38.4
10.28	322.8	424.325	1002.38	37.0	36.6	32.5
12.33	322.9	608.399	1003.75	35.7	35.0	31.2
14.4	322.9	686.864	1005.11	33.7	35.4	30.6
18.43	322.8	765.667	1007.07	34.3	35.3	29.8
20.44	322.8	791.304	1008.15	33.7	34.2	29.4
22.45	322.8	812.725	1009.13	31.9	34.7	29.1

Chiquet et al. (2007) are among the very few who studied the effect of CO_2 water interfacial tensions with pressure and temperature on the geological storage of CO_2. Their experiments concerned the pressure changing from 5 to 45 MPa and the temperature ranging from 298 K to 382 K. This range affects on deep subsurface storage environment in which pressure as well as temperature have profound effect on IFT. These findings indicate that, with increasing temperature, the value of the CO_2-water interfacial tension tends to decline and, while this tendency is more sensitive to the the pressure changes. Results that the study obtained provided evidence about the tendencies of the IFT between CO_2/water with the increase of pressure: the miscibility is improved in high-pressure conditions characteristic of deep formations (**Table 2**).

Table 2. Measured IFT and densities of the CO_2/pure water system (Chiquet et al., 2007)

P (MPa)	T (K)	ρ_{CO2} (kgm^{-3})	ρ_{H2O} (kgm^{-3})	σ (mN m^{-1})	P (MPa)	T (K)	ρ_{CO2} (kgm^{-3})	ρ_{H2O} (kgm^{-3})	σ (mN m^{-1})
5	307.4	126.3	992.7	44.3	5	364.2	86.7	970.5	45.8
7	309.6	221.7	972.6	35.2	7	362.5	152.7	973.1	39.5
10	308.1	710.5	1006.8	32.1	10	362.3	211.2	974.6	32.5
15	307.8	813.3	1004.9	30.8	15	363.5	353.6	976.7	29.2
20	308.1	863.9	1010.2	30.9	25	363.2	623.8	983.6	27.6
25	307.6	899.2	1018.2	32.0	30	363.6	693.3	986.0	25.9
30	308.1	927.2	1020.8	31.1	40	363.2	782.5	991.7	25.8
40	308.8	970.0	1024.3	29.3	45	363.3	814.4	994.3	27.0
45	309.0	987.5	1026.1	28.5					
5	322.8	105.0	996.2	45.5	5	383.2	80.8	950.6	43.7
7	323.7	172.2	995.8	38.8	7	384.2	117.0	954.1	38.0
10	324.2	377.0	995.9	34.9	10	383.3	181.1	953.6	34.4
15	323.6	691.5	999.6	32.6	15	383.5	303.2	958.0	30.8
20	323.1	778.3	1004.4	29.2	20	383.0	435.7	965.9	28.3
25	323.5	829.0	1007.6	29.7	30	383.6	622.8	974.4	25.5
30	323.3	865.9	1009.9	28.4	40	382.9	727.7	977.5	23.4
40	323.6	919.1	1016.0	28.2	45	382.9	763.2	979.8	22.8
45	324.4	939.7	1019.0	28.0					
5	343.6	94.5	985.0	45.2					
7	342.3	144.6	986.5	42.6					
10	342.1	245.3	989.8	36.3					
15	343.0	484.1	986.5	32.5					
20	343.1	645.4	990.4	27.5					
25	343.7	727.1	989.9	25.0					
30	342.7	779.7	998.3	26.7					
40	343.3	849.9	1002.4	25.4					
45	342.9	876.3	1006.5	27.5					

From the table reported in the Chun et al. (1995) study, 125 data points were identified specifically related to IFT values in high pressure CO_2 mixtures using capillary rise method (**Table 3**). This set of data covers a broad range of pressures, enabling one to understand various aspects of how CO_2 acts on different fluids under the conditions typical for subsurface use. It has been established from the results that as the pressure increases, the IFT normally decreases because of improved miscibility at higher pressures. This wide-ranging dataset offers a solid foundation for developing process models of CO_2 interactions in high-pressure conditions that is important for fluids behavior with respect to CO_2 injection and storage and improved oil recovery.

Table 3. Experimental data for water-carbon dioxide systems (Chun et al., 1995)

5 C		10 C		15 C		25 C		30 C		35 C	
P (MPa)	γ (mN/m)	P (MPa)	γ (mN/m)	P (MPa)	γ (mN/m)	P (MPa)	γ (mN/m)	P (MPa)	γ (mN/m)	P (MPa)	γ (mN/m)
0.1	74.27	0.1	73.66	0.1	72.95	0.1	71.03	0.1	70.49	0.1	69.66
2.07	61.26	2.07	61.31	2.07	61.44	2.07	61.15	2.07	60.52	2.07	60.38
2.75	52.05	3.45	47.96	3.45	47.74	4.14	46.12	3.45	52.33	3.45	52.19
3.44	45.62	4.14	41.99	4.14	44.05	6.2	32.11	4.83	45.48	4.14	48.95
3.79	42.91	4.48	55.56	4.83	48.14	6.89	42.87	6.2	38.87	6.2	40.86
4.14	47.71	4.83	50.07	5.17	51.57	7.24	29.25	6.89	35.15	6.89	37.21
4.48	51.95	5.17	25.19	5.52	26.86	7.58	29.17	7.24	33.85	7.58	35.79
4.83	52.72	5.52	25.15	5.86	25.26	7.93	27.52	7.58	33.04	7.93	31.55
5.51	22.28	6.2	24.9	6.2	25.01	8.27	28.18	7.93	29.94	8.27	20.97
6.2	21.33	7.58	23.27	6.89	24.14	10.34	27.41	8.27	23.99	8.62	18.27
6.89	22.06	8.27	22.52	8.27	23.47	12.4	26.06	8.96	22.35	8.96	21.92
8.27	20.97	8.96	20.85	10.34	24.15			12.41	27.17	9.31	25.68
10.34	22.85									10.34	26.41
										12.41	27.98
										13.79	27.73
										15.51	25.79

In the Bachu et al. (2009) study, 189 data points concentrating upon the IFT CO_2-brine and the influence of aquifer conditions were identified (**Table 4**). The data were obtained between temperature of 309 K to 398 K, pressures of 2 MPa to 27 MPa and salinity concentrations 0% to 33.4% of sodium chloride (NaCl) which are relevant to geologically reservoir storage conditions. This result ordains the fact that IFT increases with salinity because ionic content leads to stronger dispersion forces at the water surface. On the other hand, high pressures decrease IFT and temperature shows moderate effects of decreasing IFT.

Table 4. Experimental IFT data for CO2 and 334,010 mg/l brine systems (Bachu et al., 2009).

Pressure (MPa) Temperature (°C)	2	4	6	8	12	17.4	27
36	66.5	60.1	52.4	46.4	39.5	35.1	31.5

41	67.4	61.4	53.5	48.6	41.2	36.8	34.9
60	67.9	62.8	56.6	52.1	46.1	42.0	36.7
75	69.3	64.4	59.5	55.8	49.9	44.7	40.1
100	69.7	65.9	62.5	58.6	53.1	46.4	41.1
125	70.5	67.8	64.5	62.4	56.0	48.6	42.5

In the study done by Bikkina et al. (2011), high pressure of about 1-20 MPa and moderate temperatures of between 298K and 333K were considered. These conditions were selected to provide the conditions commonly found associated with subsurface CO_2 storage applications. These data show that IFT decreases with pressure while the observation of the effect of increasing pressure on the confinement of CO_2 in geological formations is beneficial to the understanding of CO_2 behaviour in aquifer and reservoir conditions.

Table 5. IFT Measurements of the CO2/Water System (Bikkina et al., 2011)

P (MPa)	T (K)	ρ_{CO2} (kgm^{-3})	ρ_{water} (kgm^{-3})	γ (mN/m)
1.48	298.15	28.4	1002.0	59.66 ± 0.14
2.86	298.15	60.0	1006.0	50.25 ± 0.06
4.24	298.15	100.0	1010.0	44.09 ± 0.08
5.62	298.15	158.9	1013.0	35.95 ± 0.08
8.38	298.15	756.3	1015.0	25.65 ± 0.17
10.44	298.15	795.6	1016.0	25.15 ± 0.07
13.89	298.15	843.0	1018.0	24.85 ± 0.08
17.34	298.15	878.4	1020.0	24.9 ± 0.07
20.79	298.15	907.1	1022.0	25 ± 0.06
1.48	313.15	26.6	995.2	57.52 ± 0.45
2.86	313.15	55.4	998.6	51.32 ± 0.09
4.24	313.15	89.7	1002.0	47.50 ± 0.16
5.62	313.15	133.1	1004.0	42.17 ± 0.12
8.38	313.15	448.6	1007.0	22.23 ± 0.21
10.44	313.15	649.9	1009.0	22.16 ± 0.28
13.89	313.15	739.3	1010.0	23.33 ± 0.20
17.34	313.15	792.8	1012.0	23.41 ± 0.2
20.79	313.15	832.4	1014.0	25.07 ± 0.22

In the paper by Liu et al. (2015), specific attention was paid to the IFT and contact angle measurements for the CO_2-brine system. Some of the experiments were conducted at temperatures between 300 K and 313 K and pressure between 3 and 9 MPa representative of subsurface conditions for CO_2 storage. The saline water was prepared to have 0.102 and 1 mol/kg

concentrations of NaCl, and the result was used to compare the impact of salinity on IFT. These measurements are useful for studying the effect of CO_2 - brine on the porous media and the flow characteristics.

Table 6. Interfacial tension of CO2 and NaCl solution at different temperatures, pressures, and concentrations (Liu et al., 2015).

	Interfacial tension (mN/m)					
	0.102 mol/L			**1.0 mol/L**		
Pressure (MPa)	**27°C**	**35°C**	**40°C**	**27°C**	**35°C**	**40°C**
3.0	51.81	52.33	53.91	52.93	54.11	54.30
4.0	47.17	48.03	49.60	48.40	49.29	,50.20
5.0	42.12	45.07	45.76	43.52	45.71	46.28
6.0	36.75	40.83	41.55	38.20	41.69	42.47
7.0	30.28	36.17	37.53	32.40	36.57	38.85
8.0	29.48	27.62	33.59	32.20	29.65	34.52
9.0	30.34	27.74	26.40	31.42	28.88	29.67

From table in the study by Hebach et al. (2002), IFT for the water + CO_2 system at elevated pressures of 0.1–20 MPa and temperatures of 278–333 K were considered. The results of IFT demonstrate that as pressure increases, there is a generally positive trend towards IFT reducing, and therefore improving the solubility of CO_2 in water, which is essential for realising CO_2 storage subsurface pressures. In a similar manner, an increase in temperature was observed to lead to a decrease on the IFT but this is not as dramatic as that of pressure. This temperature dependence is in line with molecular motion where the higher the temperature, the better miscibility although the situation becomes a bit complicated at high pressure. The presented results are valuable for designing machine learning algorithms for CO_2 behavior forecasting in geological structures.

Table 7. IFT Measurements of the CO2/Water System (Hebach et al., 2002)

p/MPa	T/K	σ/ mN m^{-1}	p/MPa	T/K	σ/ mN m^{-1}
0.1	278.4	74.0 ± 0.0	0.1	307.9	70.9 ± 0.0
1.0	278.4	64.5 ± 0.0	2.06	308.0	59.0 ± 0.0
2.0	278.5	55.1 ± 0.0	4.05	308.0	48.8 ± 0.0
2.99	278.5	46.1 ± 0.0	5.04	308.1	44.2 ± 0.0
4.6	279.1	27.4 ± 0.3	6.04	308.1	40.1 ± 0.0
5.02	279.0	27.5 ± 0.0	7.05	308.1	36.0 ± 0.0
6.03	279.0	27.1 ± 0.0	7.55	308.1	33.7 ± 0.0
6.98	279.0	26.5 ± 0.0	8.01	308.1	31.3 ± 0.1
9.99	279.0	24.6 ± 0.1	9.03	308.2	31.0 ± 0.0
16.13	279.0	19.4 ± 0.1	10.02	308.2	30.3 ± 0.0
20.0	279.0	12.4 ± 0.2	12.51	308.2	29.1 ± 0.0
			15.02	308.2	28.5 ± 0.0
0.1	287.3	73.7 ± 0.0	17.55	308.2	27.9 ± 0.0
1.0	287.1	65.2 ± 0.0	20.03	308.2	27.2 ± 0.0
2.0	287.3	56.7 ± 0.0	0.1	318.7	69.3 ± 0.0
3.01	287.7	49.5 ± 0.0	2.03	318.5	59.0 ± 0.0
4.01	287.8	42.4 ± 0.0	4.03	318.5	50.5 ± 0.0
5.01	287.8	33.9 ± 0.0	6.05	318.4	43.0 ± 0.0
6.07	287.9	29.1 ± 0.0	7.03	318.4	39.8 ± 0.0
6.97	287.7	28.8 ± 0.0	8.04	318.4	35.7 ± 0.0
8.0	287.6	28.4 ± 0.0	9.07	318.4	29.6 ± 0.0
9.91	287.6	27.5 ± 0.0	10.03	318.5	31.3 ± 0.0
14.97	287.6	25.2 ± 0.1	11.02	318.4	31.0 ± 0.1
19.96	287.6	22.4 ± 0.1	12.05	318.4	30.7 ± 0.0

In the study by Li et al. (2012), the dataset covers pressures of 2–50 MPa, including temperatures in the range from 298 to 448 K, and a series of NaCl and KCl concentrations (total molalities: 0.95 up to 4.95 mol/kg). IFT first decreases with increasing the pressure, leading to CO_2-brine miscibility. Similarly higher temperatures also frequently result in decreased IFT although again this effect can be complicated by variables such as salt type or molality influencing fluid properties and phase interactions within subsurface environments.

Table 8. Interfacial Tension for CO_2 + brine at Total Salt Molality m = 4.95 mol/kg (Li et al., 2012)

T (K)	P (MPa)	Δρ (kg·m^{-3})	γ (mN·m^{-1})	T (K)	P (MPa)	Δρ (kg·m^{-3})	γ (mN·m^{-1})
323.15	2	1117.5	65.8	373.15	2	1092.8	61.3
323.15	4	1075.0	57.2	373.15	4	1061.0	57.8
323.15	6	1019.4	50.7	373.15	6	1025.1	53.2
323.15	8	936.2	44.8	373.15	8	984.5	49.4
323.15	10	771.6	41.8	373.15	10	937.6	46.1
323.15	12	572.2	40.1	373.15	12	885.5	43.9
323.15	14	485.5	39.3	373.15	14	827.1	42.1

323.15	16	436.4	38.9	373.15	16	765.6	40.6
323.15	18	402.1	38.4	373.15	18	705.2	39.5
323.15	20	375.2	38.0	373.15	20	649.5	38.0
323.15	25	327.7	37.0	373.15	25	544.4	36.7
323.15	30	292.2	36.6	373.15	30	471.8	35.3
323.15	35	266.3	36.2	373.15	35	421.4	34.8
323.15	40	242.5	35.6	373.15	40	380.6	34.2
323.15	45	225.1	35.4	373.15	45	350.1	33.8
323.15	50	206.6	34.7	373.15	50	321.9	33.2
343.15	2	1107.9	64.9	423.15	2	1062.8	55.7
343.15	4	1070.9	58.6	423.15	4	1036.5	52.4
343.15	6	1026.3	52.9	423.15	6	1008.5	49.8
343.15	8	970.5	47.7	423.15	8	978.6	46.8
343.15	10	897.3	44.3	423.15	10	948.3	44.3
343.15	12	800.1	42.3	423.15	12	913.4	42.6
343.15	14	690.1	40.8	423.15	14	878.5	40.9
343.15	16	599.8	39.7	423.15	16	842.5	39.6
343.15	18	536.1	38.8	423.15	18	805.9	38.2
343.15	20	490.1	38.3	423.15	20	771.3	37.4
343.15	25	414.2	37.2	423.15	25	683.0	35.3
343.15	30	365.0	36.3	423.15	30	610.6	34.0
343.15	35	328.8	35.5	423.15	35	547.1	32.8
343.15	40	300.1	34.8	423.15	40	499.5	31.9
343.15	45	276.3	34.3	423.15	45	455.7	31.5
343.15	50	256.0	33.5	423.15	50	423.6	31.0

In the study done by Park et al. (2005), the experiments cover near and supercritical CO_2 conditions: pressure range up to 20 MPa and temperatures 293–344 K. The data are used to describe the effect of pressure on IFT and the results show negative slope indicating improvement of miscibility of CO_2 in water at high pressure near the critical point. This dataset proves a good starting point to evaluate IFT in the CO_2 + pure water system, from which information in real CO_2-brine systems can be built on, given the effects of salinity and ionic interactions.

Table 9. Interfacial Tension Data for the Water + CO_2 System Measured at (293.15, 298.15, 311.15, and 344.15) K (Park et al., 2005)

T/K=293.15		T/K=298.15		T/K=311.15		T/K= 344.15	
P (MPa)	γ (mN·m^{-1})	P (MPa)	γ (mN·m^{-1})	P (MPa)	γ (mN·m^{-1})	P (MPa)	γ (mN·m^{-1})
0.1	65.69	0.1	78.01	1.79	56.61	0.10	64.84
2.43	51.95	1.12	70.3	2.8	52.5	1.23	62.00
3.36	46.27	2.29	63.3	4.79	41.17	2.20	57.49
4.15	41.91	4.81	43.34	6.93	30.53	3.29	53.27

4.77	37.95	6.37	12.94	14.12	27.28	5.44	47.23
5.66	10.22	8.08	20.48	16.28	24.85	7.45	41.68
6.56	17.92	10.82	14.76	20.28	20.55	9.54	37.25
7.71	17.24	13.32	11.83			12.00	31.42
8.71	18.37					15.69	27.57
9.85	18.36					17.32	26.83
11.93	15.68						

In the work by Georgidis et al. (2010), IFT of the $H_2O + CO_2$ system at pressures 2 to 40 (MPa) and temperature 298- 373 (K) values were covered. The trends show that interfacial tension decreases with pressure following a trend related to CO_2 solubility in water at high pressure. Temperature variation has a somewhat less prominent effect solely for IFT, but, in general, IFT lowers slightly with the rising temperature since molecular activity increases. This dataset improves the understanding of how the IFT behaviour in pure water systems might change under the conditions more close to the CO_2 sequestration.

Table 10. Interfacial Tension Results of the ($H_2O + CO_2$) System at 298 and 312K (Geogidis et al., 2010)

P (MPa)	T (K)	Δρ (kg·m^{-3})	γ (mN·m^{-1})
1.01	297.8	979	65.73 ± 0.27
2.0	297.9	958	58.90 ± 0.21
3.0	297.9	934	52.42 ± 0.36
4.0	297.9	906	47.02 ± 0.32
5.01	297.9	867	41.29 ± 0.20
6.01	297.9	804	36.00 ± 0.24
7.02	297.9	250	30.12 ± 0.11
8.02	297.9	221	30.28 ± 0.08
10.01	297.9	181	29.66 ± 0.20
14.99	297.9	126	27.73 ± 0.10
19.99	297.9	90	25.99 ± 0.09
1.0	312.9	975	63.55 ± 0.26
2.0	312.9	956	58.79 ± 0.27
3.01	312.8	935	51.15 ± 0.11
4.01	312.8	910	46.94 ± 0.27
5.02	312.8	881	43.93 ± 0.23
6.0	312.8	845	40.21 ± 0.17
7.02	312.9	796	36.87 ± 0.19
8.02	312.9	715	33.47 ± 0.19
10.0	312.9	363	31.20 ± 0.15
15.0	312.9	216	29.17 ± 0.13
20.02	313.2	161	28.33 ± 0.16

24.92	312.9	124	27.14 ± 0.09

Based on the findings of Yang et al. (2005), 19 data points were obtained in the case of CO_2 - brine system with NaCl concentration of 0.427%. It covers pressures up to 30 MPa, and all experiments have been carried out at 27°C and 58°C. The behavior of IFT with pressure variation plotted in this dataset appears to decline in general as pressure increases, a characteristic of CO_2-brine systems, particularly because of the increasing solubility of CO_2 in the brine phase at higher pressures. Hence, temperature differences exhibit a relatively close increase in IFT, implying that higher temperatures may decrease the solubility of CO_2 in the brine and the interfacial characteristics.

Table 11. Measured Equilibrium Interfacial Tensions of the Reservoir Brine + CO_2 System at Different Pressures and Two Temperatures (Yang et al., 2005)

t (°C)	P (MPa)	γ(mN·m^{-1})
26.85	0.121	49.3937
26.87	1.027	42.0751
26.64	4.013	30.1697
27.02	8.506	35.305
27.04	12.907	27.144
27.23	16.927	27.6708
27.12	21.403	25.3535
27.07	24.98	22.2715
27.28	30.068	17.7078
57.89	0.13	69.4472
58.38	1.031	68.1403
58.33	4.192	54.096
58.04	7.41	42.4628
27.06	0.112	24.4109
27.19	1.292	22.6225
27.04	4.122	14.2078
27.07	8.879	2.2335
26.87	12.248	1.5462
26.85	16.114	0.8881

2.4. CO2-Oil system

2.4.1. The Importance of IFT in CO_2-Oil Systems

IFT modelling in CO_2-oil system is very important for EOR and CO_2 storage operations. Knowledge of IFT is important since it determines successful interactions between CO_2 and crude oil when injecting CO_2 into reservoir rocks for enhanced oil recovery and sequestration. A lower IFT typically improves the miscibility of CO_2 with oil hence prospecting the improved recovery rates. For instance, it is revealed that the presence of nanoparticles in the CO_2-oil system can bring substantial down the IFT and enhance the oil recovery under high pressure and temperature (Al-Anssari et al., 2020). Interfacial characteristics are highly sensitive to oil composition as variations in the types of hydrocarbons and molecular weights may have several effects. For example, the addition of surfactants change the value of IFT by changing the interfacial behavior between the CO_2 and the oil phase (Park et al., 2005) . Temperature and pressure are other parameters that always affect IFT characteristics. IFT drops with increase in temperature because of an increase in molecular motion and a decrease in cohesive forces (Wang et al., 2023) and an increase in pressure likewise causes decrease in IFT since it increases solubility of the CO_2 in the oil phase (Yang et al., 2005) .

Several experimental works explain why IFT is important. For instance, Al-Anssari et al. (2020) showed that under the pressure drop conditions, the IFT of CO_2-oil systems could be lowered significantly to enhance the oil displacement. Furthermore, Wang et al. (2023) have found similar behaviors, signifying that changes in temperature and pressure impact on the CO2- oil phase stability which relates to the EOR processes clearly. These papers collectively give the basis for accurate IFT modeling to obtain the best shot of CO_2 injection, maximize the execution of oil recovery, and augment the feasibility of CO_2 storage.

2.4.2. Traditional IFT Models for CO_2-Oil Systems

The prediction of interfacial tension (IFT) in CO_2-oil systems has been attempted through several empirical and theoretical methods. These models try to mimic relationships between CO_2 and several types of oils, the components of which, are frequently heterogeneous. One of the conventional approach to predict IFT in CO_2-oil systems is the Gibbs adsorption isotherm. This model links IFT to the concentration of surfactants at the interface meaning that the addition of these substances can considerably reduce IFT through changing the energy barriers at the interface

(Mahboob & Sultan, 2016). However, many of these theoretical approaches still necessitate a substantial amount of information concerning the thermophysical characteristics of the system and may entail substantial discrepancies due to the wide variation in the chemical makeup of crude oils.

Issues with accuracy are also realized due to differences in oil compositions that prevail in the different reservoirs. For instance, the crude oils include hydrocarbons, waxes, and asphaltenes that have variants impacts on the IFT. As a result, while empirical models or designs are optimized to particular oils, it may not be capable of being applied to other types of crude (Yang et al., 2005). Notably, the nature of the relationship between CO_2 and IFT is not linear because increased solubility of CO_2 has a large impact on interfacial behavior (Liu et al., 2015).

Both recent publications show that existing models provide only limited value in explaining the specifics of interactions between various forms of CO_2 and oil. For instance, Liu et al. (2015) observed that the use of conventional IFT empirical correlations in the prediction of IFT in models of CO_2-brine-oversaturated oil systems under different pressure and temperature conditions provided very high errors. This goes a long way to show why there is a need for the development of more elaborate modeling techniques capable of accounting for the various characteristics of the crude oils as well as their relations with CO_2.

2.4.3. Machine Learning Applications for IFT Prediction in CO_2-Oil Systems

Application of ML for IFT prediction in CO_2-oil and CO_2-brine systems has been identified as promising already because of the ability of ML to deal with complicated nonlinear relations between the inputs and outputs that any attempts to create empirical models for would be difficult. IFT plays a critical role in the design of both EOR and CO_2 sequestration projects since the interactions between CO_2-oil under different conditions determine system behavior.

It is well noted that in the realm of large datasets, the performance of the ML models is highly commendable given that it is able to work on the frameworks for the IFT where creating predictive systems is needed when working in high dimensional spaces. For example, Maleki et al. (2023) successfully applied ML for modeling IFT fluctuations linked to hydrogen storage. The study shows how data-driven modeling can detect changes in wettability and IFT across various condtions, data valuable for CO_2 storage settings. In the same way, Hosseini et al. (2022) applied

AI techniques in forecasting CO_2-brine IFT and noticed that ML-based models could represent the impacts of pressures and compositions far better than regular models crucial for CO_2-oil systems.

Khan et al. (2021) used machine learning in prediction of IFT in CO_2-brine systems proving that the proposed machine learning approach can effectively use big data for increasing the prediction accuracy. In their study, they revealed how the ML models had the potential to assess the IFT behaviour when injecting carbon dioxide at different depths and pressures, fundamental aspects of carbon geostorage. It is also applicable for CO_2-oil system where pressure and composition variations seriously affect IFT. Along the same line of thought, Zhang et al. (2020) trained supervised models on the IFT of CO_2 and brine with a strengthen on the extent of CO_2 sequestration depth, to great accuracy, depth and pressure being significant factors not only in EOR but in CO_2 storage in oil reservoir as well.

Other evidence of the efficiency of ML is presented in Mouallem et al. (2019) revealing that ML could make the estimation of CO_2-brine IFT with high results and in geostorage where the complicated subterrain conditions might hinder the accuracy of the conventional models. Their observations support the hypothesis that interaction ML can identify multivariate conditions in multiphase interactions, which are important for both CO_2-brine and CO_2-oil systems. Tavakolian et al. (2018) utilised ML to predict the gas sorption capacity in tight reservoirs through the strengths of ML in solving reservoir heterogeneity problems, especially in the system of CO_2-oil reservoir.

In combination, these works demonstrate that ML does improve predictive ability in IFT modeling by combining disparate and intricate data sets, and that the resulting structures are also modular and can be customized to fit different storage and EOR contexts. It is here that the superiority of ML becomes evident in the potential interactions of, and the sensitivity of, temperature, pressure, salinity, and composition, in providing distinct, more accurate, and real time IFT predictions imperative for the efficient handling of the CO_2.

2.4.4. Key Data Sources for CO_2-Oil IFT Modeling

In the CO_2-oil system, Al-Anssari et al., demonstrated the interfacial tension (IFT) measurements under high pressure and temperature. The experiments describe temperature and pressure effects on IFT for the CO_2-oil system and which are different when nanoparticles are added to reduce IFT

and promote better dispersion of CO_2 in the oil phase. This reduction of IFT with adding nanoparticles is beneficial in enhancing mobility at EOR because it enhances the miscibility of the injected CO_2 and the oil under reservoir condition. The pressure dependency obtained in this work corresponds to conventional tendencies, in which higher pressure leads to reduced IFT and enhanced CO_2 injection methods.

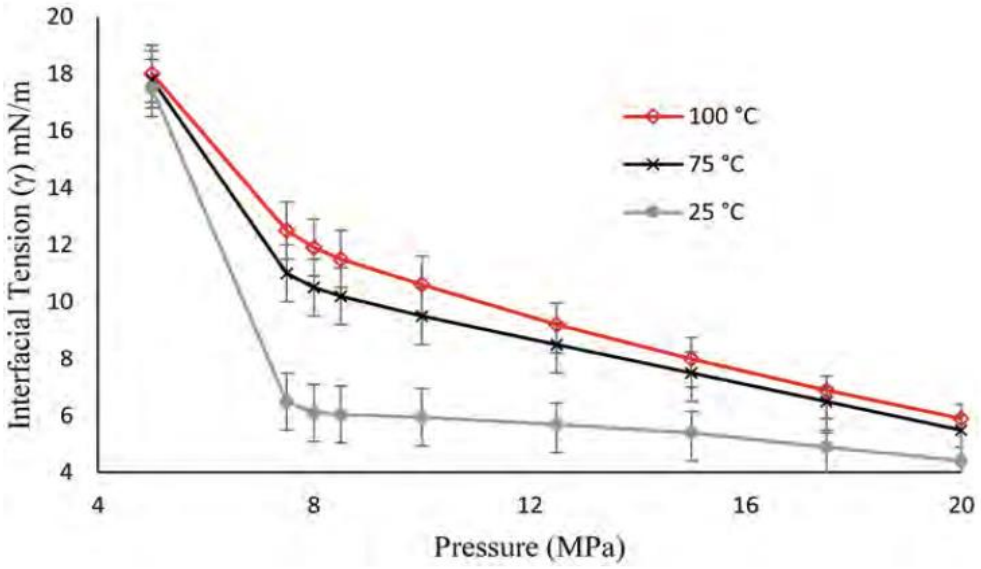

Figure 3. IFT CO2/oil system with increased pressure at three different temperatures (Al-Anssari et al., 2020)

Wang et al. (2023) examined the impact of IFT on the stabilization of CO_2-oil system employing diesel as the oil phase at elevated temperature and pressure conditions. For this study, 60 data values were retrieved from the plots based on temperatures between 25 °C and 100 °C and pressures of between 0.1 and 11 MPa. This data is important to assess foam characteristics in EOR where formation of stable CO_2-based foams leads to better sweep efficiency. These results suggest that IFT is a decreasing function of temperature and pressure and that the increasing tendency of oil stability due to the suppression of gas bubble coalescence would promote the steady formation of oil structure under reservoir like conditions. The results help to enhance understanding of oil stability – an important parameter for successful application of CO_2 flooding in EOR, particularly when diesel or other hydrocarbon phases are used as the oil phase.

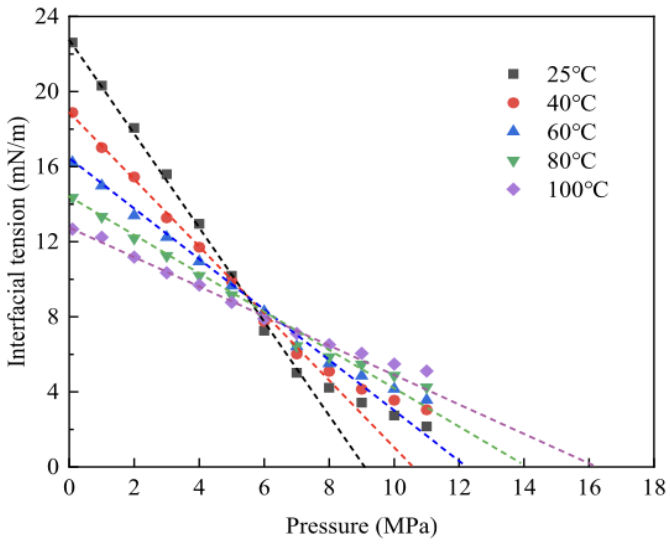

Figure 4. CO_2-diesel IFT under different temperatures and pressures (Wang et al., 2023)

Yang et al. 2004, have looked at the interfacial phenomena between crude oil and CO_2 at different temperatures and pressures. In this work, 15 data points were obtained from graph including the temperature of 27 and 58°C and pressure range of 0.17-28.37MPa. Here in this dataset, crude oil is considered as the oil phase, and from these specified temperature and pressure ranges, it determines the relationship between IFT and that affects the effectiveness of the CO_2 injection in EOR. The research evidence implies that as pressure builds up, IFT reduces which enhances miscibility of CO_2 with crude oil, a critical process for oil displacement in the subsurface reservoirs. This work therefore provides important information of the interfacial properties of crude oil-CO_2 system towards the enhancement of CO_2 EOR processes.

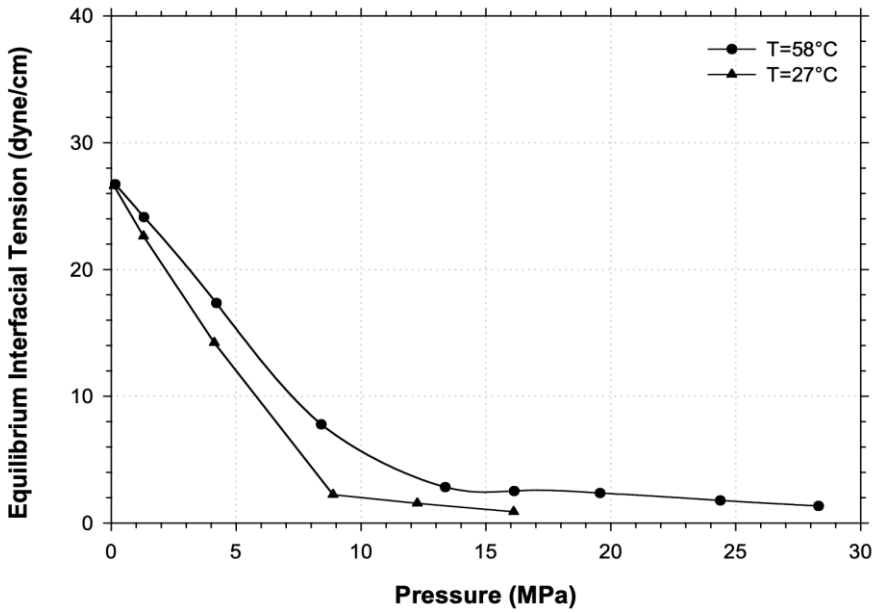

Figure 5. Measured equilibrium IFT of the crude oil-CO2 system vs pressure at two different temperatures

Yang et al., (2005) studied the nature of the interfacial tension between crude oil, reservoir brine and CO_2 during different pressure ranges. Presented in this work are the 9 data points gleaned from tables measured at 331 K and at pressure levels of 0.1 – 28 MPa. The results also show that the rising pressure consistently leads to the reduction of interfacial tension, which is essential for CO_2 solubility with crude oil, an element vital to the CO_2-based EOR. This dataset is especially important to investigate the behavior of the CO_2-brine-crude oil interphase under conditions diverting those of the subsurface reservoirs and it will be crucial to the design and optimization of EOR methods.

Table 12. Measured Equilibrium Interfacial Tensions of the crude oil + CO_2 System at Different Pressures and Two Temperatures (Yang et al., 2005)

t (°C)	P (MPa)	γ (mN·m⁻¹)
58.4	0.154	25.9951
57.99	1.305	24.1342
57.88	4.207	17.3381
57.87	8.404	7.7785
57.74	13.362	2.8275
57.74	16.131	2.5182
57.65	19.567	2.3562
57.89	24.38	1.7814

57.89	28.31	1.3449

Erpeng et al. in their study conducted in 2018, focused on the interfacial tension characteristics when using supercritical CO_2 and steam injection to extra-heavy oil reservoirs which is important an effective recovery mechanism in tight high viscosity reservoirs. In taking the 27 data points from plots the study covered the temperature parameter from 15°C and the pressure component up to 18 MPa. The results depicted below show that as pressure increases, interfacial tension of CO_2 and extra-heavy oil reduces, and this provides increased miscibility essential for CO_2 displacement and enhanced flow of extra-heavy oil within the reservoir. Additionally, temperature variations also show a marked effect: it has been observed that at high temperatures, the decrease in interfacial tension with pressure is even further realized. This implies that, high temperatures in combination with high pressures plays a major role in the enhancement of flow and collaboratively the co-injection technique for extra-heavy oil deposit.

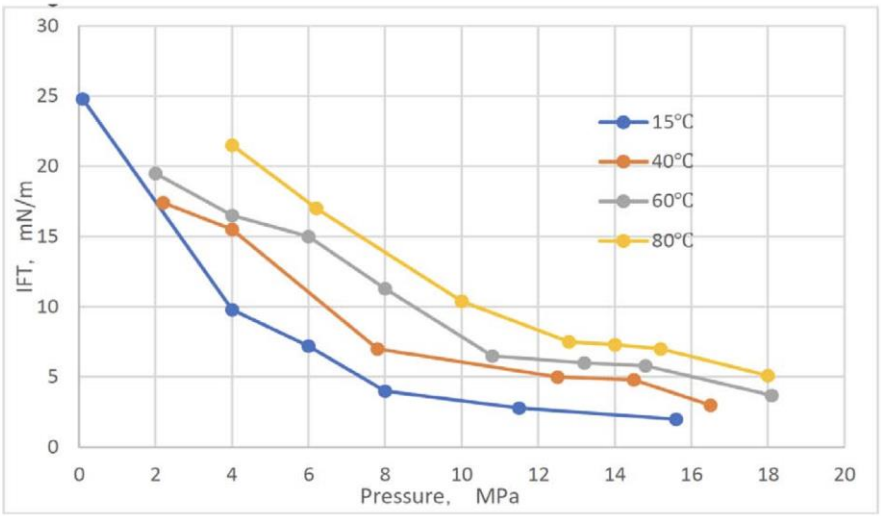

Figure 6. Variation of IFT between CO2 and oil under different conditions (Erpeng et al., 2018).

Al-Anssari et al. (2020) studied a relationship between the nanoparticles and the interfacial tension (IFT) of the CO_2-oil system, which is important for EOR processes due to high pressure and temperature conditions. From the plots, 18 data points were obtained without adding nanoparticles, using constant pressures of 5, 10 and 20 MPa and temperatures of up to 393K. It was observed that as pressure increased, CFD observation index showed decreasing interfacial tension as

consequence of increased solubility of CO_2 in oil and improved miscibility assisting the oil displacement efficiency.

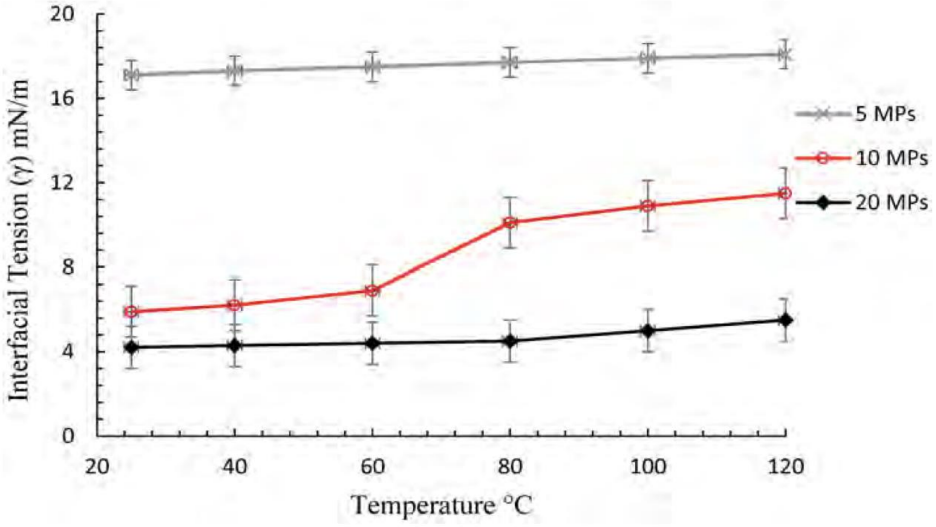

Figure 7. IFT CO2/oil system with increased temperature at three different pressures (Al-Anssari et al., 2020).

2.5. Comparing CO_2 – Water system and CO_2 – Oil system

Understanding the dependence of the IFT on various variables at CO_2 – water and CO_2 – oil interfaces plays a crucial role for processes like CCS and EOR. Each system exhibits distinct behavior under different regimes of pressure, temperature, and fluid composition, all of which significantly influence the IFT response. Therefore, a detailed analysis of IFT behavior and its variation under varying thermodynamic and compositional conditions is essential for accurate modeling and prediction in CCS and EOR applications.

2.5.1. Pressure and temperature effects:

The behavior of IFT in the system containing CO_2 and water is dependent of pressure and temperature where, IFT reduces with increase of both pressure and temperature. For instance, research has shown that at higher pressures up to 50 MPa the IFT between CO_2 and water declines this implying that the miscibility between the two phases is good which is suitable for use in CCS (Chiquet et al., 2007; Bachu et al.,2009). On the other hand, the nature of the effect of pressure on IFT in CO_2-oil systems depends on the composition of oil phase because the effect exhibits different trend. In general, raising pressure will cause the IFT to reduce but this influence can be best explained by several factors including solubility of CO_2 in the oil phase (Yang et al., 2005;

Al-Anssari et al., 2020).Temperature has been identified to be another crucial factor. In the case of CO_2-water systems, the experimental observations show that IFT is generally low at high temperatures because of increased molecular activity. In contrast, in CO_2-oil systems reduction of the IFT could be affected by the temperature and nature of the oil phase or also with the presence of additives such as surfactants (Wang et al., 2023).

2.5.2. Composition Influence:

Water salinity has a strong influence to IFT especially in CO_2-water system because an increase in water salinity resulted to lower IFT resulting from variation of electrical double layer of water CO_2 interface (Bachu et al., 2009). On the other hand, for CO_2-oil systems there is a great dependence on the type of crude oil and presence of hydrocarbons types affecting the IFT. The behavior of various crude oils varies with the density of the crude oils where the IFT of the heavier crude oils stands higher than that of the lighter crude ones (Yang et al., 2005, Al-Anssari et al., 2020).

2.5.3. Data Characteristics:

CO_2-Water Systems: The set of input parameters for CO_2-water systems is normally limited to pressure, temperature, concentration of salts, and impurities present in CO_2. The curves established here are generally relatively linear for these parameters and IFT and relatively easy to model.Compared to the data gathered in the field, the information is acquired under laboratory settings; thus, making it more reliable and consistent (Chiquet et al.,2007).

CO_2-Oil Systems: For the CO_2-oil systems, pressure and temperature are crucial factors, as they govern the extent of mass transfer between the CO_2 and oil phases, significantly influencing IFT behavior and phase equilibrium. Moreover, the datasets are normally more scattered due to the differences in crude oil composition and their specific gravity. The existence of two and more hydrocarbon phases can complicate the data because of non-linear dependencies, which make the modeling more difficult (Yang et al., 2005). This variety can potentially cause a wider range of variations of IFT with the same conditions, which needs more analysis.

2.5.4. Machine Learning Model Requirements:

CO_2-Water Systems: The relationships between variables in the data of the CO_2-water systems may be more easily understandable by simpler ML models most of the time. It might be sufficient to

apply linear regression or use decision trees what will take less time and will give acceptable accuracy (Li et al., 2012).

CO_2-Oil Systems: Contrary to this, the modeling of the CO_2-oil systems requires higher level of data complexity which in this case include ensemble approaches or deep learning approaches. The requirement for these sophisticated models stems from the fact that the existence and the stability of IFT depend on the configuration of one or multiple independent parameters and their interplay (Wang et al., 2023; Al-Anssari et al., 2020).

2.6. Machine Learning Tools

Data-driven decisions are made when machine learning tools are applied for automation of pattern recognition, predictive modeling and optimization in various domains. ANN is very good at complex, nonlinear relationships and renders well in the deep learning applications (Wu et al., 2018). Symbolic Regression-Genetic Programming (SR-GP) is an evolutionary approach to mathematical relationship discovery in data without given models (Galvan et al., 2022). Both Random Forest (RF), and Decision Trees (DT) are good ensemble and tree-based methods which help increase predictive accuracy and interpretability (Nallathambi et al., 2017). Extreme Gradient Boosting (XGBoost), a very fast boosting algorithm, is very good at structured data task (Chen et al., 2016). Support Vector Regression (SVR) are efficiently used for datasets with the small number of samples but large dimensions of features (Smola AJ et al., 2004). GBR is able to enhance predictive accuracy by adding iteratively the next weaker learner (Nait Amar et al., 2019). All machine learning tools contribute to scalable and reliable answers to real world issues.

2.6.1. Artificial Neural Network (ANN)

The modeling system of Artificial Neural Networks (ANNs) duplicates human brain processing ability to handle difficult and non-linear data forms. The system finds wide use across forecasting applications, decision-making support, pattern recognition tasks and industrial automation operations. (Gevrey et al., 2003; Wu et al., 2018).

The primary feature of ANNs is their ability to handle nonlinear input-output variable connections. ANNs adapt their processing dynamically, whereas linear regression in conventional statistical models preserves fixed variable associations (Dongare et al., 2012).

An input layer, hidden layers, and output layers make up their tiered networks of interconnected nodes (Qamar and Ali Zardari, 2023). The fundamental units of artificial neural networks (ANNs) are neurons, which take in input, calculate a weighted total, and then utilize an activation function to generate an output.

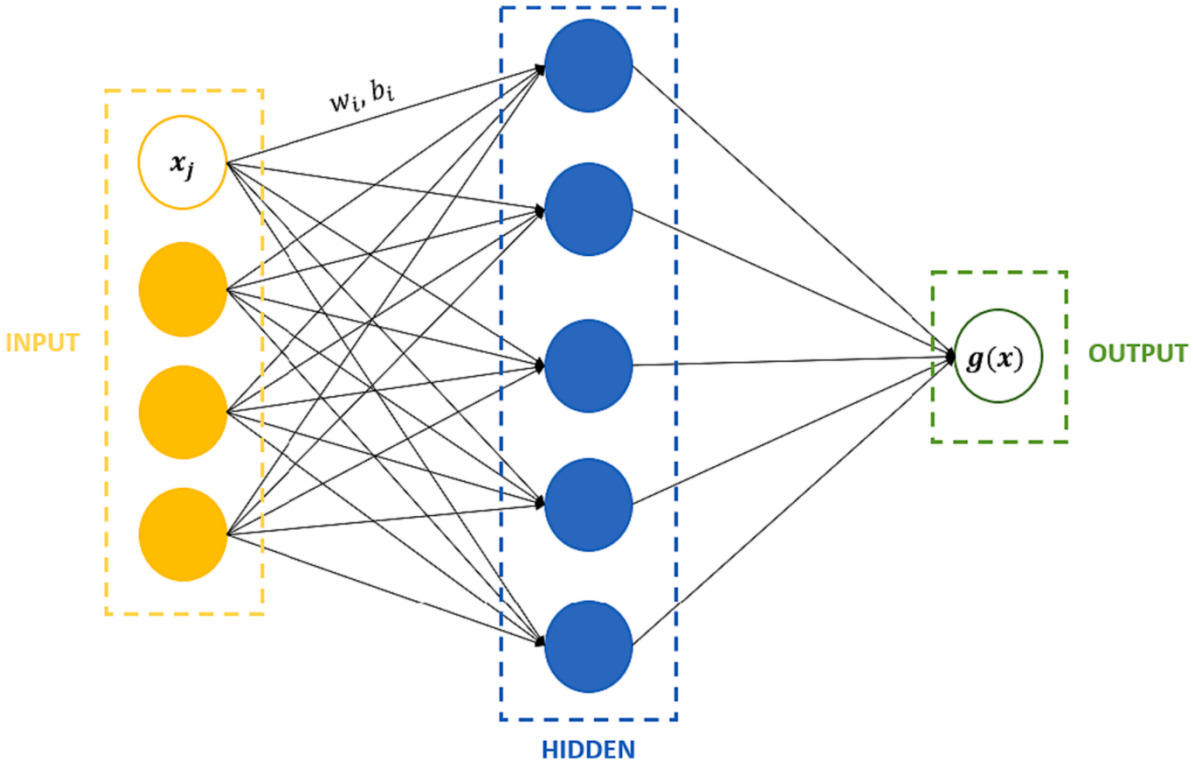

Figure 8. Model of ANN showing the input, hidden and output layers (Mouallem et al., 2024).

A mathematical description of a simple ANN structure is as follows:

$$y = \sum_{j=1}^{N_h} w_{jk} g\left(\sum_{i=1}^{N_i} w_{ij} x_i + b_{oj}\right) + b_{ok} \qquad (5)$$

The network variables include x_i representing input parameters and y representing target parameters with w_{ij} signifying weights connecting input nodes to hidden nodes, w_{jk} maintaining weights between hidden nodes to output nodes, b_{oj} referring to input layer bias linked to each

hidden node, b_{ok} describing output layer bias along with N_i indicating overall input variables, N_h counting hidden layer neurons and g representing the activation function.

An ANN trains through backpropagation which adjusts weights and biases to minimize its loss function. During the training phase the network parameters receive optimization through various updates to reach exact prediction or classification goals (M. Lopez et al., 2022). An ANN contains a set of key hyperparameters which includes its neuron count, activation function and optimizers (Kalam et al., 2023).

2.6.2. Symbolic Regression via Genetic Programming (SR-GP)

Finding symbolic mathematical expressions that provide the greatest fit for a given dataset is known as symbolic regression (SR). The search for these terms is typically done with Genetic Programming (GP) according to Galvan et al. (2022). Through an iterative process it enhances a collection of symbolic possibilities throughout the duration. In the GP method different combinations of mathematical operations together with constants are tested to search for mathematical equations. The genetic process of GP relies on mutation and crossover operators through its fitness function to measure how accurately candidate equations match the provided data set. A progressive evolution process allows SR-GP to develop more precise symbolic data representations which capture the fundamental relationships.

SR-GP features several hyperparameters where population size stands for the number of programs in each generation and number of generations to evolve while function set contains fundamental mathematical operations such as addition, subtraction, multiplication and crossover along with mutation operations are also necessary (Kalam et al., 2023).

2.6.3. Decision Tree (DT)

Decision trees are sequential models that logically incorporate a series of basic tests, each of which compares a nominal attribute to a range of potential values or a numeric attribute to a threshold value. (Kotsiantis, 2011). This model has a simple structure and is made up of branches, nodes, and leaves. Regression and classification tasks are handled by the DT models. Additionally, DT is capable of carrying out a step-by-step decision-making procedure. During each evaluation, one of the two nodes is selected, starting with the root node. The iterative process runs until it gets at the last leaf which indicates the target value. Each node in the tree functions as a decision rule. The

hyperparameters controlling DT include tree depth and the least samples to split internal nodes as well as the minimum number of samples needed to locate leaf nodes (Kalam et al., 2023).

2.6.4. Random Forest (RF)

To increase prediction accuracy and avoid overfitting, the ensemble learning method known as random forest (RF) integrates several decision trees (Borup et al., 2023). The training process of tree forest with bootstrapped data involves tree splitting analysis of randomly selected characteristics at each split point.

Integrating the predictions of many trees is the fundamental idea. For aggregation, majority voting is typically utilized, whereas regression problems are handled by averaging. This can be expressed mathematically as follows.

$$RF\ Prediction(x) = \frac{1}{N}\sum_{i=1}^{N} Tree_i(x) \qquad (6)$$

RF Prediction (x) represents the forecast and $Tree_i$ (x) denotes the i_{th} tree calculation in the ensemble forest. The combination of multiple decision trees through RF minimizes incorrect models caused by overfitting because it incorporates data from various trees. RF includes several hyperparameters which consist of the number of estimators, minimum split, leaf node samples, maximum features and maximum depth (Kalam et al., 2023).

2.6.5. Gradient Boosting Regressor (GBR)

Schapie in 1990 initially introduced the boosting method as an ensemble methodology. The central aim of this method involves linking low-performing predictors also called learners into a single enhanced predictor unit (Nait Amar et al., 2019). During sequential training sessions weak predictors enhance the performance of previously trained learners as part of their complementary work. The boosting method finds its illustration as Gradient Boosting Regression (GBR).

The decision tree (DT) approach receives an enhancement through the addition of a boosting mechanism which results in Gradient Boosting Regression being considered an advanced version of DT. Multiple GBR hyperparameters maintain logical relationships with parameters from the decision tree (DT) approach. The GBR hyperparameters consist of subsampling as well as the

number of estimators, maximum features, maximum depth together with minimum split samples and leaf node samples (Kalam et al., 2023).

2.6.6. Support Vector Machine for Regression (SVR)

Another popular and reliable machine learning approach for regression applications is Support Vector Machine for Regression (SVR). The support vector machine (SVM) algorithm, which is commonly used for classification issues, is extended by this method. SVR is predicated on the idea of optimizing the margin between data points and the regression line, just like its classification analog (Suykens JA et al., 1999). It can manage challenging regression problems and is excellent at identifying non-linear patterns in data. Finding the hyperplane that best matches the multi-dimensional data while allowing for a margin of error is the fundamental concept of SVR (Smola AJ et al., 2004). Support vectors are data points that fall inside this range. The algorithm penalizes data points that fall outside of this margin in an effort to minimize it. Furthermore, SVR can effectively handle data with non-linear patterns by supporting the use of many kernel functions, including linear, polynomial, radial basis function (RBF), and sigmoid (Cristianini et al., 2000). SVR has great precision and generalization capabilities and is commonly used in a variety of continuous-valued outcomes.

2.6.7. Extreme Gradient Boosting (XGBoost)

Extreme Gradient Boosting, or XGBoost, is a potent machine learning algorithm that is mostly employed for classification and regression problems. It is a member of the Ensemble Learning family, which builds a more robust and accurate model by combining the predictions of several separate models. For a variety of applications, XGBoost has become extremely popular and is regarded as one of the best options among data scientists and machine learning professionals. XGBoost is renowned for its computational efficiency and strong predictive performance. It enhances the idea of gradient boosting, an ensemble method that iteratively combines the predictions of weaker models to create a strong predictive model. By adding a regularized objective function and a computational structure that effectively manages missing data, reduces overfitting, and permits parallel processing, this technique improves on this methodology (Chen et al., 2016). The algorithm is a flexible tool for resolving challenging predicting issues since it includes a large set of hyperparameters that may be adjusted to tailor its behavior for various jobs.

3. METHODOLOGY

The aim of this work will be to develop and build machine learning models for evaluating IFT in both the CO_2-water and CO_2-oil phases, depending on temperature, pressure and composition. The methodology consists of three main phases: Data Gathering, Data Preprocessing and Data Processing.

3.1. Data Gathering

This study used experimental data collected from research papers, technical reports and a publicly available database. The purpose of data collection was to determine the values of interfacial tension in CO_2–water and CO_2–oil systems in a wide range of operating conditions. These include input parameters such as temperature (T, K), pressure (P, MPa), molality of monovalent (m^+, mol/kg) and bivalent (m^{2+}, mol/kg) salts, non-acidic impurities (CH_4, N_2, H_2), (X_{imp}, %) and acidic impurities (H_2S, SO_2), (X_{imp}, %) percentage for the CO_2 – water system, as well as pressure (P, MPa), temperature (T, K) and API gravity for the CO_2 – oil system.

To obtain data on the CO_2-water system, 23 research papers with experimental tables were used. The values obtained were metric, and these tables were copied with the necessary numerical values decoded accordingly for accuracy. On the other hand, the CO_2-oil system was less represented in tabular form, most of the data was obtained from graphs presented in nine research papers in the form of figures. For accurate extraction of data points, the Plot Digitizer tool was used.

Thus, 1831 data points were collected for the CO_2-water system, while 385 data points were collected for the CO_2-oil system. The summary for collected data for both systems you can see on table 13 and table 14 correspondingly. The values below have been selected specifically to account for a wide range of thermodynamic conditions related to both systems. This diversification allows to cover many possible conditions that can be implemented in industrial use.

Table 13. Summary of collected data for CO_2-water system

Author	Method	Temperature (K)	Pressure (MPa)	Molality *(mol/kg)*	Salt composition	Impurities (%)	Datapoints
Kvamme et al., 2007	PD	322.8	1.1-22.45	0	-	-	11

Chiquet et al., 2007	PD	307.4-382.9	5-45	0.349	NaCl	-	52
Chun & Wilkinson, 1995	Capillary rise	278-344	0.1-18.61	0	-	-	125
Bachu & Bennion, 2009	PD	309-398	2-27	1.331-6.39	NaCl	-	189
Bikkina et al., 2011	PD	298-333	1-20	0	-	-	36
Liu et al., 2015	PD	300-313	3-9	0.102-1	NaCl	-	42
Hebach et al., 2002	PD	278-333	0.1-20	0	-	-	85
Li et al., 2012	PD	323-448	0-50	0.98-4.95	NaCl, KCl	-	336
Park et al., 2005	Capillary rise	293-344	0.1-20.28	0	-	-	36
Georgiadis et al., 2010	PD	297-374	1-60	0	-	-	80
Yang et al., 2005	PD-ADSA	300-331	0.112-30	0.0785	NaCl	-	13
Li et al., 2012	PD-ADSA	343-423	2-50	2.5-5	$MgCl_2$, $CaCl_2$	-	208
Ren et al., 2000	PD	298-373	1-30	0	-	20-40 (CH_4)	60
Yan et al., 2001	PD	298-373	1-30	0	-	24.15-49.28 (N2)	60
Aggelopoulus et al., 2010	PD-ADSA	300-373	5-25	0.045-2.7	$CaCl_2$	-	103

Aggelopoulus et al., 2011	PD-ADSA	300-373	5-25	0.045-1.5	NaCl, $CaCl_2$	-	95
Akutsu et al., 2007	PD	318	1-16	0	-	-	14
Pereira et al., 2016	PD-ADSA	298-469	0.7-69	0	-	-	78
Pereira et al., 2017	PD	298-423	2.96-69	0.98-1.98	NaCl	-	42
Shah et al., 2008	PD	350	0.5-15.6	0	-	30 (H_2S)	14
Saraji et al., 2014	PD-ADSA	333	20.68	1	NaCl	1%; 6% (SO_2)	2
Isfehani et al., 2023	PD	323-353	3-20	0 - 3.15	NaCl	30% (H_2)	24
Liu et al., 2016	PD-ADSA	299-398	1-34	0 – 3.42	NaCl	10-49% (CH_4)	126
						Total	1831

Table 14. Summary of collected data for CO_2-oil system

Author	Method	Temperature (K)	Pressure (MPa)	º API	Datapoints
Al-Anssari et al., 2020	PD-ADSA	297 - 393	5-20	62	45
Wang et al. 2023	PD	298-373	0-11	37	60

Yang et al., 2005	PD-ADSA	300-331	0-28	23	15
Erpeng et al., 2018	PD	288-353	0-18	8	27
Yang et al., 2015	PD-ADSA	318-412	3-44	27,30	105
Xin et al., 2015	PD-ADSA	355.65	7-25	28	11
Torabi et al., 2024	PD-ADSA	338	19-22	33	3
Gajbhiye, R., 2025	PD	303-358	0.7 – 6.5	41.7, 59.4	76
Zhang et al., 2024	PD	313-333	2-22	35	43
				Total:	385

*PD refers to pendant drop method.

**PD-ADSA refers to pendant drop method with Axisymmetric Drop Shape Analysis.

The collected dataset supports the entire process of model development and evaluation, providing a reliable basis for building accurate machine learning models of interfacial tension in both CO_2–water and CO_2–oil systems.

3.2. Data Preprocessing

Data preprocessing or cleaning remains an important process for improving the quality and standard of a dataset in machine learning. However, before proceeding with the practical application of machine learning algorithms, it is necessary to solve several preprocessing problems, including the missing values, the presence of outliers, and problem with different data formats. This process makes the dataset clean, reliable, and preprocessed, which increases its convenience for modeling.

The concentration was made on the most relevant essential factors of IFT for CO_2-water and CO_2-oil systems, which consists of the temperature, pressure, and molality of mono- and bivalent salts, acidic and non-acidic impurities in CO_2 for the water phase and API gravity for the oil phase. Accurate analysis of data procured from experimental study was done to dissolve issues with missing values, data formatting and variations in data obtained from different sources. These steps were crucial to produce the dataset for strong machine learning model building process.

The unit statistics, including the mean, standard deviation, minimum, maximum, 25th and 50th and 75th percentiles of each parameter were also calculated to gain an understanding of the distribution of the data. Tables 15 and 16 below give a summary of the data set and variability of the data collected in this study. In other words, parameter ranges need to be standardized in the dataset and data discrepancies handled at the preprocessing step in order to properly train and apply the chosen model. This structured approach was solely helpful in structuring the dataset for the generation of machine learning models capable of identifying IFT at disparate thermodynamics conditions.

Table 15. Statistical analysis for CO_2-water system

	P, MPa	T, K	m^+, mol/kg	m^{2+}, mol/kg	$X_{imp(CH4, N2, H2)}$, %	$X_{imp(H2S, SO2)}$, %	γ, mN/m
count	1831	1831	1831	1831	1831	1831	1831
mean	15.19	345.36	0.98	0.5	4.84	0.23	39.98
std	12.69	40.67	1.6	1.21	12.49	2.62	12.33
min	0.05	278	0	0	0	0	4.71
25%	6	312.8	0	0	0	0	31

50%	11.6	343.15	0	0	0	0	37.74
75%	20	373.15	1.5	0	0	0	47.5
max	69.51	469	6.39	5	49.35	30	78.48

Table 16. Statistical analysis for CO_2-oil system

	Pressure, MPa	Temperature, K	API	IFT, mN/m
count	385	385	385	385
mean	11.11	338.86	37.07	9.1
std	8.93	29.23	14.6	6.34
min	0.08	288	8	0.7
25%	4.88	318	27	4.15
50%	8.62	333	35	7.87
75%	15.98	353	41.7	13.18
max	43.85	412	62	58.92

3.2.1. Boxplots

The boxplots for the CO_2-water and the CO_2-oil systems can be used to visually compare the distributions of different key parameters, in terms of the center tendencies, spread and the outliers.

For CO_2-water system, based on interquartile range data the pressure measurement varies from 5 MPa to 20 MPa with 10 MPa as the median value but includes multiple outliers ranging from 40 MPa to 70 MPa (fig.9). The widespread changes in the data signify phase transitions or variations in solution behavior. Data shows temperature follows a stable pattern with distribution limits from 310 K to 370 K and a median value at 350 K and a major outlier point above 450 K. The analysis shows pressure exhibits higher sensitivity to system factors compared to temperature which stays consistent.

The boxplots exclude secondary factors that include molality of monovalent and bivalent cation salts in addition to CO_2 gas impurity types since their data distributions are both highly variable and sparse across the study parameters. The narrow distribution of molality values makes boxplots perform poorly at depicting distribution patterns and impurity concentrations present severe right-

skewness except occasional extreme values. The effectiveness of boxplots depends on continuous variables that show evenly distributed quartiles and thus these secondary factors do not generate appropriate visual outcomes using this method. The study include all selected molality and impurity variables to achieve a broad range of input factors necessary for studying interfacial tension (IFT). Pressure and temperature stand as the main points of outliers' analysis because they demonstrate substantial variability which is critical for understanding CO_2-water thermodynamic processes.

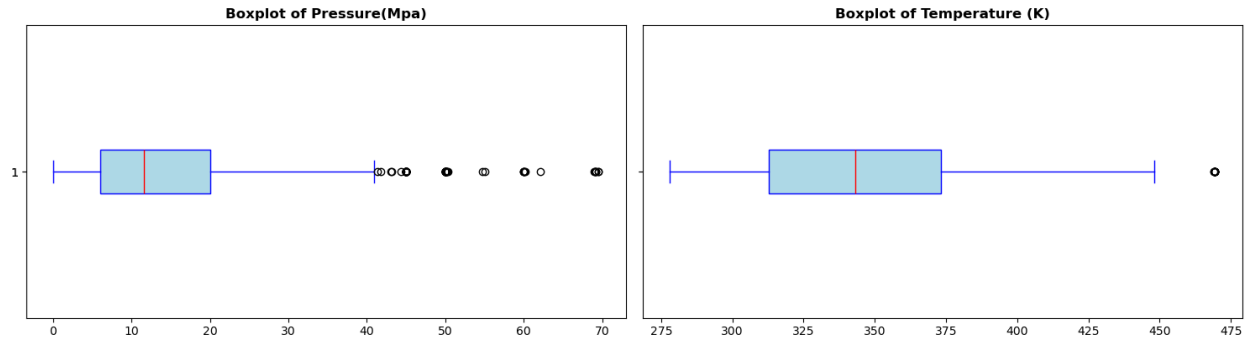

Figure 9. Boxplots for CO_2-water system

As for the CO_2-oil system, the distribution of pressure measurements ranged between 5 MPa and 15 MPa, with a median pressure value matching 8 MPa (fig.10). Multiple outliers in the data extend the whisker boundary from 30 MPa to 45 MPa, revealing considerable pressure variations. The temperature distribution in the boxplot ranges from 320 to 350 K, with a median temperature of 330 K. A single extreme high-temperature measurement exceeding 400 K functions as evidence for a rare temperature reading while the general distribution maintains consistent stability. The distribution of API gravity shows symmetry because the interval spanning 30 to 45 contains most of the data, with a median of approximately 38. The API gravity oil values extend through the entire whisker space from 8 to 60, demonstrating a wide yet distribution of measurements. Pressure varies most among the three variables because several outlier observations exist, but API gravity and temperature measurements show steadier distributions. The measured pressure fluctuations demonstrated higher sensitivity to system conditions than both temperature and API gravity, which demonstrated predictable patterns within the CO_2-oil system.

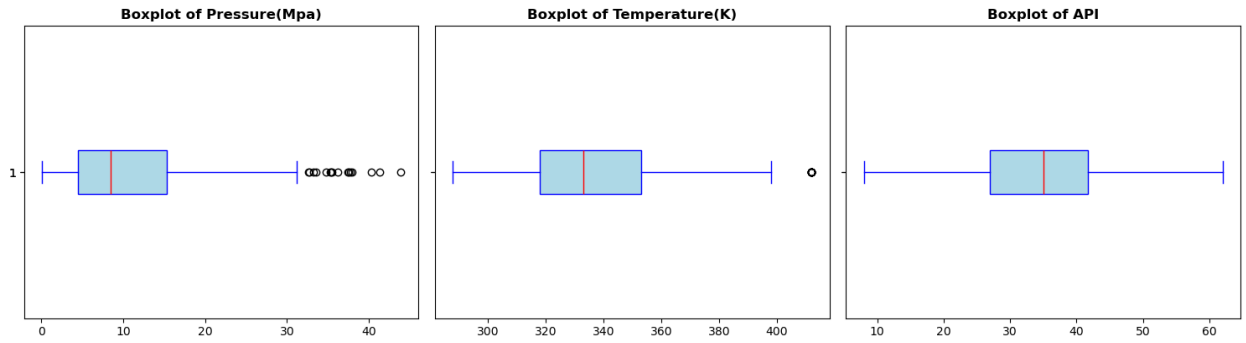

Figure 10. Boxplots for CO_2-oil system

3.2.2. Pair plots

The pair plot is a useful type of graph for a large number of variables, which allows researchers to analyze trends, correlations, and dependencies between variables. In the present analysis, to depict the correlation study of individual parameters pressure, temperature, molality of mono- and bivalent salts, impurities and interfacial tension for the CO_2-water and API gravity for CO_2-oil systems pair plots are presented. These parameters are important for assessing the behavior of CO_2 in such processes as Geological Storage and Enhanced Oil Recovery.

Scatter plots show the distribution of each variable in of CO_2–water system (fig.11). Pressure is significantly dominated by lower values, while Temperature and Molality of mono- and bivalent salts have a wider distribution, which highlights the variability of the experiments. The potential observed in the IFT values is largely confined in the range of 20 mN/m to 40 mN/m which implies that the interfacial tension is fairly stable under different conditions. One observed pattern is the negative relationship between pressure and IFT, where the pressure decreases as IFT increases. This feature correlates well with the physical properties of the CO_2 which is characterized by increased solubility in water at high pressure thus lowering the interfacial tension. IFT was found to have a weak positive relationship with the molality of salts, which suggests that increasing salt concentration could improve IFT to a negligible extent, perhaps because salt is cohesive and prevents CO_2 from immersing into water. On the other hand, temperature does not have any direct significant influence on the IFT, but the variance in the IFT values increases as temperature increases, implying that several other variables interact with temperature. The analysis of impurities revealed a distinct distribution that indicated pre-established experimental conditions instead of continuous variation.

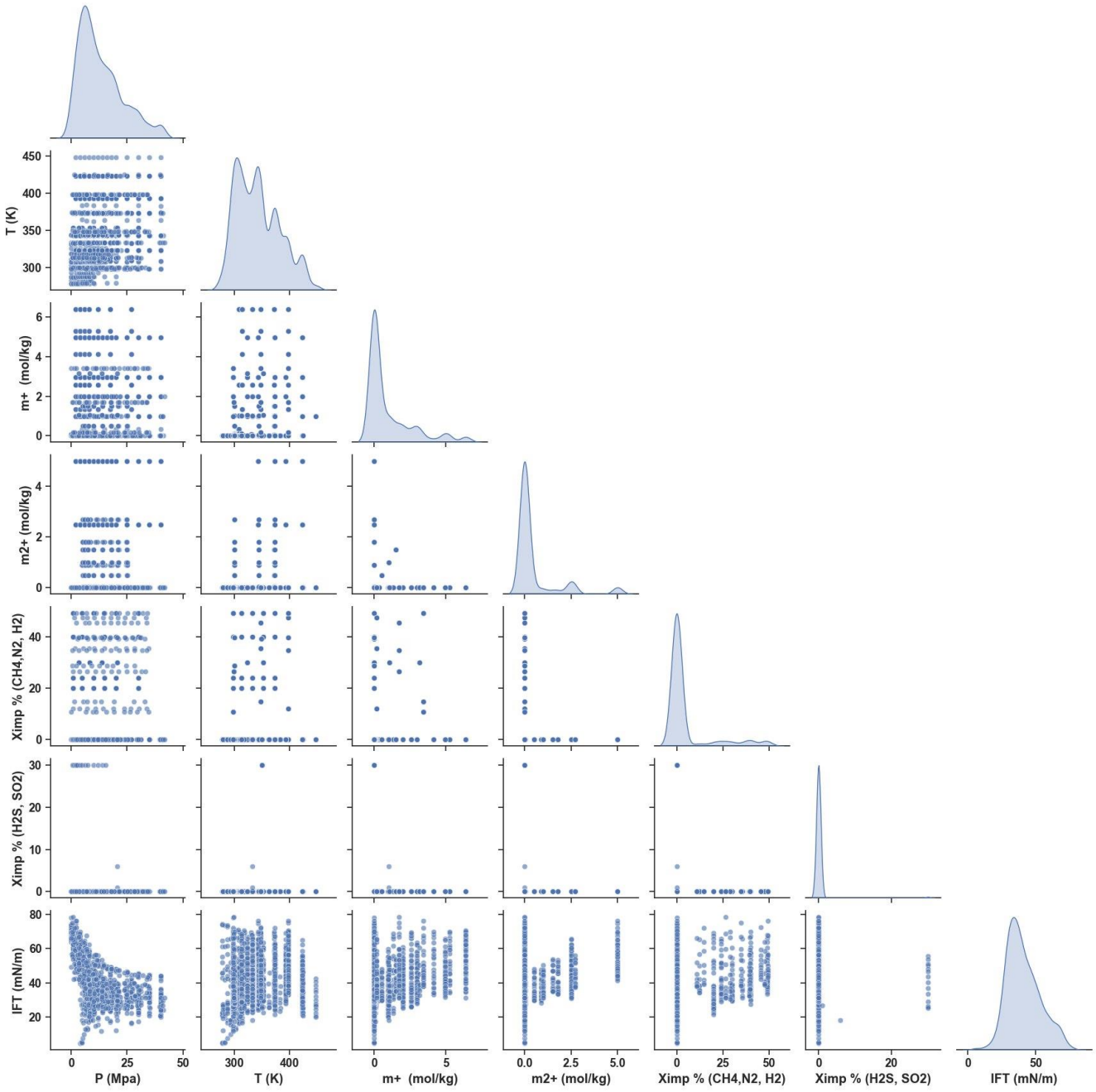

Figure 11. Pair plot showing the dependency of values for CO_2-water system

In the case of the CO_2-oil system, similar trends are noticed but with different properties of the phase behavior (fig.12). The same inverse trend can be observed between pressure and IFT. This shows that the dissolution of CO_2 in oil at high pressure is enhanced in combination with reduced interfacial tension. Temperature does not have a significant impact on the IFT, but a small fluctuation in the IFT is observable at high temperatures. The distribution reveals that pressure is

mostly focused on the lower range, while IFT is most common within the range of 0 - 20 mN/m, which suggests that the interfacial tensions in the CO_2-oil system are in general lower than that of the CO_2-water system. The API gravity values form a double-peaked distribution pattern. The dataset contains two primary types of crude oil which represent light and medium products.

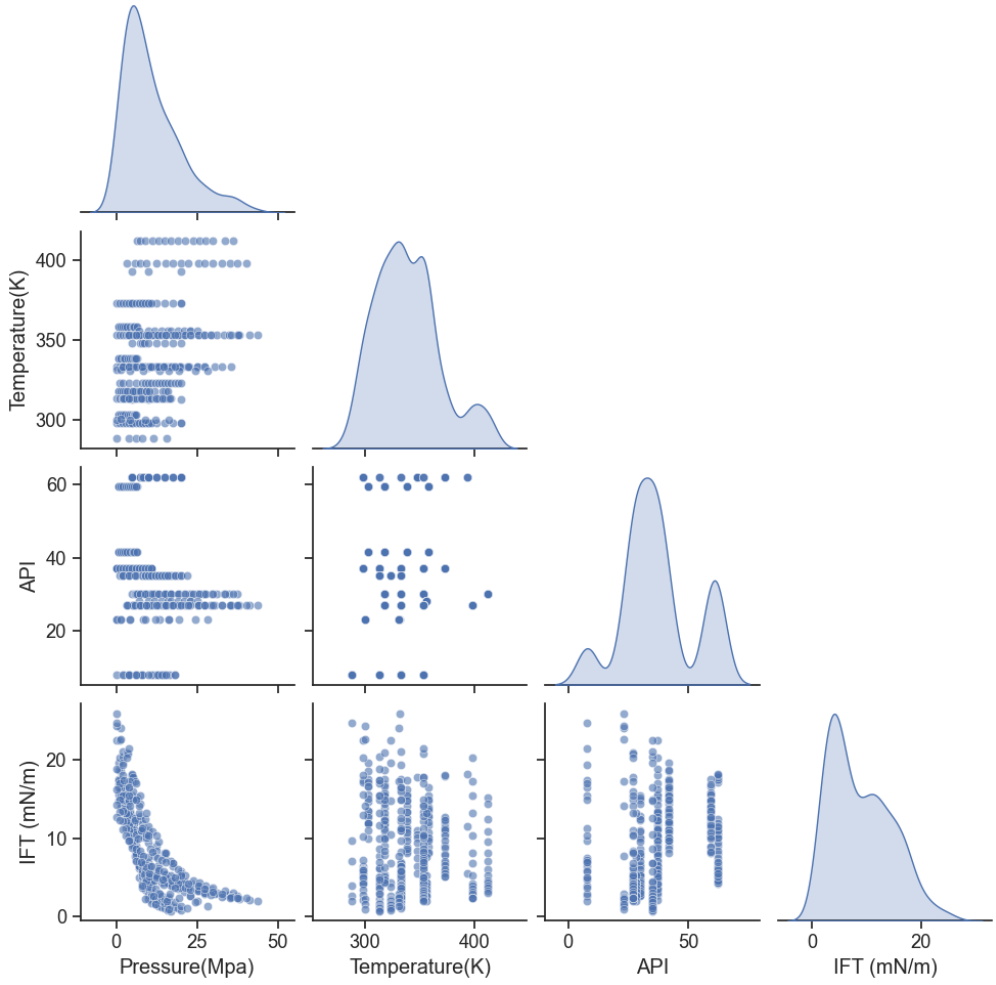

Figure 12. Pair plot showing the dependency of values for CO_2-oil system

Pressure is the primary factor influencing IFT, with a greater influence on the CO2-oil phase, according to the pair plots for CO_2-water and CO_2-oil systems. Temperature had a negligible direct impact on the IFT of both systems, and the effects of the molality of salts, impurities, and API gravity is mild. When using the observed patterns to improve model precision under various

conduct conditions, these considerations provide crucial information that serves as the foundation for improving machine learning models to forecast IFT.

3.2.3. Heat Maps

A heatmap is an essential data interaction technique that allows users to explore the correlations between variables in large, dynamic systems. This shows the degree and direction of relationships and can therefore be used to determine which factors are most salient and how prediction models should be built. The heatmaps below (fig.13, fig.14) illustrate correlation coefficients indicating the relationship of pressure (MPa), temperature (K), molality of mono- and bivalent salts (mol/kg), acidic, non-acidic impurities, and IFT (mN/m) for CO_2-water and pressure (MPa), temperature (K), and API gravity for CO_2-oil system.

The findings presented for CO_2-water system offer several important implications. First, the obtained negative coefficient between pressure and IFT (-0.56) is reasonable and corresponds to the physical law, with higher pressure favoring the dissolving of CO_2 in water and resulting in lower interfacial tension. The temperature correlated less with IFT, which indicates that temperature had a less impact on IFT in the given dataset. IFT has a positive relationship with the molality of salts (0.17 and 0.19), implying that the ionic strength can slightly advance the interfacial tension in cases of high salinity.

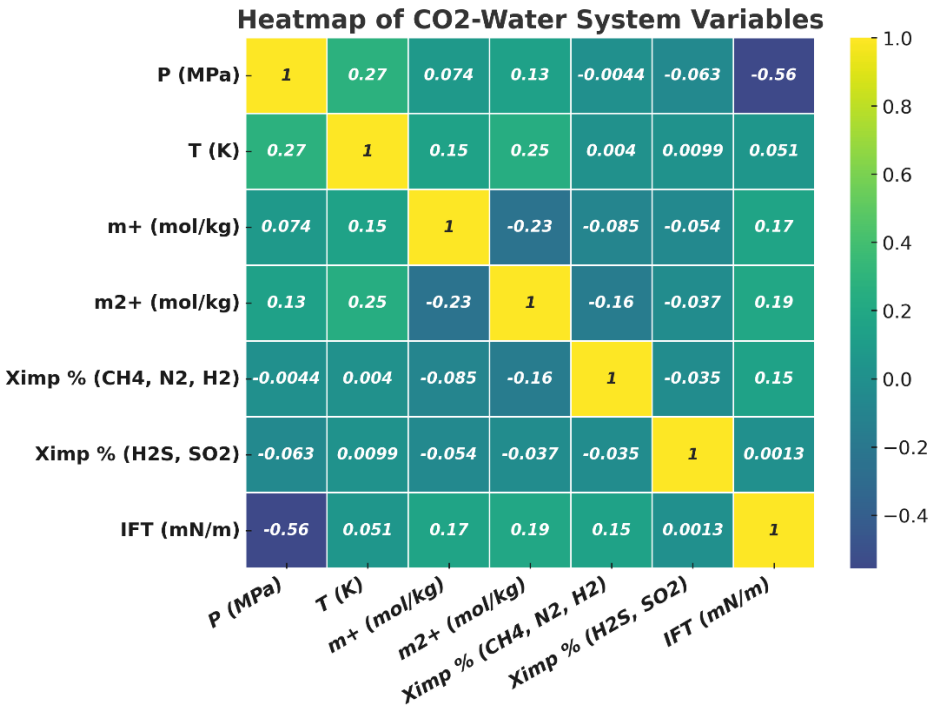

Figure 13. Heat map for CO_2-water system before preprocessing

Analyzing parameters for CO_2- oil system (fig.14) such as pressure and IFT correlation, it was -0.62, which indicates that higher pressure definitely leads to a reduction in interfacial tension, as per actual data, because of higher CO_2 solubility and miscibility. Temperature exhibited a very low correlation (-0.09) with IFT, which demonstrates that changes in temperature do not reasonably modify interfacial tension levels. The correlation results indicate that interfacial behavior has a minimal influence on the crude oil density measured by API gravity through its relationship with mild positive values of 0.17. The correlation between pressure and API holds a negative value of -0.27 indicating that elevated pressure systems are associated with heavier crude oil types. The heatmap indicates that the operational conditions lead to a moderate positive correlation between pressure and temperature, with a value of 0.35. Data indicates no substantial relationship exists between crude oil density and temperature since the correlation between API and temperature is -0.05. Pressure is the main factor in lowering interfacial tension, although temperature and API gravity have only marginal impacts.

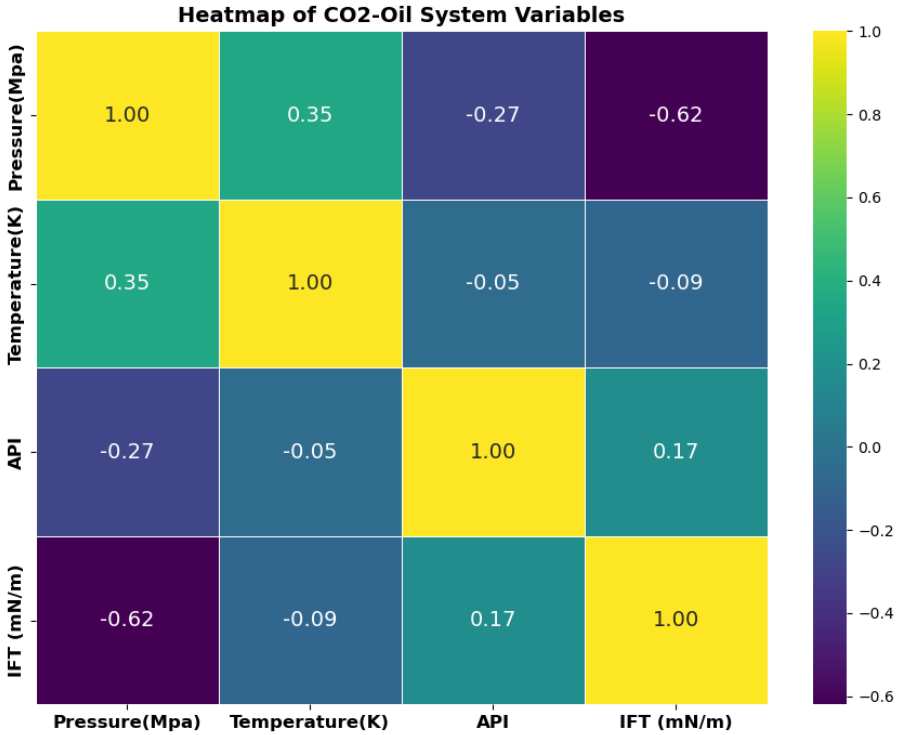

Figure 14. Heat map for CO_2-oil system before preprocessing

After cleaning the data, the CO_2–water system dataset was reduced to 1725 data points, whereas, the CO_2–oil system dataset was reduced to 382 data points. Table 17 and table 18 display the statistical analysis of the cleaned dataset and includes the skewness, kurtosis, mean, standard deviation, minimum, and maximum values for CO_2-water and CO_2-oil systems, respectively. This preprocessing was successful in accomplishing the main goal of outlier removal; as a result, the ranges of averaged values were more uniform and compact for both systems.

Table 17. Statistical summary for CO_2-water system of cleaned data

Feature	Sign	Unit	Count	Minimum	Maximum	Mean	Standard Deviation	Skewness	Kurtosis
Pressure	P	MPa	1725	0.05	41.72	13.21	9.78	0.95	0.214
Temperature	T	K	1725	278	448.15	343.16	39.15	0.55	-0.54
Molality of monovalent salts	m^+	mol/kg	1725	0	6.39	0.98	1.61	1.79	2.404

Molality of bivalent salts	m^{2+}	mol/kg	1725	0	5	0.49	1.18	2.65	6.409
Impurities (CH_4, N_2,H_2)	X_{imp}	%	1725	0	49.35	5.14	12.81	2.37	4.198
Impurities (H_2S, SO_2)	X_{imp}	%	1725	0	30	0.25	2.69	10.93	117.865
IFT	σ	mN/m	1725	4.71	78.48	40.68	12.26	0.54	-0.014

Table 18. Statistical summary for CO_2-oil system of cleaned data

Feature	Sign	Unit	Count	Minimum	Maximum	Mean	Standard Deviation	Skewness	Kurtosis
Pressure	P	MPa	382	0.079	43.852	11.038	8.925	1.239	1.224
Temperature	T	K	382	288	412	338.863	29.35	0.661	0.081
API	API	-	382	8	62	37.108	14.646	0.256	-0.304
IFT	σ	mN/m	382	0.696	25.995	8.877	5.652	0.598	-0.507

A comparison between the data distributions before and after removal of the outliers shows that there is a better correlation between the data as well as a more equal spread of the parameters across the various distributions (fig. 15; fig. 16). They improve the data sets' suitability for later modeling and analysis by reducing noise, thereby preserving the patterns of the data better than before. Such refinements help to create a clearer and more accurate model in modeling endeavors.

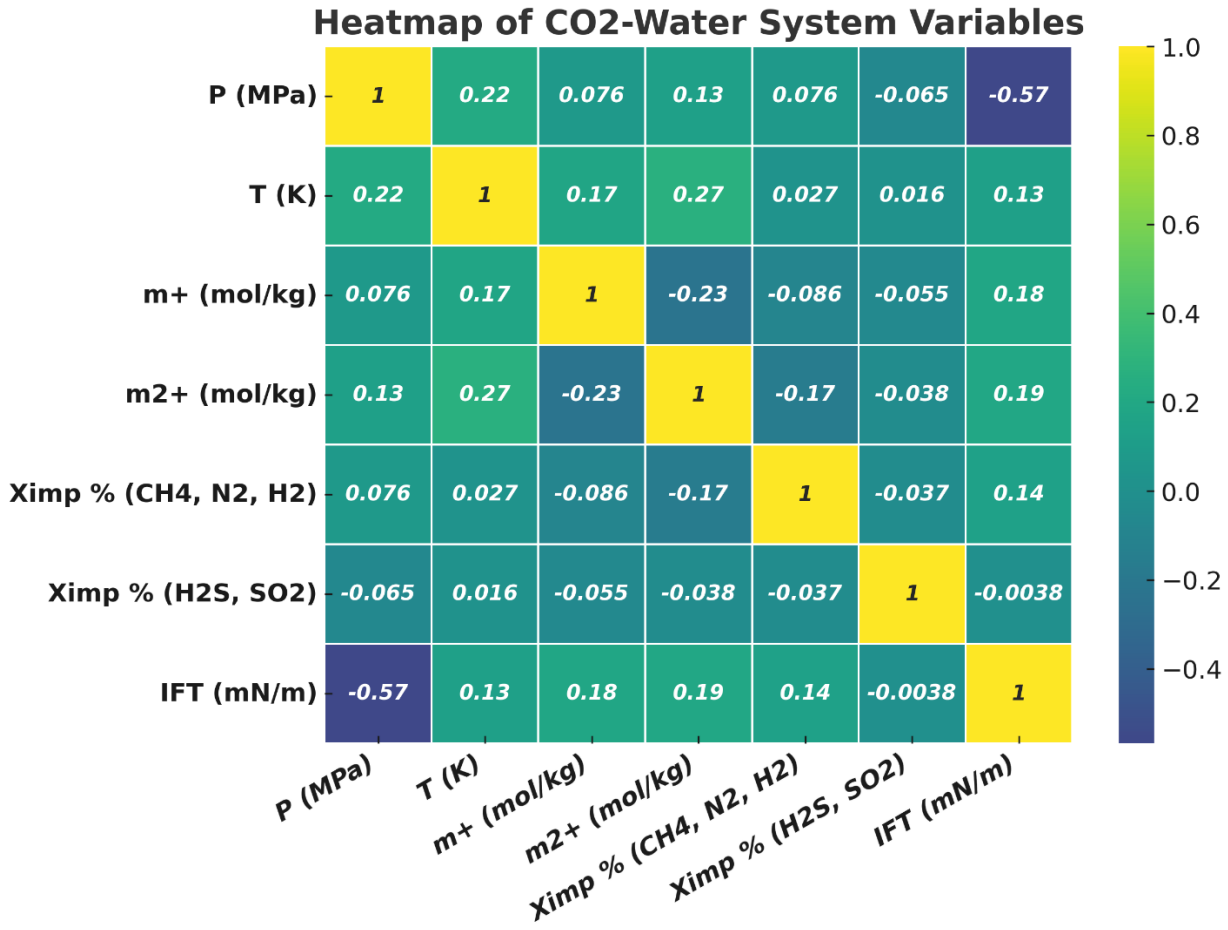

Figure 15. Correlation coefficient heatmap for CO2-water system dataset after data cleaning.

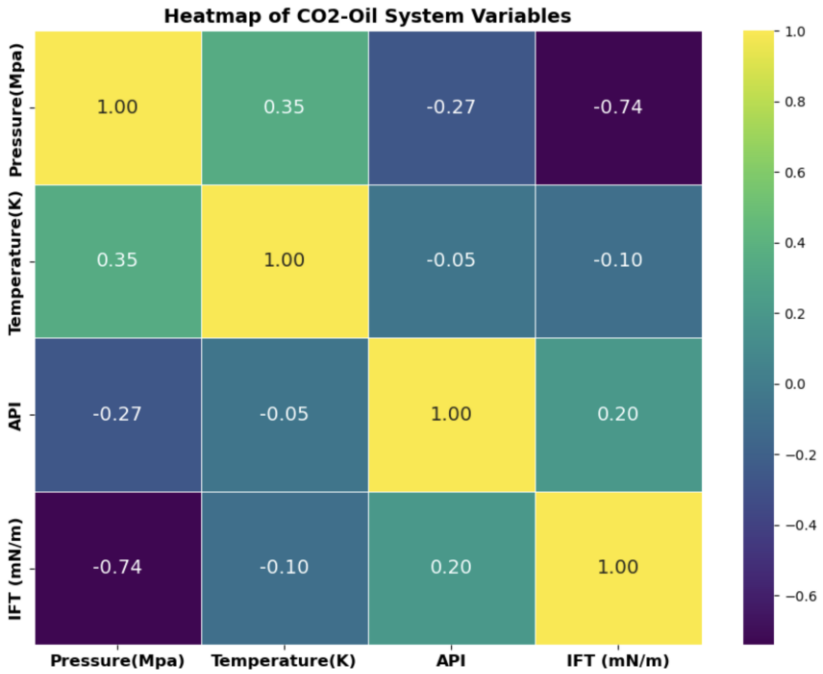

Figure 16. Correlation coefficient heatmap for CO2-oil system dataset after data cleaning.

3.3. Data Processing

3.3.1. Model Selection

In this project, seven machine learning models were used for predicting IFT:

- **Artificial Neural Network (ANN):** ANNs are excellent at complex, nonlinear relationships and renders well the deep learning applications (Wu et al., 2018).
- **Symbolic Regression-Genetic Programming (SR-GP):** SR–GP is an evolutionary approach to mathematical relationship discovery in data without a given model (Galvan et al., 2022).
- **Decision Tree (DT):** DT is a sequential model that logically incorporates a series of basic tests, each of which compares a nominal attribute to a range of potential values or a numeric attribute to a threshold value (Kotsiantis, 2011).
- **Random Forest (RF):** Using the decision tree, which is an example of Ensemble learning that does not easily overfit because it also captures the complexities of the data through

nonlinear separability. It gives variable importance scores to assist in feature selection. (Maleki et al., 2024)

- **Gradient Boosting Regression (GBR):** Its main objective is to combine poor predictors, often known as "learners," to produce a more capable predictor. Each of these weak predictors improves the performance of its predecessors during a phase of sequential training (Nait Amar et al., 2019).
- **Support Vector Machine for Regression (SVR):** SVR can manage challenging regression problems and is excellent at identifying non-linear patterns in data. Finding the hyperplane that best matches the multi-dimensional data is the fundamental concept of SVR (Smola AJ et al., 2004)
- **Extreme Gradient Boosting (XGBoost):** An algorithm for boosting gradients, well-known for high performance and its applicability to instances with non-linear interactions. XGBoost was sued for its effectiveness on tabular data and naturally for handling missing values. (Khan et al., 2024)

3.3.2. Model training and testing

To ensure consistency, the entire dataset was divided into separate categories, namely the training and testing data. In the splitting strategy, special attention was given to the fact that data should not leak and that the models' performance on unseen data should be evaluated. The following steps were implemented:

- **Training Set (80%):** This set included 80% of the entire dataset. This subset was used by the models to identify patterns, associations, and interdependencies between features (inputs) and the output variable (IFT). The training set was used to fit the model and determine the optimal parameters for maximum model performance.
- **Testing Set (20%):** The remaining 20% was used for testing. While training, this subset was employed to evaluate the performance of the model on data not used during training to control aspects like the number of epochs or the learning rate for example. The same subset was used to test the final model after training on the available data.

3.3.3. Hyperparameter tuning

Hyperparameter tuning is an important part of modeling because it improves the predictive accuracy and efficiency of ML tools. Both systems is modeled using various ML techniques, such as Artificial Neural Networks (ANN), Symbolic Regression-Genetic Programming (SR-GP), Decision Trees (DT), Random Forest (RF), Gradient Boosting Regression (GBR), Support Vector Regression (SVR), and XGBoost. The performance of each algorithm was dependent on a set of hyperparameters that were tuned to achive the best performance.

For the CO_2-water system the summary table of the optimized hyperparameters is presented in Table 19:

ANN: 1 - 5 hidden layers and 8 - 256 neurons were optimized, with an optimum value of 4 hidden layers and 256 neurons, which provided a well-structured network. A better convergence and gradient updates are achieved by selecting of the “relu” activation function and “rmsprop” optimizer.

SR-GP: The combination of 2000 population size and 30 generations received optimized values in SR-GP to reach the peak of evolutionary expression identification. The search for correlations involves addition, subtraction, multiplication, division, square root, log, absolute value, negation and inversion, along with other functions.

DT: A compromise between model complexities and overfitting prevention was achieved by selecting 15 as the maximum depth and 20 as the minimum sample split.

RF: The evaluation of computational efficiency vs variance reduction was achieved through adjustments of the maximum features set to “sqrt” paired with 800 estimators and a maximum depth of 15.

GBR: the model was maximized with 500 estimators, a maximum depth of 7, and a minimum sample split of 2 to capture the underlying data patterns with minimal overfitting.

SVR: “rbf” kernel was selected to provide nonlinear transformation ability compared to other existing kernel functions, and C (1000), epsilon (10^{-7}), and gamma (0.01) were tuned to enhance the performance of the model.

XGBoost: The optimized parameters were the number of estimators of 1000, maximum depth of 6, and learning rate of 0.01 to achieve a strong boosting effect with less overfitting.

Table 19. Statistical summary of hyperparameters for all ML models of CO_2-water system.

Model	Hyperparameter	Range	Optimization
ANN	Hidden layer	1-5	4
	Neurons	8-256	256
	Activation function	relu, sigmoid, tanh	relu
	Optimizer	adam, nadam, rmsprop	rmsprop
	Generations	10-50	30
	Population size	1000-2000	2000
	Tournament size	10-60	15
SR - GP	Function set	add, sub, mul, div, sqrt, log, abs, neg, inv	add, sub, mul, div, sqrt, log, abs, neg, inv
	P crossover	0.9	0.9
	P subtree mutation	0.05-0.1	0.05
DT	Max depth	3-15	15
	Min samples split	5-40	20
	Min samples leaf	1	1
	Max features	auto, sqrt, log2, None	None
RF	N estimators	200-800	800
	Max features	sqrt, log2, None	sqrt
	Max depth	5-15	15
	Min samples split	2-8	2
	Min samples leaf	2-4	2
	bootstrap	True, False	False
	N estimators	100-500	500

	Max features	sqrt, log2	sqrt
GBR	Max depth	3-7	7
	Min samples split	2-8	2
	Min samples leaf	1	1
	Kernel	sigmoid, rbf	Rbf
SVR	C	1-1000	1000
	epsilon	10^{-7}-10^{-9}	10^{-7}
	gamma	0.001-1	0.01
	N estimators	200-1000	1000
	Max depth	3-6	6
	Learning rate	0.01	0.01
	Min child weight	2-10	4
XGBoost	Gamma	0	0
	Subsample	1	1
	Colsample bytree	1	1
	Alpha	0	0
	Lambda	1	1

For the CO_2-oil system, a summary of the optimized hyperparameters is presented in Table 20:

ANN: The optimal architecture consisted of four hidden layers containing 256 neurons because it effectively balanced the computational efficiency and model complexity. A sigmoid function was selected as the activation function for gradient smoothness control, and an "adam" optimizer was used for quick convergence via adaptive learning rates.

SR – GP: The number of generations (50) and population size (1500) ensured sufficient evolutionary iterations for symbolic regression. In addition, the search space of symbolic models was varied by the function set, which included addition, subtraction, multiplication, division, square root, logarithm, absolute value, negation, and inversion.

DT: Maximum depth (10), minimum samples split (2) and the minimum samples per leaf (2) balanced model interpretability with generalization while avoiding overfitting.

RF: The bootstrapping option has been disabled, resulting in more deterministic learning outcomes; hyperparameters have been fine-tuned to 500 estimators, the maximum depth to 8, and "sqrt" is used as the max function, ensuring dependable group learning while maintaining computational efficiency.

GBR: the model was maximized with 500 estimators, a maximum depth of 4, and a minimum samples split of 4 to capture the underlying data patterns with minimal overfitting.

SVR: "rbf" kernel was selected since the "rbf" kernel is capable of handling the relationship effectively and nonlinearly. The regularization parameters C = 100, epsilon 0.1, and gamma 0.1 were tuned to enhance the model performance.

XGBoost: 500 estimators, maximum depth of 4, and a learning of 0.05 were the optimized parameters for XGBoost, which offers good gradient boosting and regularization for optimal performance.

Table 20. Statistical summary of hyperparameters for all ML models of CO_2-oil system.

Model	Hyperparameter	Range	Optimization
ANN	Hidden layer	1-5	4
	Neurons	8-256	256
	Activation function	relu, sigmoid, tanh	sigmoid
	Optimizer	adam, nadam, rmsprop	adam
SR - GP	Generations	10-50	50
	Population size	1000-3000	1500
	Tournament size	15-60	15
	Function set	add, sub, mul, div, sqrt, log, abs, neg, inv	add, sub, mul, div, sqrt, log, abs, neg, inv
	P crossover	0.9	0.9
	P subtree mutation	0.05-0.1	0.05

DT	Max depth	4-10	10
	Min samples split	2-6	2
	Min samples leaf	2-4	2
	Max features	auto, sqrt, none	None
RF	N estimators	300-800	500
	Max features	sqrt, log2	sqrt
	Max depth	4-8	8
	Min samples split	4-6	4
	Min samples leaf	2-4	2
	bootstrap	True	True
GBR	N estimators	300-500	500
	Max features	sqrt, log2	sqrt
	Max depth	3-4	4
	Min samples split	2-6	4
	Min samples leaf	1-5	5
SVR	Kernel	rbf	Rbf
	C	1-100	100
	epsilon	0.01-0.1	0.1
	gamma	Scale, 0.01, 0.1	0.1
XGBoost	N estimators	200-500	500
	Max depth	2-10	4
	Learning rate	0.03-0.05	0.05
	Min child weight	5-8	8
	Gamma	0, 1	0
	Subsample	0.6, 0.8	0.6
	Colsample bytree	0.6, 0.8	0.8
	Alpha	0, 0.5	0

	Lambda	1	1

3.3.4. Model evaluation

The evaluation was perfomed out using various metrics and visualization techniques. They are given by equations 7 to 12:

- **Mean Squared Error (MSE):** Measures the average that is squared of the difference between the actual and predicted values. An interval scale has been used to measure performance; the lower the value, the better the performance (Iowast et al., 2020).

$$MSE = \frac{1}{n}\sum_{i=1}^{n}(x_{measured} - x_{pred})^2 \qquad (7)$$

- **Root Mean Squared Error (RMSE):** The square root of MSE, which is more comprehensible because it expresses an average error in the original measurement units of the target variable (Khan et al, 2021).

$$RMSE = \sqrt{\frac{1}{n}\sum_{i=1}^{n}(x_{measured} - x_{pred})^2} \qquad (8)$$

- **Mean Absolute Percentage Error (MAPE):** An indicator of a statistical forecasting method's prediction accuracy is the mean absolute percentage error (MAPE). The average error is compared to the actual value (Kim et al., 2016).

$$MAPE = \frac{1}{n}\sum_{t=1}^{n}\left|\frac{x_{measured} - x_{pred}}{x_{measured}}\right| \qquad (9)$$

- **Akaike Information Criterion (AIC):** Model selection is based on the use of the AIC, which balances the goodness of fit of a model and its complexity. It penalizes models with a larger number of parameters to avoid overfitting and selects the model that best fits the data with the smallest number of parameters (Akaike, 1974).

$$AIC = -2\ln(likelihood) + 2P_n \qquad (10)$$

Here, k is the number of estimated parameters in the model and L is maximized value of the likelihood function for the model

- **Bayesian Information Criterion (BIC):** Like AIC, BIC is also used for model selection, with the penalty being larger for increasing the number of parameters, mainly the larger the sample size. This criterion is based on Bayesian probability and selects the true model from the set of candidate models assuming that the true model exists.

$$BIC = -2\ln(likelihood) + [\ln(n)]P_n \qquad (11)$$

- **R^2 Score (Coefficient of Determination):** Shows how effectively complex variation of the target variable is captured and uncovered by the model. The higher (closer to 1) the result, the better the performance; however, negative values indicate present poor generalizability (Zhang et al., 2022).

$$R^2 = 1 - \sum_{i=1}^{n}(x_{measured} - x_{pred})^2 \,/\, \sum_{i=1}^{n}(x_{measured} - x_{avr\ measured})^2 \qquad (12)$$

where $x_{measured}$ is actual values, x_{pred} is predicted values, n is number of datapoints, P_n is number of parameters in the model

4. RESULTS AND DISCUSSION

4.1. CO_2-water system

Various error metrics were used to evaluate the performance of Artificial Neural Networks (ANN) in predicting interfacial tension (IFT) measurements of CO_2-water system with varying numbers of hidden layers (from one to five). The evaluation included Root Mean Square Error (RMSE), Mean Squared Error (MSE), coefficient of determination (R^2), Mean Absolute Percentage Error (MAPE), Akaike Information Criterion (AIC) and Bayesian Information Criterion (BIC) to assess the training and testing datasets (Table 21).

Table 21. The model evaluation results for ANN with different numbers of hidden layers

	Error Metrics	One Layer	Two Layers	Three Layers	Four Layers	Five Layers
Training Data	RMSE, mN/m	4.484	4.172	4.994	3.525	4.034
	MSE, mN/m	20.106	17.4	24.94	12.42	16.27
	R^2	0.866	0.884	0.834	0.917	0.892
	MAPE, %	10.397	9.938	10.616	7.722	8.918
	AIC	4155.467	3956.479	4452.89	3490.944	3863.725
	BIC	4192.076	3993.088	4489.5	3527.553	3900.334
Testing Data	RMSE, mN/m	4.114	3.824	4.98	3.534	4.337
	MSE, mN/m	16.924	14.622	24.8	12.489	18.8
	R^2	0.886	0.902	0.833	0.915	0.873
	MAPE, %	8.47	7.894	9.668	6.760	8.37
	AIC	989.934	939.587	1121.77	884.995	1026.36
	BIC	1016.839	966.492	1148.68	911.90	1053.26

The four-layer ANN model demonstrated optimal performance for the training data with an overall RMSE of 3.525 mN/m, MSE of 12.42 mN/m, MAPE of 7.722% and R^2 value of 0.917. These performance metrics demonstrate both high accuracy and a strong relationship between the predicted IFT values and the experimental results. The results show that the four-layer model has optimal AIC (3490.944) and BIC (3527.553) values, which validate its statistical robustness alongside model parsimony. The two-layer model also showed good performance but did not outperform the four-layer structure as it achieves an R^2 of 0.884 but a slightly higher MAPE of 9.938%. The testing data results indicate that the four-layer model offers the best predictive capabilities by producing minimal RMSE (3.534 mN/m) along with MSE (12.489 mN/m) and achieved the lowest MAPE (6.760%) and highest R^2 (0.915). The model demonstrated robust generalization capabilities, which proves that it makes predictions from factual understanding rather than memorizing training data. The two-layer model demonstrates marginally superior generalization over the five-layer model (R^2 = 0.902 versus 0.873), but produces higher error values (RMSE = 3.824 mN/m, MAPE = 7.894%) than the four-layer approach. Among all tested architectures, the three-layer ANN model exhibited the least effective performance during training and testing since its R^2 values reach 0.834 for training and 0.833 for testing while demonstrating

the highest RMSE and MSE values. The selected architecture appears insufficiently developed to detect nonlinear connections in the dataset. The training performance of the five-layer model achieves $R^2 = 0.892$, but the testing results suffered from its excessive complexity.

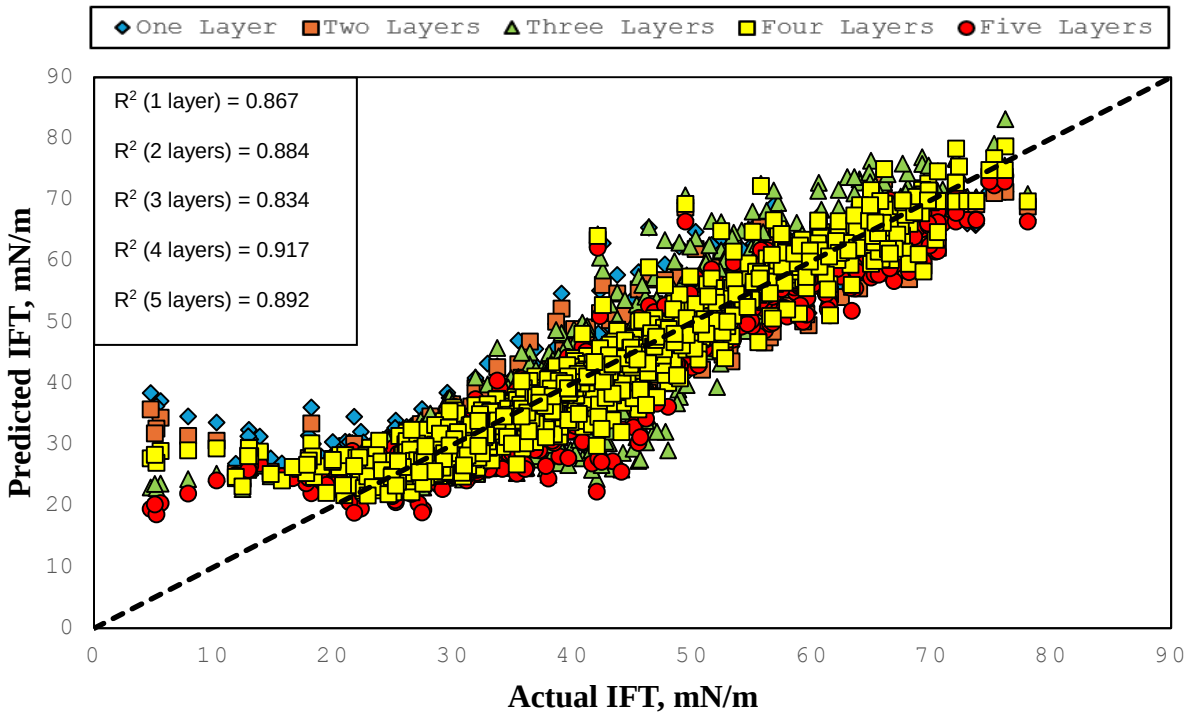

Figure 17. Actual vs Predicted IFT for the training dataset by ANN model

The results in Table 21 are further supported through Figures 17 and 18, which visualize the ANN model predictions using scatter plots for training and testing datasets corresponding to different hidden layer numbers. The model with four hidden layers demonstrated the best alignment between the actual and predicted IFT values based on training data analysis (Figure 17). This observation supports its optimal R^2 value of 0.917 since it indicates superior learning capabilities. Training with the three-layer model resulted in the widest prediction scatter and the lowest R^2 of 0.834 value which indicates weaker prediction accuracy and correlation rates.

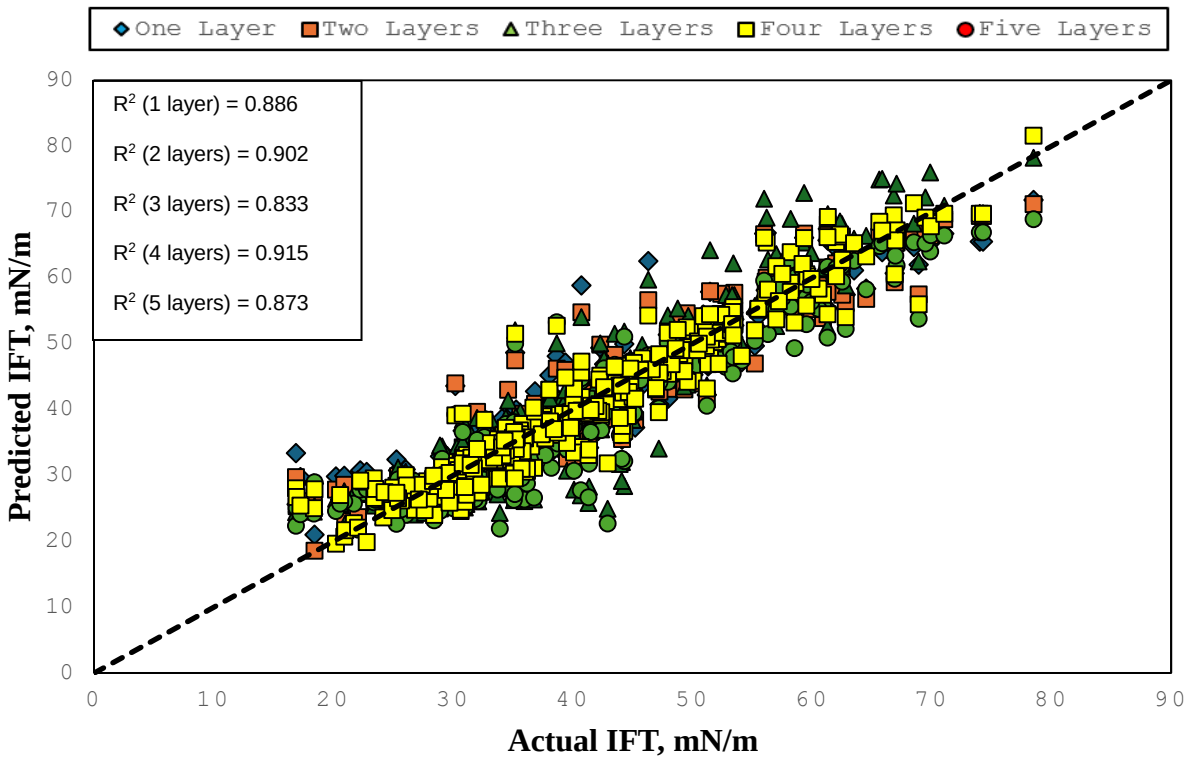

Figure 18. Actual vs Predicted IFT for the testing dataset by ANN model

Figure 18 shows the ANN configuration performance results on the testing dataset. The four-layer model achieves the best generalization ability when evaluating testing data based on an R^2 value of 0.915 while maintaining tight matching of predicted and actual data points with the diagonal line. The two-layer model provides reliable predictions with an R^2 value of 0.902, although it demonstrates some moderate dispersion between actual and predicted values. Analysis of the three-layer model revealed continued underperformance, resulting in an R^2 value of 0.833 because its predicted values extended far from the ideal trend. The five-layer model yielded a high R^2 value during training with 0.892 but achieved lower $R^2 = 0.873$ performance on the testing subset.

The observed visual data points support the statistical results from Table 21 and validate the four-layer ANN structure's optimal blend of learning ability and generalization capability for CO_2–water interfacial tension prediction.

Table 22 shows the error metrics for the machine learning models which include Artificial Neural Networks (ANN), Symbolic Regression Genetic Programming (SR-GP), Decision Tree (DT), Random Forest (RF), Gradient Boosting Regression (GBR), Support Vector Regression (SVR),

and XGBoost. The table measures different error metrics of these models through testing and training data evaluation procedures. The Artificial Neural Network model generates training metrics of 3.525 mN/m for RMSE and 12.425 mN/m for MSE together with an R^2 value of 0.917, indicating good performance. GBR surpasses ANN because it delivers 1.367 mN/m RMSE and R^2 at 0.988. RF and XGBoost demonstrate robust performance similarly to GBR, as they possess R^2 scores amounting to 0.982 and 0.98, respectively. The performance of SR-GP was inferior to other models because it displays lower R^2 metrics. The Decision Tree and SVR models demonstrated good predictive strength through its R^2 value reaching 0.938 and 0.945, respectively, according to the performance data.

The testing dataset revealed reliable performance of the ANN based on its 3.534 mN/m RMSE, 12.489 mN/m MSE, and 0.915 R^2 value. However, GBR and XGBoost models achieved the best R^2 value ratings at 0.96 and 0.954, respectively. The generalization capabilities of the RF and SVR models remained strong because it achieves an R^2 score of 0.941 and 0.942. The SR-GP model provides less application benefit because its higher RMSE values and MAPE results indicate poor accuracy rates. GBR combined with XGBoost proved superior to deep machine learning tools as ANN for predicting CO_2-water system IFT since they delivered the best performance in all training and testing data applications. RF and SVR present themselves as solid alternatives that demonstrate high accuracy at the same time exhibit strong capabilities in generalization.

Table 22. The model evaluation results for all ML models.

		ANN	SR-GP	DT	RF	GBR	SVR	XGBoost
Training Data	RMSE, mN/m	3.525	6.127	3.058	1.671	1.367	2.867	1.717
	MSE, mN/m	12.425	37.54	9.35	2.792	1.869	8.219	2.948
	R^2	0.917	0.75	0.938	0.982	0.988	0.945	0.98
	MAPE	7.722	13.674	6.328	3.574	2.274	4.948	3.578
	AIC	3490.944	5017.151	3099.305	1430.235	876.128	2921.706	1505.724
	BIC	3527.553	5053.76	3135.914	1466.844	912.73	2958.315	1542.33
Testing Data	RMSE, mN/m	3.534	5.581	4.120	2.959	2.416	2.926	2.61

MSE, mN/m	12.489	31.147	16.974	8.755	5.837	8.561	6.81
R^2	0.915	0.79	0.885	0.941	0.96	0.942	0.954
MAPE	6.760	10.862	7.497	5.27	3.93	4.876	4.494
AIC	884.995	1200.421	990.954	762.751	622.866	754.718	676.579
BIC	911.90	1227.326	1017.859	789.655	649.771	781.623	703.484

The predicted and actual IFT values comparison for the training and testing datasets appears in figures 19 and 20 using machine learning model scatter plots. GBR with XGBoost and RF demonstrated high prediction accuracy because their results aligned optimally along the diagonal line in figure 19 which shows the training dataset. The predicted outcomes from the ANN excelled, although they demonstrated greater variability than the GBR and RF results. The SR-GP displayed inconsistent prediction results because their data points were spread largely across the analysis area. The analysis of figure 20 shows that GBR, XGBoost, and RF maintain their predictive strength with the testing data. The ANN and SVR systems deliver reliable performance but achieve slightly inferior results than GBR-based prediction. The predictions of SR-GP significantly deviated from the ideal diagonal line demonstrating their low accuracy.

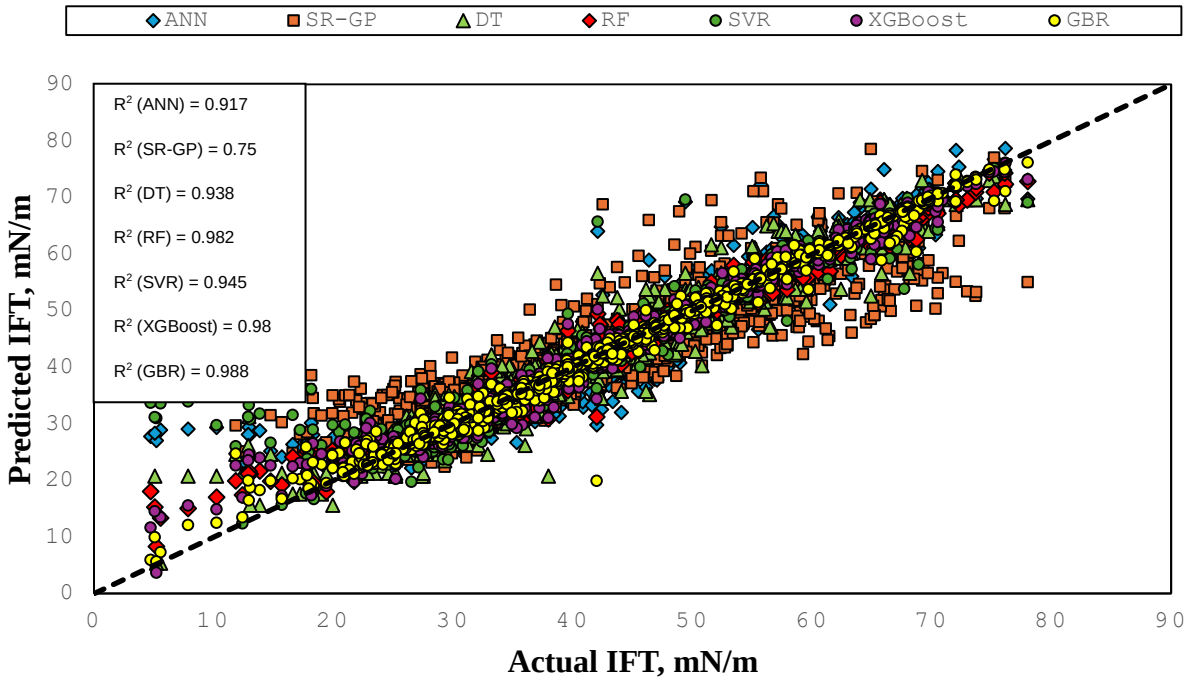

Figure 19. Actual vs Predicted IFT for the training dataset by all ML models

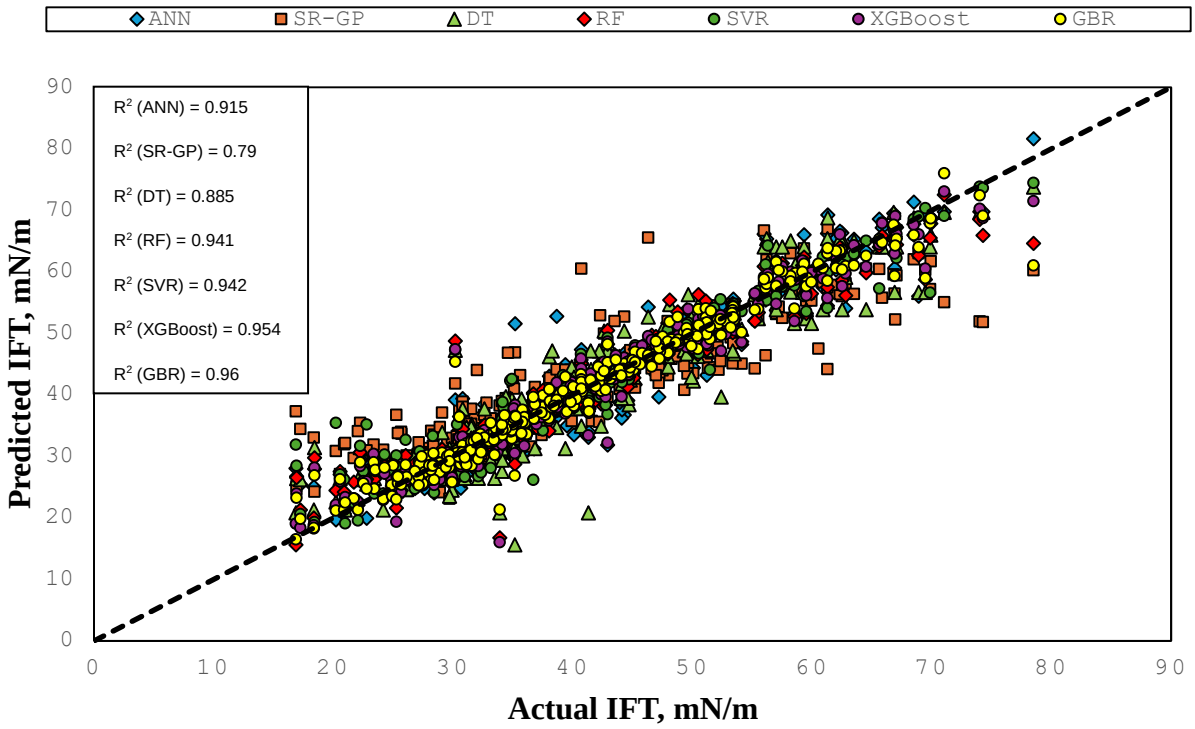

Figure 20. Actual vs Predicted IFT for the testing dataset by all ML models

The results show that GBR and XGBoost yield the most accurate predictions of IFT in CO_2-water systems based on their low RMSE and high R^2 values in addition to their tight fits in Figures 19 and 20. The RF model demonstrates stability in predicting results, but GBR and XGBoost produce more accurate results than RF. ANN and SVR also demonstrate good performance, which make them acceptable alternatives to RF. DT is far less effective than GBR, RF, and XGBoost, but nevertheless remains a good and reliable tool prediction of IFT in CO_2-water system. SR-GP demonstrates inferior results compared to other models rendering it less effective for this application.

An additional validation step was performed on the error metrics results via Kernel Density Estimation (KDE) plot analysis (fig. 21). The plots provide visual evidence about predicted data versus actual data distribution, which enhances the understanding of model accuracy and reliability. The data distribution of GBR, RF, XGBoost, and SVR matches closely with the actual data in figure 21a (Testing Dataset) due to their reliable predictive abilities. The ANN shows matching behavior with respect to actual density concentrations, although it exhibits slight

deviations from the original patterns. The distribution pattern of DT matches the main trend, yet its minor tail deviations might affect precision during certain predictions. SR-GP shows large deviations from actual density distribution patterns which implies that it fails to detect fundamental data patterns relative to the other models. The actual distribution in Figure 21b (Training Dataset) shows strong similarity with most models including GBR, RF, XGBoost, SVR, ANN, and DT. Although DT reproduces the data distribution patterns effectively, it demonstrates small discrepancies in the density areas when compared with other leading models. The SR-GP model shows the lowest level of alignment with the actual data distribution which supports its previous performance evaluations.

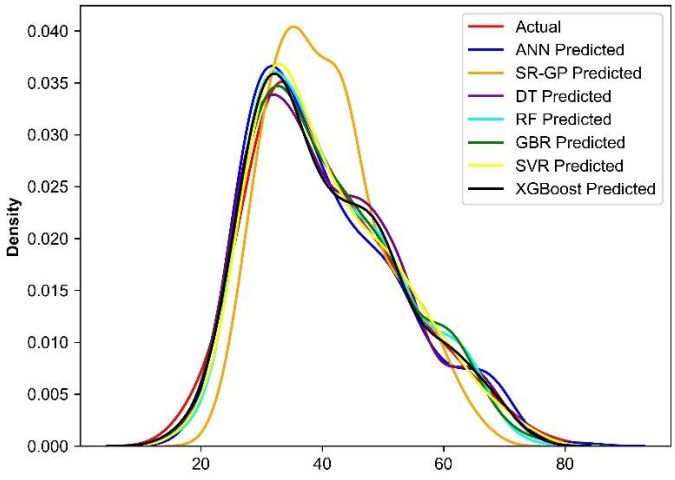

a)

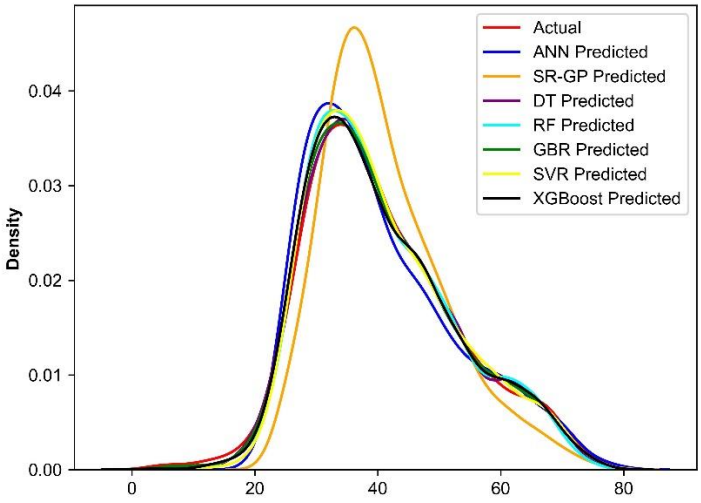

b)

Figure 21. Analysis of KDE plots comparing actual data and all ML models using a) testing dataset and b) training dataset

The KDE analysis verified the assessment from table 22 that GBR, RF, and XGBoost deliver the best predictions for IFT values in CO_2-water systems. The ANN, DT, and SVR models demonstrate performance success by identifying the main distribution patterns in CO_2-water system predictions. SR-GP generates poor outcomes when measuring actual density since it stands as the least dependable model. The quality of the predictive models improves when their alignment appears better in KDE plots and this relationship strengthens their predictive capabilities.

Below, the effect of key influencing parameters on interfacial tension (IFT) trend is analyzed. Different variations of IFT behaviour in CO_2–water system depending on the pressure, temperature, salinity, salt type, and presence of impurities are presented. They strongly influence the interfacial properties and affect the behavior of the entire system. The solid markers in the figures correspond to the actual experimental values, while the dashed lines are the predicted values using Gradient Boosting Regression (GBR), which is the best performing model for CO_2-water system.

The visual comparison between actual IFT values and predicted values by Gradient Boosting Regression (GBR) demonstrating the effect of pressure and temperature on IFT at constant molality of 0 mol/kg with no impurities is represented in figure 22. The information presented in this figure demonstrates the underlying thermodynamic characteristics of IFT when different test conditions are implemented. In all tested temperature ranges, the IFT showed continual decrease as the pressure increased. The high - pressure environment increases CO_2 water solubility thus lowering the interfacial forces. At lower pressure ranges between 0 and 10 MPa, the IFT exhibits its highest sensitivity to changes. The system achieved stabilized interfacial conditions as the pressure increased above 10 MPa since it reached an equilibrium state under increased pressure conditions. The research demonstrates that the increasing temperature from 309 K to 398 K causes the IFT values to rise steadily throughout the experiments. The gap between temperatures at lower and higher pressures showed greater variations in interfacial tension but diminished when the pressure rose because the effect of temperature became stronger at lower pressures. The predicted values based on the GBR model match the experimental data points very well, which demonstrates the outstanding precision of the model for representing IFT changes between different thermodynamic states.

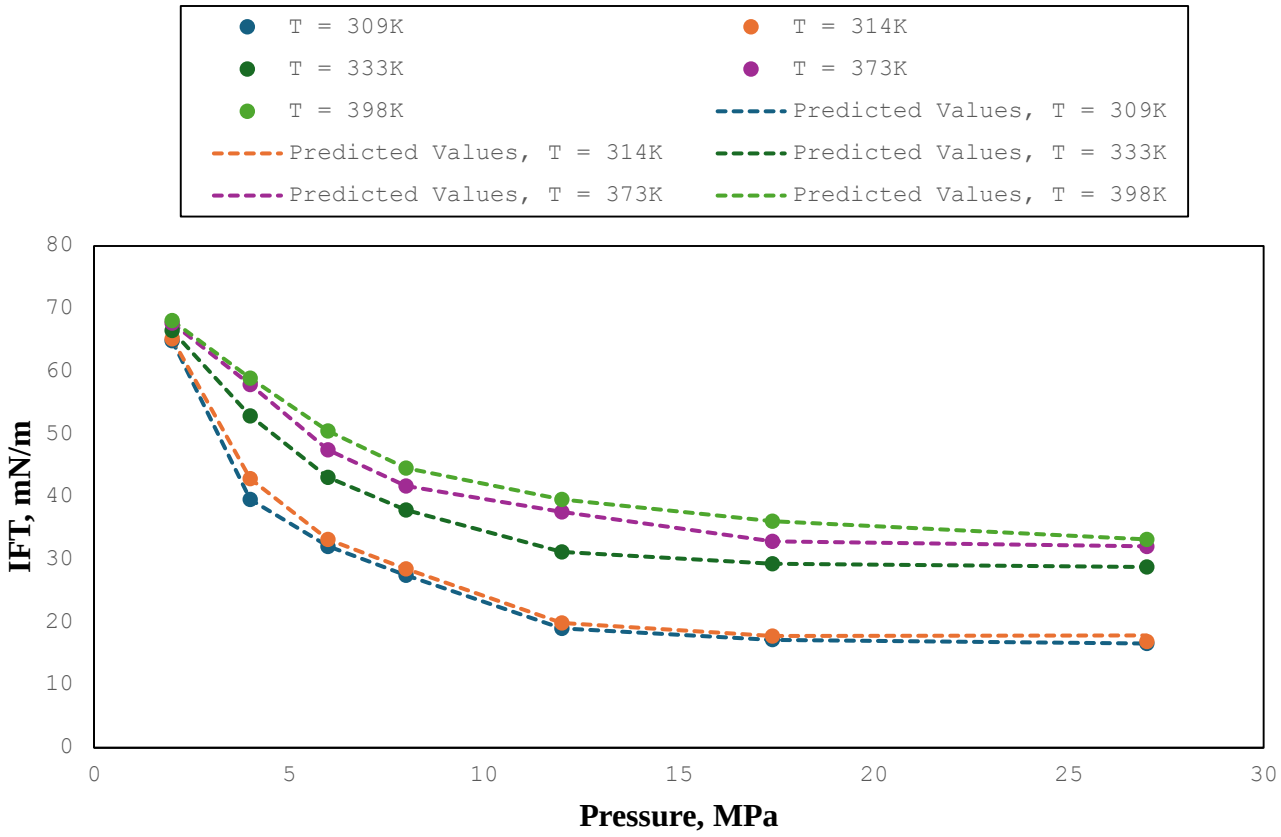

Figure 22. Analysis of actual and predicted values by GBR, demonstrating the effect of pressure and temperature on IFT at a constant molality of 0 mol/kg with no impurities.

The effect of salinity on interfacial tension (IFT) in a CO_2 water system at a constant temperature of 314 K without impurities is shown in figure 23 with actual and predicted values obtained using Gradient Boosting Regression (GBR). The experimental data shows that interfacial tension increases when salt concentration rises under defined pressure conditions. The interfacial tension was elevated by the presence of NaCl across all pressure points. The highest interfacial tension was observed at high sodium chloride concentrations (6.39 mol/kg NaCl) and reached its lowest level with pure water at zero sodium chloride concentration (0 mol/kg NaCl). The increase in IFT results from the salting-out effect, which occurs when NaCl molecules decrease CO_2 solubility in water solutions. A weaker bond forms between CO_2 and water molecules, resulting in increased interfacial tension. NaCl ions strengthen the cohesive forces of water, enhancing its resistance to the disruption of surfaces by CO_2 molecules.

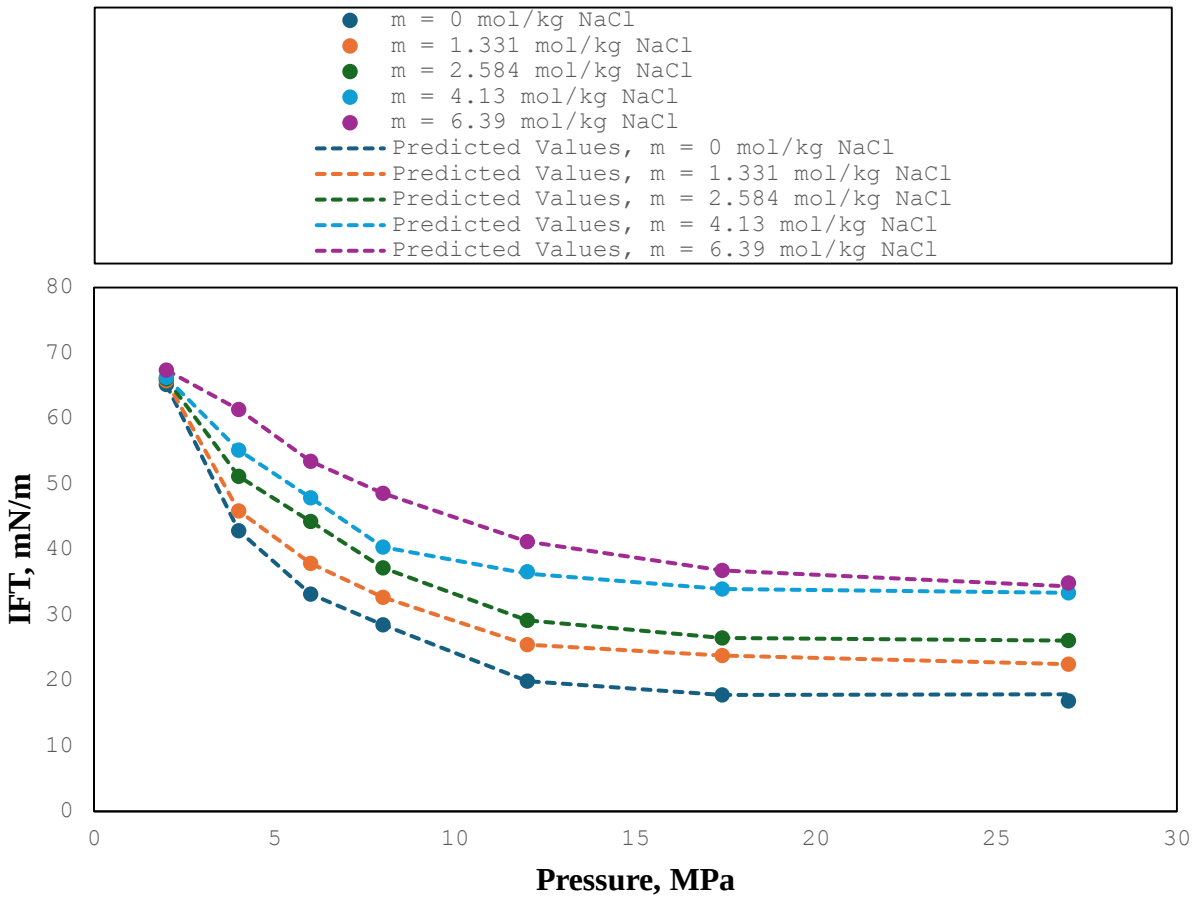

Figure 23. Analysis of actual and predicted values by GBR, demonstrating the effect of different salinities on IFT at a constant temperature (314K) with no impurities.

Figure 24 shows how non-acidic impurities affect the interfacial tension between CO_2 and water at 298 K and a zero - molality concentration. The IFT measurements showed higher values when the system contained increased amounts of CH_4 impurities across all tested pressures. A system containing pure CO_2 had the lowest interfacial tension measures whereas the system with 40% of CH_4 reaches the maximum interfacial tension at every pressure measurement. The CH_4 molecules produce interfacial stabilization which reduces CO_2 water solubility effects and enhances the rise in interfacial tension. The competitive adsorption mechanism explains how CH_4 impurities enhance IFT values. The interface stabilizing impact of CH_4 molecules on water is weaker than CO_2 molecules due to their lower water solubility properties. Adding CH_4 to the system decreases the CO_2 concentration available at the interfaces leading to stronger intermolecular forces between water molecules and resulting in higher interfacial tension.

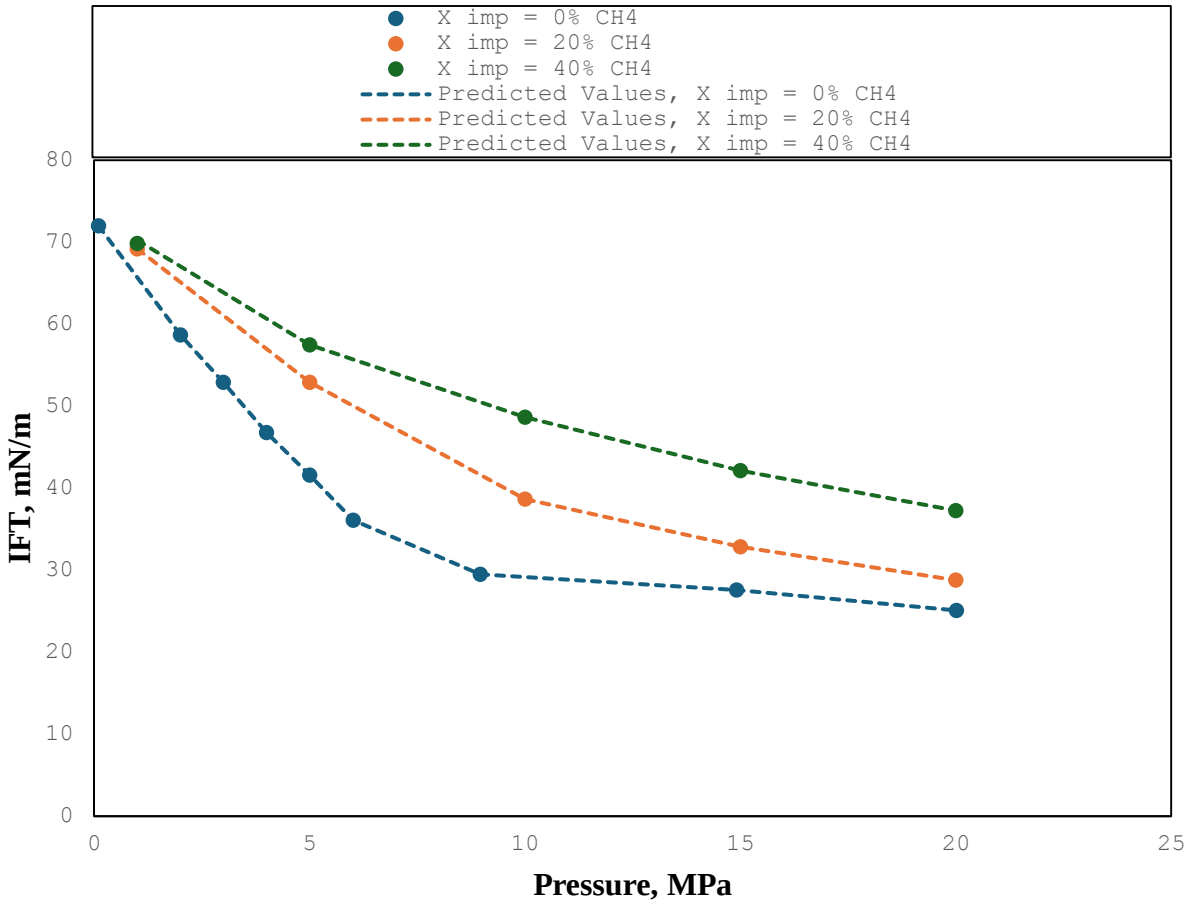

Figure 24. Analysis of actual and predicted values by GBR, demonstrating the effect of impurities on IFT at a constant temperature (298K) and molality (0 mol/kg).

Figure 25 shows the effects of salt types NaCl and $CaCl_2$ on CO_2-water system interfacial tension (IFT) measurements at a constant temperature of 343 K and zero impurity conditions. In solutions containing $CaCl_2$ the measured interfacial tension values remained higher than those measured in NaCl at all applied pressures. The IFT values from $CaCl_2$ solution consistently exceed those from the NaCl solution readings indicating bivalent Ca^{2+} salts produce stronger IFT elevation than monovalent Na^+ salts. The interfacial tension (IFT) remained higher in $CaCl_2$ solutions due to bivalent calcium ions (Ca^{2+}) forming more robust electrostatic bonds than monovalent sodium ions (Na^+). The stronger electrostatic interactions between Ca^{2+} ions in the aqueous phase strengthen the water's cohesive forces, leading to an increase in interfacial tension. A solution of $CaCl_2$ at equivalent molality shows enhanced ionic strength, resulting in a higher salting-out effect that decreases CO_2 solubility and raises IFT values.

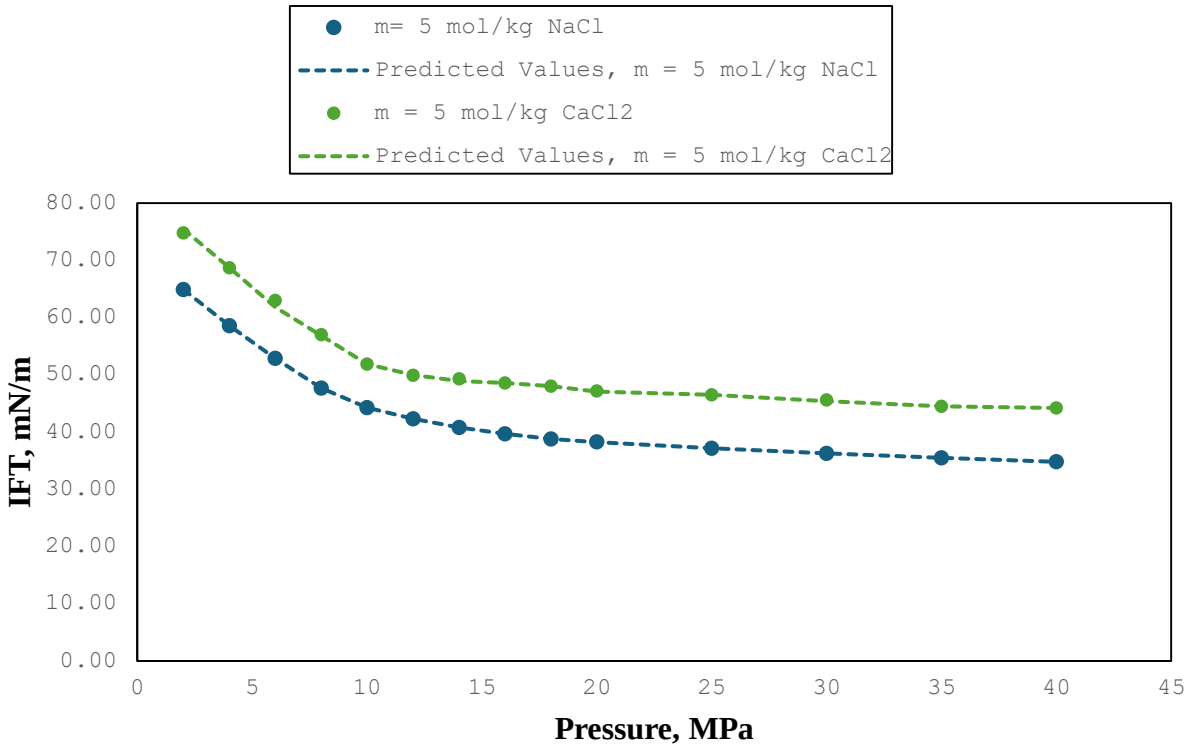

Figure 25. Analysis of actual and predicted values by GBR, demonstrating the effect of salt types on IFT at a constant temperature (343K) with no impurities.

The figure 26 shows interfacial tension measurements (IFT) between CO_2 and water at 343K for bivalent salts $CaCl_2$ and $MgCl_2$ under no impurity conditions. $CaCl_2$ and $MgCl_2$ show the same behavior on interfacial tension (IFT) as their data points produce substantial overlap throughout all measured pressure ranges. The results show that both salts perform similarly by attracting water molecules through ionic bonds which drives their equivalent IFT results. The impact of $CaCl_2$ and $MgCl_2$ on IFT are similar because both salts possess similar ionic strengths and hydration effects. The bivalent cations (Ca^{2+} and Mg^{2+}) in the salts produce powerful electrostatic forces with water molecules, enhancing water cohesion and thereby increasing the interfacial tension.

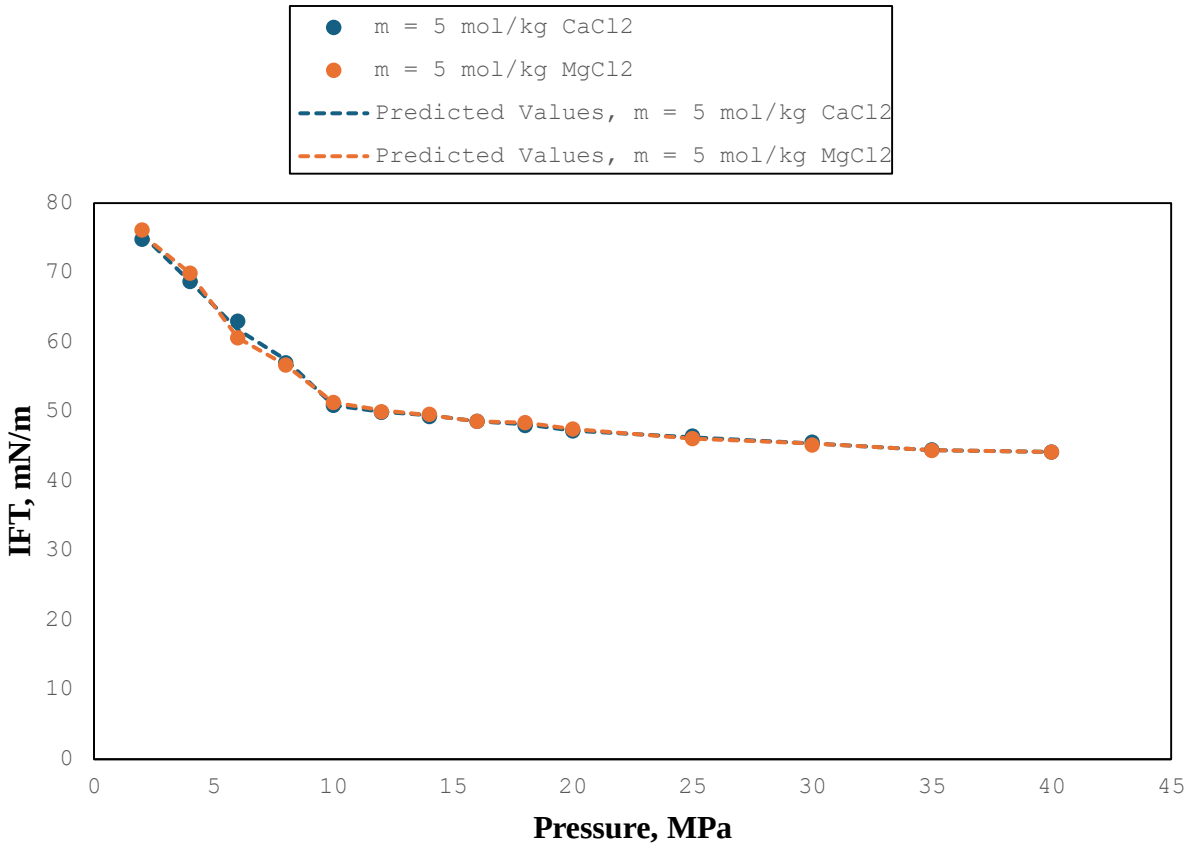

Figure 26. Analysis of actual and predicted values by GBR, demonstrating the effect of the same valent salt types on IFT at a constant temperature (343K) with no impurities

An examination of figure 27 demonstrates how interfacial tension (IFT) changes when impurities H_2S at 30% and CH_4 at 30% interact with a CO_2-water system compared to pure CO_2 without impurities. It is important to mention that the experimental data absence for pure CO_2 at 353 K conditions required the use of Gradient Boosting Regressor (GBR) to predict interfacial tension (IFT) since GBR proved to be the most precise machine learning model throughout this investigation. The analysis requires pure CO_2 to establish the baseline IFT behavior for determining how impurity changes affect interfacial properties. The results show that IFT measurements steadily decline with pressure elevation across the entire testing range as elevated pressures create higher CO_2 water solubility which weakens interfacial forces. The addition of 30% H_2S to CO_2 solution produces lower interfacial tension values than pure CO_2 because H_2S functions as a surfactant to reduce IFT more than CO_2 alone. The solubility of H_2S in water exceeds CO_2 by itself allowing H_2S to disrupt water cohesive forces to a greater extent. The measured interfacial

forces reach their maximum values when the system contains 30% CH_4 compared to the other samples. CH_4 shows lower water solubility than pure CO_2 and H_2S so it does not substantially contribute to interfacial disruption. The addition of CH_4 to the system stabilized the interface and produced higher IFT compared to both systems containing pure CO_2 and systems containing CO_2 and H_2S. The pure CO_2 - measurement appears between these two test conditions indicating that H_2S creates lower IFT values, whereas CH_4 produces higher values.

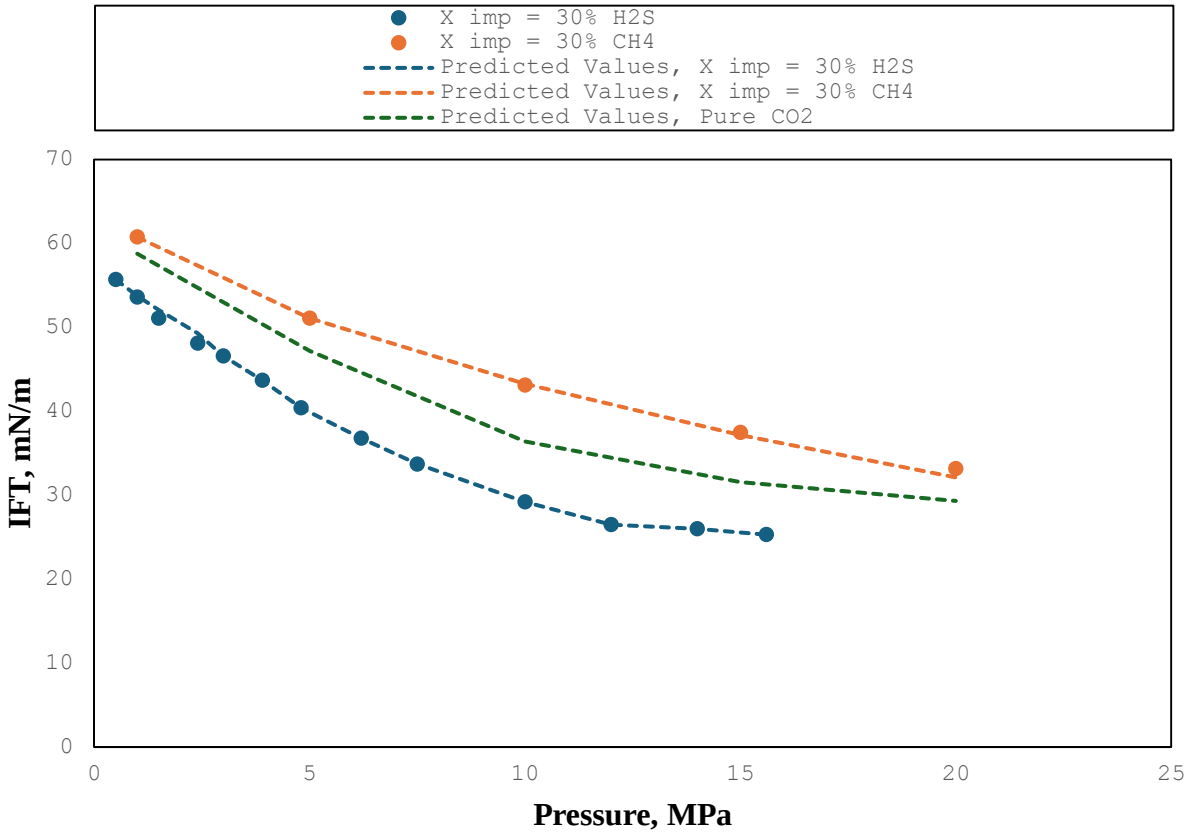

Figure 27. Analysis of actual and predicted values by GBR, demonstrating the effect of the type of impurities on IFT at a constant temperature (353K) and molalities (0 mol/kg)

4.2. CO_2-oil system

Various error metrics were used to evaluate the performance of Artificial Neural Networks (ANN) in predicting interfacial tension (IFT) measurements of CO_2-oil system with varying numbers of hidden layers (from one to five). The evaluation includes Root Mean Square Error (RMSE), Mean Squared Error (MSE), coefficient of determination (R^2), Mean Absolute Percentage Error (MAPE),

Akaike Information Criterion (AIC) and Bayesian Information Criterion (BIC) to assess the training and testing datasets (Table 23).

Table 23. The model evaluation results for ANN with different numbers of hidden layers

	Error Metrics	One Layer	Two Layers	Three Layers	Four Layers	Five Layers
Training Data	RMSE, mN/m	1.786	1.775	1.766	1.583	1.830
	MSE, mN/m	3.189	3.151	3.119	2.505	3.349
	R^2	0.904	0.906	0.906	0.925	0.899
	MAPE, %	17.515	17.628	17.115	19.14	18.977
	AIC	361.820	358.009	354.865	288.28	376.735
	BIC	376.701	372.891	369.746	303.168	391.616
Testing Data	RMSE, mN/m	1.733	1.707	1.695	1.582	1.724
	MSE, mN/m	3.003	2.914	2.873	2.503	2.972
	R^2	0.884	0.888	0.889	0.903	0.886
	MAPE, %	17.143	17.604	16.254	14.687	17.259
	AIC	92.685	90.379	89.272	78.727	91.896
	BIC	102.060	99.754	98.647	88.103	101.271

The proposed four-layer ANN model demonstrated superior results to the other models when predicting the training data values. The model delivers minimal RMSE at 1.583 mN/m, MSE at 2.505 mN/m, and AIC at 288.280 while providing the highest R^2 value of 0.925 for training data fit. The model's BIC value of 303.168 is the minimum among all models, indicating that it reaches its most optimal complexity level. The three-layer model exhibits similar R^2 (0.906) compared to the four-layer architecture but shows higher numerical error and fails to reach better results for any respective metrics. Training data performance for the five-layer model produced the highest values among all models for both RMSE (1.830 mN/m) and MSE (3.349 mN/m), and a reduced R^2 (0.899) along with the maximum AIC and BIC scores.

During the testing, the four-layer model simirarly exhibited the best generalization capabilities by yielding the minimum RMSE (1.582 mN/m) combined with the minimum MSE (2.503 mN/m) and MAPE (14.687%) along with the top R^2 value of 0.903. The model demonstrated its ability to avoid training data overfitting through its excellent predictive ability on previously unseen data. The error rates along with R^2 scores for the one-, two-, and three-layer configurations were slightly worse than those of the four-layer model structure. The five-layer model demonstrates poor performance in this prediction phase, resulting in higher RMSE (1.724 mN/m), MSE (2.972 mN/m), and a reduced R^2 (0.886) similar to its training performance.

The graphical representations in Figures 28 and 29 confirm the prediction results obtained from Table 23 for ANN models with different hidden layers when addressing IFT values of the CO_2–oil system. The IFT prediction results the training data are displayed as scatterplots in Figure 28. The ANN architecture with four layers (yellow markers) shows optimal alignment with the best fit line, thus indicating its success in effectively predicting actual values. The results of the graphical analysis support the model's highest R^2 value of 0.925, which appears in Table 23. The predicted and actual IFT values match similarly for the three-layer and two-layer models, but a slightly more scattered pattern is observed with R^2 values at 0.906. The five-layer model exhibits wider deviations (R^2 = 0.899), which confirms its reduced performance.

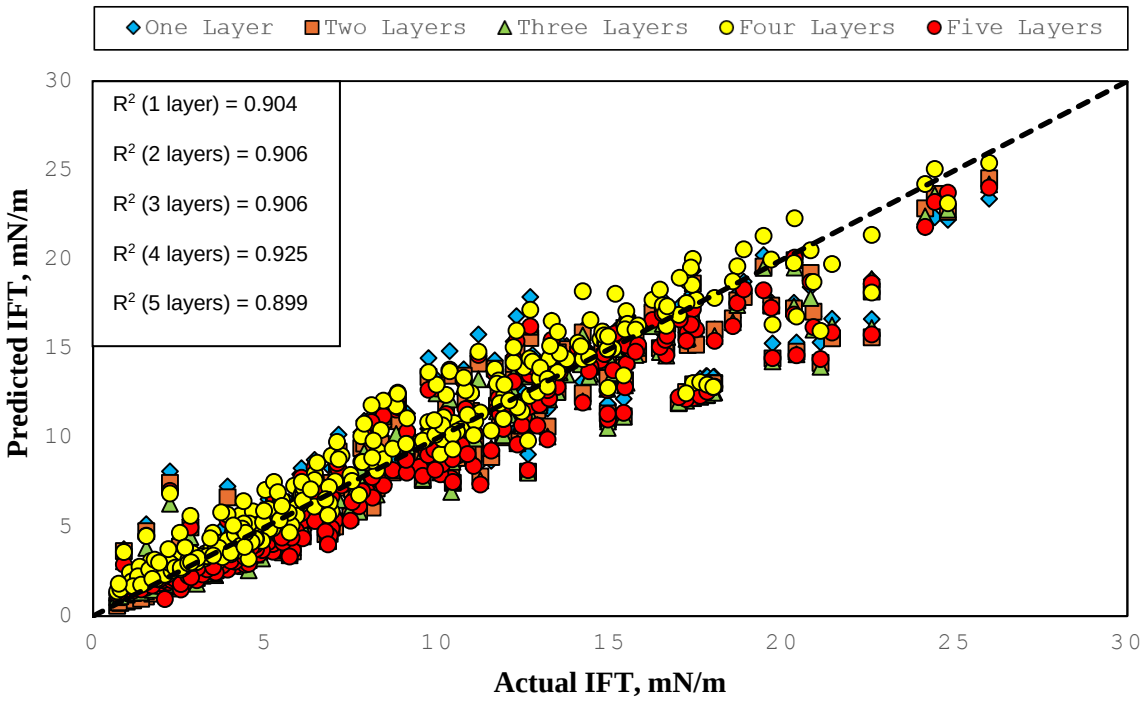

Figure 28. Actual vs Predicted IFT for the training dataset by ANN model

The examination of Figure 29 demonstrates the general predictive ability of different ANN architectures for the testing dataset. The four-layer model demonstrated the most effective predictive performance through a tight distribution of predicted values near the diagonal line and achieved the best R^2 value of 0.903. The testing results show that the three-layer (R^2 = 0.889) and two-layer (R^2 = 0.888) models deliver adequate predictions although they do not reach the accuracy level achieved by the four-layer model. The five-layer model achieves an R^2 equal to 0.886 but showed a wider spread from the perfect trend compared to other models.

The visual representations shown in these scatter plots support the statistical data presented in Table 23. The four-layer ANN model has the best capability for generalizing IFT predictions for the CO_2–oil system by learning from training data while maintaining high performance on testing data. The visual evidence in the graphs indicated that the four-layer architectural design produced the best modeling outcomes.

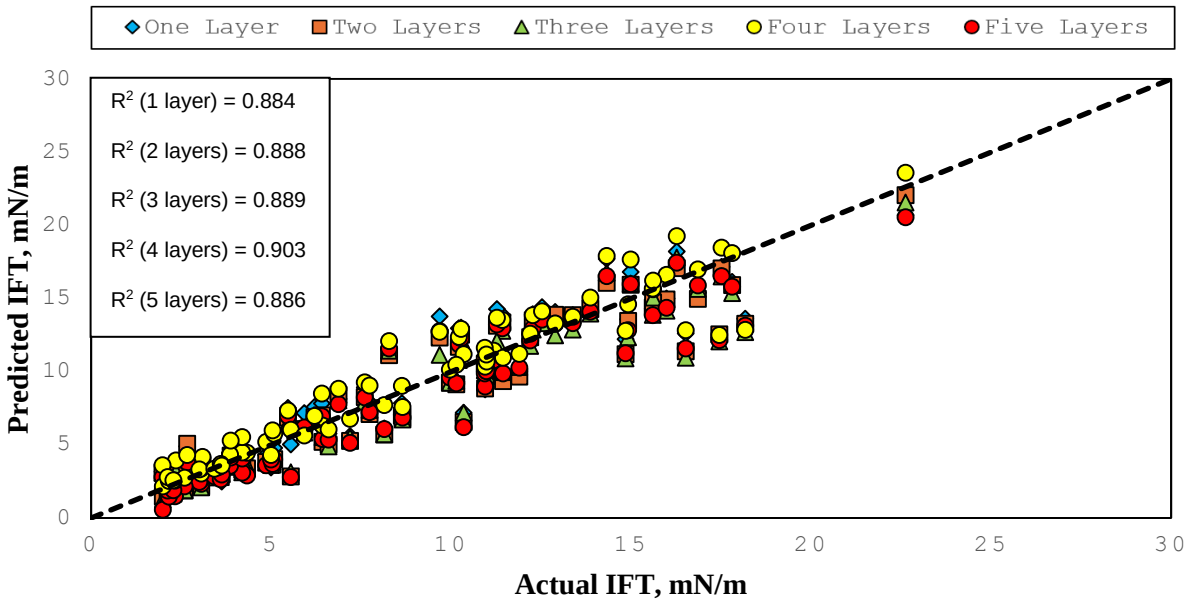

Figure 29. Actual vs Predicted IFT for the testing dataset by ANN model

Different machine learning (ML) techniques including ANN, Symbolic Regression via Genetic Programming (SR-GP), Decision Tree (DT), Random Forest (RF), Gradient Boosting Regression (GBR), Support Vector Regression (SVR), and XGBoost, were evaluated for their ability to predict

interfacial tension (IFT) in the CO_2–oil system using the performance metrics shown in Table 24. The performance assessment includes both generalization through the AIC and BIC values and accuracy evaluation using the training and testing RMSE, MSE, R^2, and MAPE.

Table 24. The model evaluation results for all ML models.

		ANN	SR-GP	DT	RF	GBR	SVR	XGBoost
Training Data	RMSE, mN/m	1.583	2.731	0.671	1.124	0.370	1.291	0.522
	MSE, mN/m	2.505	7.458	0.45	1.263	0.136	1.667	0.272
	R^2	0.925	0.776	0.987	0.962	0.996	0.95	0.991
	MAPE	19.14	27.335	6.014	14.475	4.78	10.08	6.393
	AIC	288.28	620.962	-235.23	79.804	-597.69	164.114	-387.43
	BIC	303.168	635.844	-220.35	94.685	-582.82	179.021	-372.55
Testing Data	RMSE, mN/m	1.582	2.926	1.397	1.347	0.662	1.456	0.805
	MSE, mN/m	2.503	8.561	1.951	1.814	0.438	2.12	0.649
	R^2	0.903	0.670	0.923	0.93	0.983	0.918	0.974
	MAPE	14.687	25.350	12.33	16.85	7.43	12.02	7.939
	AIC	78.727	173.387	59.53	53.885	-55.5	65.83	-25.24
	BIC	88.103	182.761	68.91	63.26	-46.125	75.2	-15.867

The training results demonstrate that the GBR and XGBoost models outperform the other models because they present the lowest RMSE values (0.370, 0.522 mN/m) while obtaining R^2 values of 0.99 which indicates superior learning ability. The prediction results indicate that GBR delivers a small deviation from the actual values through its MAPE of 4.78%, whereas XGBoost shows a similarly low value of 6.39%. The GBR and XGBoost models show extreme efficiency and strong model fit, as indicated by their highly negative AIC and BIC scores, where the GBR model has AIC = -597.69, and BIC = -582.82 while XGBoost model has AIC = -387.43, and BIC = -372.55. The training performance of the DT and RF models shows high R^2 values at 0.987 and 0.962 respectively but their MAPE outcomes stood at 6.014% and 14.47%. SR-GP attains the most

inferior performance because it generates RMSE (2.731 mN/m) outcomes along with MAPE (27.335%) while achieving R^2 (0.776).

Testing confirmed the highest generalization capability of GBR through its superior overall performance, which included a low RMSE of 0.662 mN/m, MSE of 0.438 mN/m, and MAPE of 7.43%, along with a high R^2 value of 0.983. The machine learning models achieved almost similar results, as DT (R^2 = 0.923, MAPE = 12.33%) followed RF by maintaining R^2 = 0.93 alongside error metrics of RMSE = 1.347 mN/m, MAPE = 16.85%. The ANN model achieved acceptable performance scores compared with the ensemble-based models due to its R^2 value of 0.903 and MAPE value of 14.687%. It produced reliable but less precise predictions. The generalization capabilities of the XGBoost predictions are strong R^2 = 0.974 and MAPE = 7.939% compared with SR-GP, which exhibit the lowest R^2 value (0.670). The model comparison metrics AIC and BIC validate these findings by showing that GBR had the lowest statistical values (AIC = -55.5, BIC = -46.12) surpassing both XGBoost and RF. The ANN model has statistical reliability based on its AIC and BIC values (that are AIC = 78.727, BIC = 88.103), but it falls behind the most efficient ensemble methods.

The data in Table 24 which compares ML models on CO_2–oil systems receives strong confirmation from the scatter plot visualizations shown in Figures 30 and 31. Figures 30 and 31 display actual IFT measurements against predicted values for training and testing datasets under all applied ML models thus providing quantitative data with visual qualitative assessments for prediction accuracy.

The scatter plot for training data demonstrates an ideal match between Gradient Boosting Regression (GBR) and XGBoost predicted results and the reference line in Figure 30, thus validating a nearly perfect prediction. Both models confirmed their ability to identify complex nonlinear relationships in the data through their R^2 values exceeding 0.99. The actual values match well with DT and RF predictions because these models produce R^2 values of 0.987 and 0.962, respectively. The SVR model produced adequate results (R^2 = 0.95), yet its data points spread across the graph to a greater extent than ensemble models. SR-GP reveals substantial deviations from the diagonal line because its R^2 value stands at 0.776, indicating inferior learning capability.

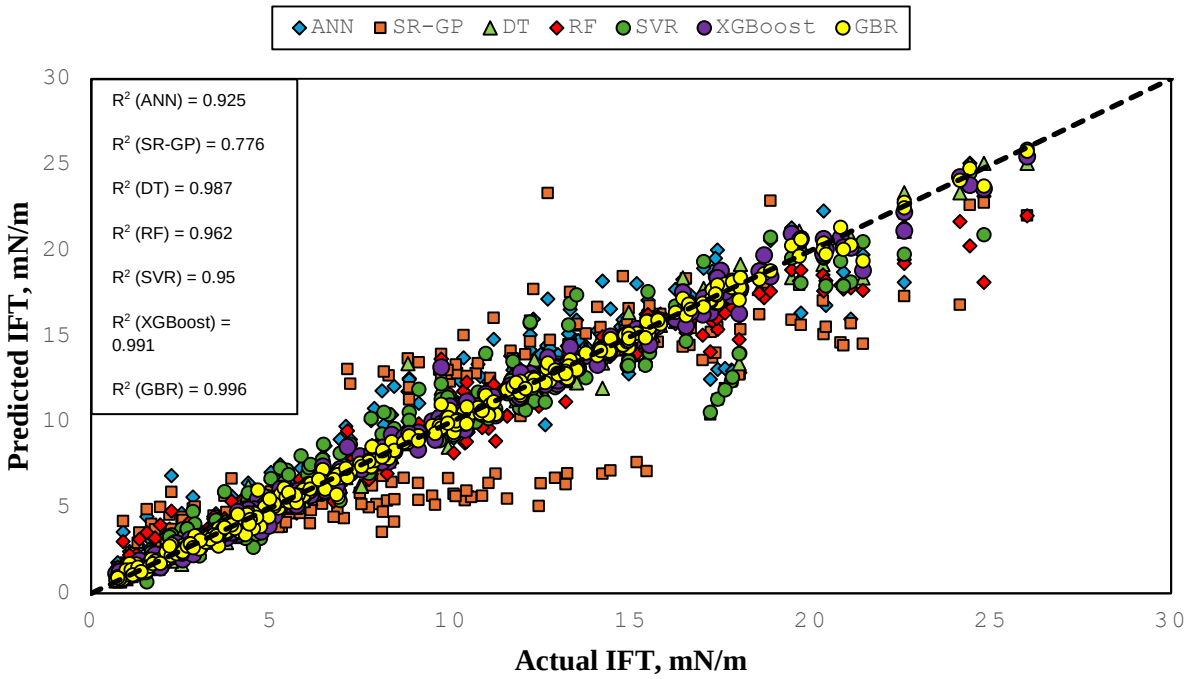

Figure 30. Actual vs Predicted IFT for the training dataset by all ML models

The scatter plot of the testing dataset in Figure 31 evaluates the model generalization with higher complexity. XGBoost (R^2 = 0.974) together with GBR (R^2 = 0.983) demonstrate their superior predictive accuracy by producing predictions that align very closely to the diagonal reference line. The model generalization capability of RF remains strong (R^2 = 0.93) during testing. The ANN model produces more reliable yet less precise predictions than the ensemble methods while maintaining a R^2 value of 0.903. This model generates predictions with moderate dispersion. The predictive outcome of Decision Tree (DT) model exhibited high prediction variability while maintaining an R^2 value of 0.923. SVR and RF models also showed high generalizabilty of 0.918 and 0.93, correspondingly. Only SR-GP (R^2 = 0.670) demonstrated significant spread in their data points while providing the worst fit to actual values during generalization. Figures 30 and 31 expand the numerical data from Table 24 in visual representation. The performance metrics demonstrate that the GBR, XGBoost, and DT models actively achieve the best results through training processes as well as testing phases with accurate value matches while keeping errors to a minimum. The analysis results demonstrated that the ensemble tree-based models especially GBR and XGBoost demonstrated the strongest reliability and accuracy for IFT prediction in CO_2–oil

systems. The scatter plots confirm the visual evidence of their strong R^2 values which validate their exceptional generalizability.

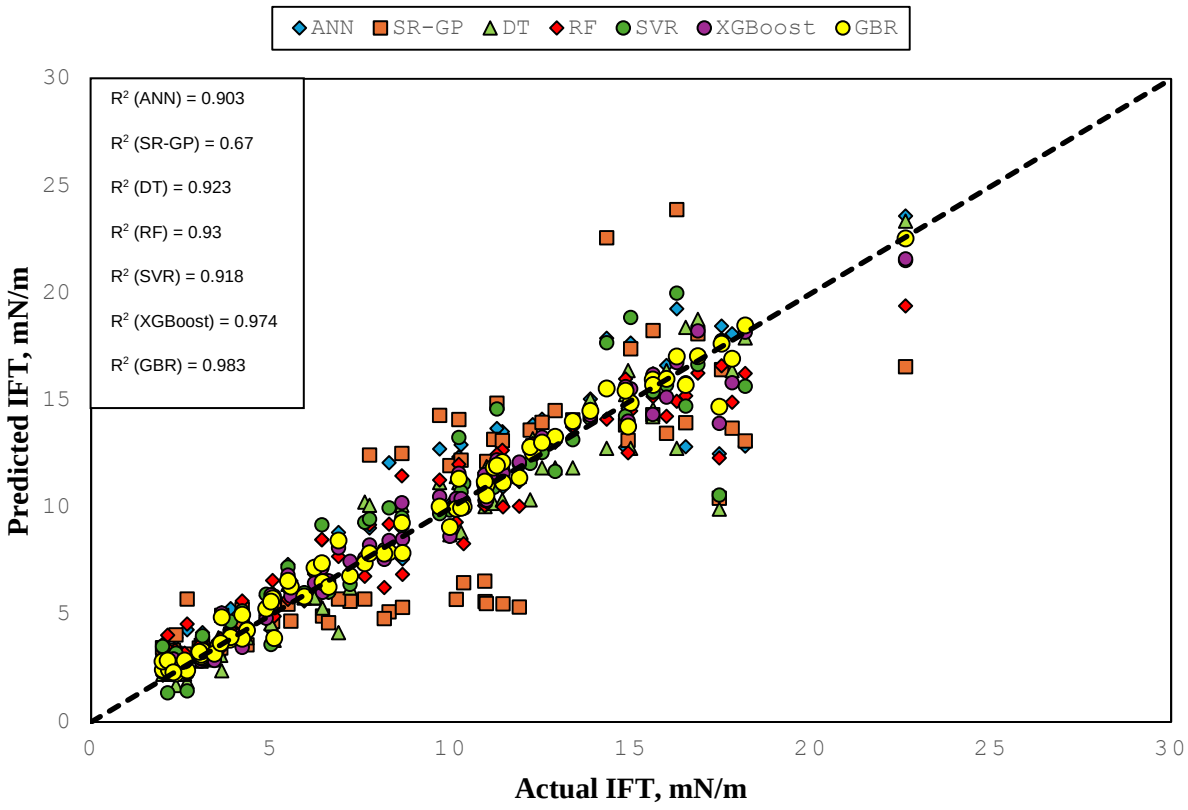

Figure 31. Actual vs Predicted IFT for the testing dataset by all ML models

The Kernel Density Estimation (KDE) plots in figure 32 show the predictive accuracy of the machine learning models for the IFT values by measuring their compliance with CO_2–oil system actual data distribution patterns. KDE visualization helps model evaluation by displaying probability density distributions, which enables performance assessment in addition to traditional error metrics. In the testing data subplot (a) the GBR , XGBoost, and DT model KDE curves precisely match the actual data (red) distribution, demonstrating effective reproduction of the IFT values distribution. As shown in Table 24 and Figures 30–31 these models demonstrate an exceptional ability to deliver the minimum error metrics combined with the highest R^2 values. The ANN model shows excellent generalizability in matching actual data points with small deviations. The distribution of SR-GP deviates significantly from the actual curve by having a sharp peak with visible shifts toward the predictive values due to its poor ability to align with the data as shown

previously through error metrics and scatter plots. RF and SVR relate between these two extremes by accurately showing the general pattern with minor inconsistencies in distribution density and spread. The subplot in (b) displays the training dataset results and shows identical patterns between the different models. The KDE curves for GBR, DT and XGBoost demonstrate identical alignment with actual data points during training due to the strong learning ability of the underlying data distribution. The alignment between the predicted data points and actual data points explains the high R^2 values together with the observed low RMSE/MAPE metrics. The training performance of SR-GP remained unsatisfactory because it displayed incorrect peak locations and shape misalignment, demonstrating its inability to learn proper data characteristics correctly. SVR and ANN deliver more accurate predictions than the testing phase, although they deviate from the actual KDE curve.

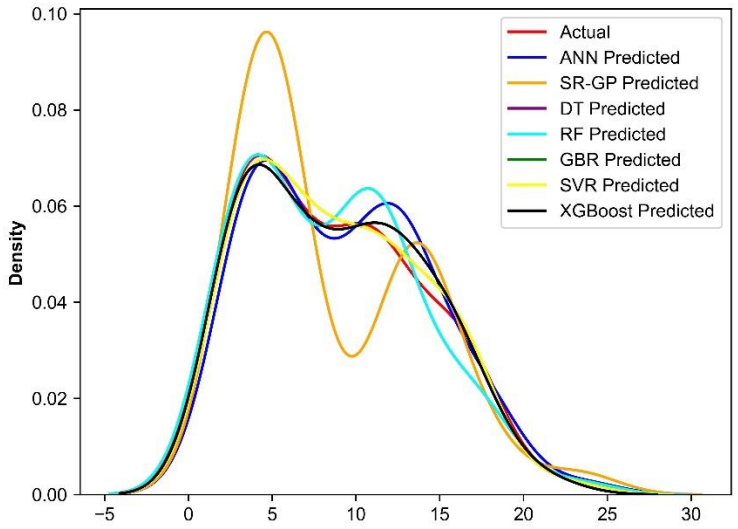

a)

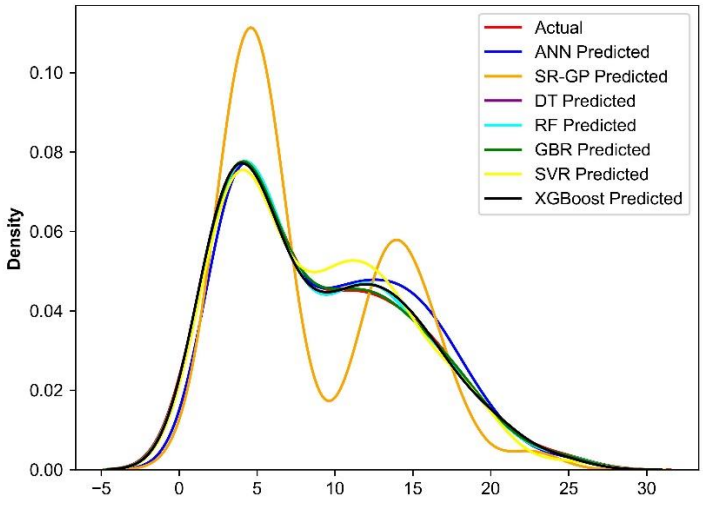

b)

Figure 32. Analysis of KDE plots comparing actual data and all applied ML models using a) testing dataset and b) training datasets

The impact of pressure and temperature on CO_2–oil interfacial tension IFT can be observed through figure 33 by analyzing actual and GBR-predicted IFT values at a fixed API gravity of 37°. The experimental data were obtained by testing pressures up to 11 MPa and temperatures in the range of 298 to 353 K. The interfacial tension exhibits a specific decreasing pattern throughout each measured temperature stage when the pressure levels increase. Higher pressure decreases CO_2-oil interfacial tension because CO_2 increases its solubility in oil while lowering the tension at different phase interfaces. The IFT exhibits its greatest response magnitude to changing pressure when measured from 0 to 5 MPa, thus indicating the system's sensitivity at this specific pressure level. The rate of IFT reduction became slower than in the previous stages when the pressure exceeded 6 MPa because the system reached an equilibrium state. Temperature is as an important factor that influences the IFT behavior. At a given pressure, the IFT decreases with increasing temperature. All datasets across the figure demonstrate that IFT reached maximum values at 298 K and minimum values at 353 K. High temperature levels enable better mixing and lower interfacial tension by increasing molecular activity and decreasing viscosity. The system behavior

became strongly influenced by the pressure as its value increased while the temperature sensitivity decreased at higher pressures. The GBR model-generated predicted values precisely match the experimental observations since the dashed predicted lines precisely follow the solid actual marker data points throughout all temperature ranges. The GBR model shows excellent match with the underlying thermodynamic principles that control interfacial tension in CO_2-oil mixtures through all experimental conditions. The model exhibits strong precision in predicting IFT with minimal variation across all pressure and temperature points during the test conditions.

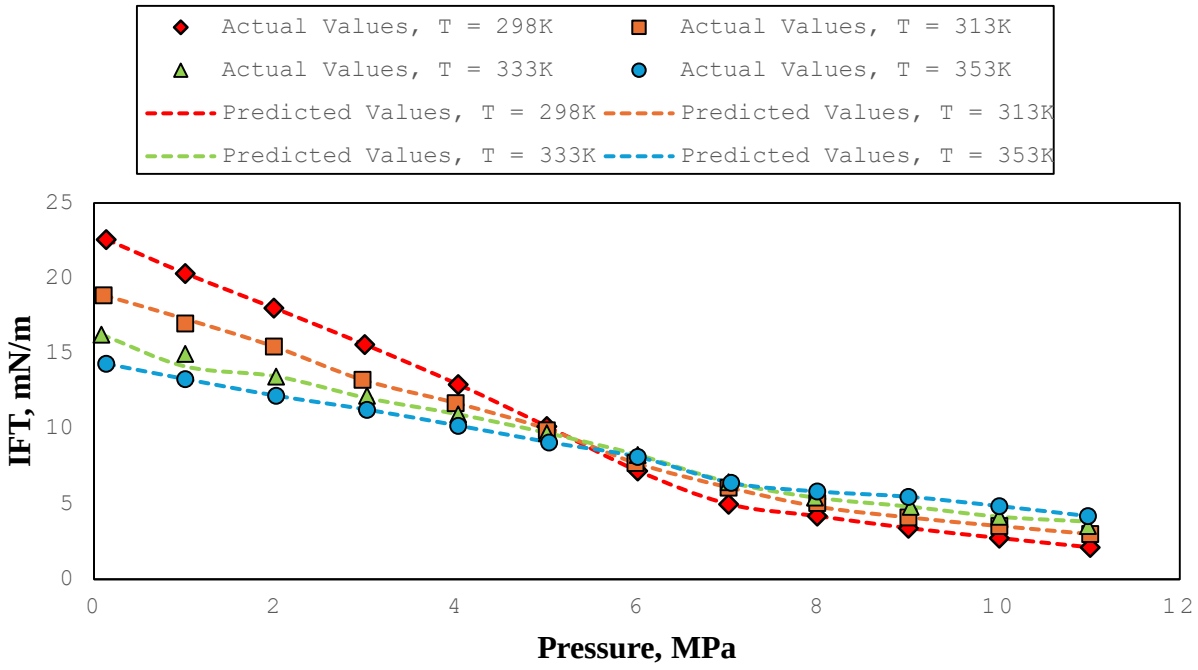

Figure 33. Analysis of actual and predicted values by GBR model, demonstrating the effect of pressure and temperature on IFT at a constant API = 37°

Figure 34 shows how changes in pressure affect the interfacial tension (IFT) of the CO_2–oil system under conditions of 333 K and various oil gravity levels expressed as API degrees. Experimental data from three crude oil types with API gravity of 8 and 27 and 35 were compared to prediction results generated by Gradient Boosting Regression (GBR) modeling software. Pressure increases cause Interfacial Tension (IFT) to decrease systematically throughout all API levels in CO_2–oil systems as per typical CO_2–oil system behavior. The IFT value decreases proportionally with increasing API gravity under standard pressure conditions. During the entire pressure range, the

35°API oil maintains lower interfacial tension than both 27 °API and 8 °API oils. The decreased viscosity of high API gravity oils enables CO_2 to diffuse more easily throughout the interface, which contributes to greater IFT reduction. Higher API crudes have lower viscosity characteristics, which allows CO_2 to mix easily at the interface, thus decreasing Interfacial Tension values. For all API levels, the GBR model successfully replicated the experimental data trends and predicted outcomes. The prediction lines on the graph show near-perfect agreement with actual data points, which indicates that GBR correctly replicates the complex interrelation between the pressure and oil composition on the IFT values.

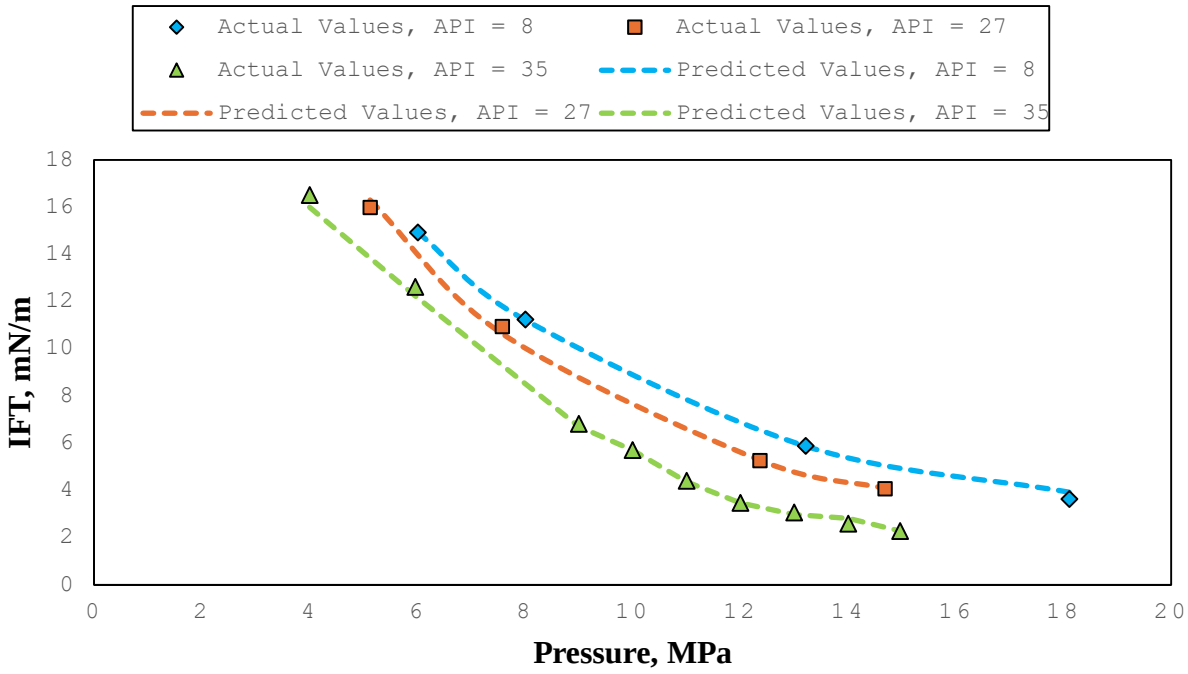

Figure 34. Analysis of actual and predicted values by GBR model, demonstrating the effect of pressure and API on IFT at a constant T = 333 K

5. CONCLUSION

This research evaluated a machine learning models that predict interfacial tension measurements between CO_2/water and CO_2/oil systems across diverse thermal and material compositions. The machine learning evaluation utilized seven models including Artificial Neural Networks (ANN), Symbolic Regression–Genetic Programming (SR-GP), Decision Trees (DT), Random Forest (RF), Gradient Boosting Regression (GBR), Support Vector Regression (SVR), and XGBoost which

were tested using RMSE, MSE, R^2, MAPE, AIC, and BIC error metrics. To visually examine data alignment Scatter Plots and the Kernel Density Estimation (KDE) graphical method were implemented.

When applied to CO_2–water systems, Gradient Boosting Regression (GBR) proved to be the most effective model for predicting surface tension according to testing assessments such as training R^2 at 0.99 and testing R^2 at 0.96 and minimum RMSE at 1.367 mN/m in training and MAPE at 2.27%. XGBoost and Random Forest models achieved testing results that exceeded $R^2 = 0.94$ and maintained low error levels in the datasets. A four-layer ANN achieved stable performance at $R^2 = 0.917$ in training and 0.915 in testing; however, ensemble models based on trees displayed superior results. The results of SR-GP revealed the weakest predictive ability when examining both training $R^2 = 0.75$ and testing $R^2 = 0.79$ alongside maximum MAPE values.

The experimental data revealed corresponding patterns during CO_2–oil interaction. GBR established itself as the most reliable model for IFT prediction by producing R^2 values of 0.996 during training and 0.983 during testing coupled with minimal RMSE and MAPE values of 0.662 and 7.43%, respectively, since it showed the best ability to quantify IFT dependencies on pressure and crude oil properties and temperature adjustments. DT and XGBoost provided comparable predictive outcomes with R^2 scores surpassing 0.96 thus proving their capability for various oil types and operating conditions. The results demonstrated that the ANN model was potentially reliable when its optimization was performed correctly because it generated training $R^2 = 0.925$ and testing $R^2 = 0.903$. The predictive abilities of SVR and RF fell between acceptable rankings but SR-GP demonstrated the poorest performance with R^2 scores of 0.776 for training and 0.670 for testing thus indicating restricted applicability for these complex interfacial systems.

The accuracy of the GBR, RF and XGBoost models was further confirmed through scatter plot analysis (Figures 17–18, 28–29, 30–31) because their data points showed minimal deviation from the perfect prediction line during testing. KDE plots verified the reliability of these predictive models because their predicted distributions closely matched the measured data distributions.

The models correctly represented key physical trends based on their sensitivity analyses. Both experimental systems demonstrated that pressure increases led IFT to decrease, but this reduction became less pronounced at elevated pressures which indicates the appearance of stabilization effects. Both salinity elevation and CH_4 presence enhanced CO_2–water interfacial tension, whereas

elevated temperature decreased the interfacial tension in the CO_2–water system. The IFT-increasing effect of bivalent salts (like $CaCl_2$) exceeded that of monovalent salts (like NaCl), and minor variations developed between different bivalent salt types (between $CaCl_2$ and $MgCl_2$). The experimental system of CO_2 in contact with oil showed decreasing IFT values as both the temperature and API gravity increased according to physical theory. The best performing models, particularly GBR demonstrated the capacity to accurately reflect these patterns along with their representation of meaningful physicochemical relationships.

This research shows that ensemble learners namely GBR and XGBoost are exceptional tools for estimating interfacial tension in CO_2–fluid systems. These models provide an effective alternative solution for precise and efficient and expandable predictions of interfacial tension that replace traditional experimental or theoretical approaches. These prediction systems possess the potential for enlargement or inclusion in reservoir simulators and optimization platforms, which enable better decision-making during CO_2-based enhanced oil recovery (EOR) carbon capture storage (CCS) and corresponding subsurface engineering operations.

6. RECOMMENDATIONS

- **Utilization of Ensemble Models for IFT Prediction**

The implementation of Gradient Boosting Regression (GBR) together with Random Forest (RF) and XGBoost represents the best choice for future IFT prediction tasks due to their reliable precision outcomes. The prediction models showed outstanding performance across all tested systems which included water and oil mixing with CO_2.

- **Application to Real-Time and Field-Scale Predictions**

The integrated models can run in simulation tools of enhanced oil recovery (EOR) and carbon sequestration workflows to produce quick and trustworthy IFT estimations during real-time delivery without requiring continuous experimental measurements.

- **Development of Hybrid or Physics-Informed ML Models**

Thermodynamic equations have the potential to be combined with ML to drive hybrid models that can improve extrapolation outside of training conditions. In this study SR-GP was used to create equations based on mathematical relationships in datasets. While SR-GP perfomed poorly in this study, alternatives to the current symbolic regression tool may create better, more generalizable mathematical equations providing deeper understanding of underlying physical relationships.

- **Expansion of Capillary Rise Experimental Dataset**

The volume of experimental data obtained using the capillary rise method should be increased for future research. In this study, some models did not show good predictive performance when they were applied to dataset generated from this technique, possibly because of limited sample size. Increasing the amount of data points from capillary rise experiments may improve the model training, reduce the bias, and improve the overall predictive accuracy of any ML model used.

7. REFERENCES

Aggelopoulos, C. A., Robin, M., Perfetti, E., & Vizika, O. (2010). CO2/CaCl2 solution interfacial tensions under CO2 geological storage conditions: influence of cation valence on interfacial tension. *Advances in Water Resources*, *33*(6), 691-697.

Aggelopoulos, C. A., Robin, M., & Vizika, O. (2011). Interfacial tension between CO2 and brine (NaCl+ CaCl2) at elevated pressures and temperatures: The additive effect of different salts. *Advances in Water Resources*, *34*(4), 505-511.

Akaike, H. (1974). A new look at the statistical model identification. *IEEE transactions on automatic control*, *19*(6), 716-723.

Akutsu, T., Yamaji, Y., Yamaguchi, H., Watanabe, M., Smith Jr, R. L., & Inomata, H. (2007). Interfacial tension between water and high pressure CO2 in the presence of hydrocarbon surfactants. *Fluid phase equilibria*, *257*(2), 163-168.

Al-Abri, A., & Amin, R. (2009, December). Experimental investigation of interfacial interactions of condensate/brine/SC-CO2 systems at high pressure and high temperature conditions. In *IPTC 2009: International Petroleum Technology Conference* (pp. cp-151). European Association of Geoscientists & Engineers.

Al-Anssari, S., Arain, Z. U. A., Shanshool, H. A., Ali, M., Keshavarz, A., Iglauer, S., & Sarmadivaleh, M. (2020, November). Effect of nanoparticles on the interfacial tension of co2-oil system at high pressure and temperature: an experimental approach. In *SPE Asia Pacific Oil and Gas Conference and Exhibition* (p. D013S101R009). SPE.

Al-Yaseri, A., Yekeen, N., Ali, M., Pal, N., Verma, A., Abdulelah, H., ... & Sarmadivaleh, M. (2022). Effect of organic acids on CO2-rock and water-rock interfacial tension: Implications for CO2 geo-storage. *Journal of Petroleum Science and Engineering*, *214*, 110480.

Amar, M. N., Shateri, M., Hemmati-Sarapardeh, A., & Alamatsaz, A. (2019). Modeling oil-brine interfacial tension at high pressure and high salinity conditions. *Journal of Petroleum Science and Engineering*, *183*, 106413.

Andreas, J. M., Hauser, E. A., & Tucker, W. B. (2002). Boundary tension by pendant drops1. *The Journal of Physical Chemistry*, *42*(8), 1001-1019.

Arashiro, E. Y., & Demarquette, N. R. (1999). Use of the pendant drop method to measure interfacial tension between molten polymers. *Materials Research*, *2*, 23-32.

Bachu, S., & Bennion, D. B. (2009). *Dependence of CO_2-brine interfacial tension on aquifer pressure, temperature and water salinity.* Energy Procedia, 1(1), 3157–3164. https://doi.org/10.1016/j.egypro.2009.02.098

Bikkina, P. K., Shoham, O., & Uppaluri, R. (2011). Equilibrated interfacial tension data of the CO2–water system at high pressures and moderate temperatures. *Journal of Chemical & Engineering Data*, *56*(10), 3725-3733.

Borup, D., Christensen, B. J., Mühlbach, N. S., & Nielsen, M. S. (2023). Targeting predictors in random forest regression. *International Journal of Forecasting*, *39*(2), 841-868.

Chalbaud, C., Robin, M., Lombard, J.-M., Martin, F., Egermann, P., & Bertin, H. (2009). Interfacial tension measurements and wettability evaluation for geological CO_2 storage. *Advances in Water Resources*, 32(1), 98–109.

Chiquet, P., Daridon, J. L., Broseta, D., & Thibeau, S. (2007). *CO_2/water interfacial tensions under pressure and temperature conditions of CO_2 geological storage.* Energy Conversion and Management, 48(3), 736–744. https://doi.org/10.1016/j.enconman.2006.09.011

Chen, T., & Guestrin, C. (2016, August). Xgboost: A scalable tree boosting system. In *Proceedings of the 22nd acm sigkdd international conference on knowledge discovery and data mining*(pp. 785-794).

Chun, B., & Wilkinson, G. T. (1995). Interfacial tension in high-pressure carbon dioxide mixtures. *Industrial & Engineering Chemistry Research*, *34*(12), 4371–4377. https://doi.org/10.1021/ie00039a029

Cristianini, N., & Shawe-Taylor, J. (2000). *An introduction to support vector machines and other kernel-based learning methods*. Cambridge university press.

Del Rıo, O. I., & Neumann, A. W. (1997). Axisymmetric drop shape analysis: computational methods for the measurement of interfacial properties from the shape and dimensions of pendant and sessile drops. *Journal of colloid and interface science*, *196*(2), 136-147.

Dongare, A. D., Kharde, R. R., & Kachare, A. D. (2012). Introduction to artificial neural network. *International Journal of Engineering and Innovative Technology (IJEIT)*, *2*(1), 189-194.

Drelich, J., Fang, C., & White, C. L. (2006). Interfacial tension measurement in fluidfluid systems. *Encyclopedia of Surface and Colloid Science. New York: Marcel Dekker Inc*, 2966.

Drelich, J., Fang, C., & White, C. L. (2002). Measurement of interfacial tension in fluid-fluid systems. *Encyclopedia of surface and colloid science*, *3*, 3158-3163.

Duan, Z., & Sun, R. (2003). An improved model calculating CO_2 solubility in pure water and aqueous NaCl solutions from 273 to 533 K and from 0 to 2000 bar. *Chemical Geology*, 193(3–4), 257–271.

Erpeng, G., Yongrong, G., Youwei, J., Yunjun, Z., Zhigang, C., & Yao, W. (2018, March). Super critical CO2 and steam co-injection process for deep extra-heavy oil reservoir. In *SPE EOR Conference at Oil and Gas West Asia* (p. D022S003R001). SPE.

Fordham, S. (1948). On the calculation of surface tension from measurements of pendant drops. *Proceedings of the Royal Society of London. Series A. Mathematical and Physical Sciences*, *194*(1036), 1-16.

Gajbhiye, R. (2025). Impact of gas composition, pressure, and temperature on interfacial Tension dynamics in CO_2-Enhanced oil recovery. *Scientific Reports*, *15*(1), 3821.

Galván, E., Trujillo, L., & Stapleton, F. (2022). Semantics in multi-objective genetic programming. *Applied Soft Computing*, *115*, 108143.

Georgiadis, A., Maitland, G., Trusler, J. M., & Bismarck, A. (2010). Interfacial tension measurements of the (H2O+ CO2) system at elevated pressures and temperatures. *Journal of Chemical & Engineering Data*, *55*(10), 4168-4175.

Gevrey, M., Dimopoulos, I., & Lek, S. (2003). Review and comparison of methods to study the contribution of variables in artificial neural network models. *Ecological modelling*, *160*(3), 249-264.

Haider, G., Khan, M. A., Ali, F., Nadeem, A., & Abbasi, F. A. (2022, October). An intelligent approach to predict minimum miscibility pressure of injected CO2-oil system in miscible gas flooding. In *Abu Dhabi International Petroleum Exhibition and Conference* (p. D032S172R006). SPE.

Hebach, A., Oberhof, A., Dahmen, N., Kögel, A., Ederer, H., & Dinjus, E. (2002). *Interfacial tension at Elevated Pressures: Measurements and correlations in the water + Carbon dioxide system.* Journal of Chemical & Engineering Data, 47(6), 1540–1546. https://doi.org/10.1021/je025569p

Hoorfar, M., & Neumann, A. W. (2006). Recent progress in axisymmetric drop shape analysis (ADSA). *Advances in colloid and interface science*, *121*(1-3), 25-49.

Hosseini, A. H., Ghadery-Fahliyany, H., Wood, D., & Choubineh, A. (2020). Artificial intelligence-based modeling of interfacial tension for carbon dioxide storage. *Gas Processing Journal*, *8*(1), 83-92.

Iowast, A.G., & Kumari, K.A. (2020). Predictive analytics approaches for software effort estimation: A review. *Indian journal of science and technology, 13*, 2094-2103.

Isfehani, Z. D., Sheidaie, A., Hosseini, M., Fahimpour, J., Iglauer, S., & Keshavarz, A. (2023). Interfacial tensions of (brine+ H2+ CO2) systems at gas geo-storage conditions. *Journal of Molecular Liquids*, *374*, 121279.

Kalam, S., Arif, M., Raza, A., Lashari, N., & Mahmoud, M. (2023). Data-driven modeling to predict adsorption of hydrogen on shale kerogen: implication for underground hydrogen storage. *International Journal of Coal Geology*, *280*, 104386.

Kamal, M. S., Sultan, A. S., Al-Mubaiyedh, U. A., & Hussein, I. A. (2015). Review on surfactant flooding: Phase behavior, retention, IFT, and field applications. *Energy & Fuels*, 29(8), 4258–4283.

Khan, M. R., Tariq, Z., Ali, M., & Murtaza, M. (2024, February). Predicting Interfacial Tension in CO2/Brine Systems: A Data-Driven Approach and Its Implications for Carbon Geostorage. In *International Petroleum Technology Conference* (p. D031S144R001). IPTC.

Kim, S., & Kim, H. (2016). A new metric of absolute percentage error for intermittent demand forecasts. *International Journal of Forecasting*, *32*(3), 669-679.

Kotsiantis, S. B. (2013). Decision trees: a recent overview. *Artificial Intelligence Review*, *39*, 261-283.

Kvamme, B., Kuznetsova, T., Parmar, K., & Danielsen, S. (2007). *Measurements and modeling of interfacial tension for water + carbon dioxide systems at elevated pressures.* Journal of Chemical & Engineering Data, 52(5), 1810–1818. https://doi.org/10.1021/je7001855

Li, D., Li, X., Zhang, Y., Sun, L., & Yuan, S. (2019). Four Methods to Estimate Minimum Miscibility Pressure of CO2-Oil Based on Machine Learning. *Chinese Journal of Chemistry*, *37*(12), 1271-1278.

Li, X., Boek, E., Maitland, G. C., & Trusler, J. P. M. (2012). *Interfacial Tension of (Brines + CO_2): (0.864 NaCl + 0.136 KCl) at Temperatures between (298 and 448) K, Pressures between (2 and 50) MPa, and Total Molalities of (1 to 5) mol·kg^{-1}.* Journal of Chemical & Engineering Data, 57(2), 1078-1088. https://doi.org/10.1021/je201062r

Liu, Y., Li, H. A., & Okuno, R. (2016). Measurements and modeling of interfacial tension for CO2/CH4/brine systems under reservoir conditions. *Industrial & Engineering Chemistry Research*, *55*(48), 12358-12375.

Liu, Y., Mutailipu, M., Jiang, L., Zhao, J., Song, Y., & Chen, L. (2015). *Interfacial tension and contact angle measurements for the evaluation of CO_2-brine two-phase flow characteristics in porous media.* Environmental Progress & Sustainable Energy, 34(6), 1756–1762. https://doi.org/10.1002/ep.12160

Mahboob, A., & Sultan, A. S. (2016, April). An experimental study of interfacial tension and contact angles of CO2/brines/surfactants/oil systems with dolomite rock. In *SPE Kingdom of Saudi Arabia Annual Technical Symposium and Exhibition* (pp. SPE-182839). SPE.

Maleki, H., Keshavarz, P., Shahbazi, S., & Shahrabi, M. (2023). *Investigation of Wettability and IFT Alteration during Hydrogen Storage Using Machine Learning.* Energy, 248, 123263. https://doi.org/10.1016/j.energy.2022.123263

Montesinos López, O. A., Montesinos López, A., & Crossa, J. (2022). Fundamentals of artificial neural networks and deep learning. In *Multivariate statistical machine learning methods for genomic prediction* (pp. 379-425). Cham: Springer International Publishing.

Mouallem, J., Raza, A., Glatz, G., Mahmoud, M., & Arif, M. (2024). Estimation of CO2-brine interfacial tension using machine learning: implications for CO2 geo-storage. *Journal of Molecular Liquids*, *393*, 123672.

Myles, A. J., Feudale, R. N., Liu, Y., Woody, N. A., & Brown, S. D. (2004). An introduction to decision tree modeling. *Journal of Chemometrics: A Journal of the Chemometrics Society*, *18*(6), 275-285.

Nallathambi, S., & Ramasamy, K. (2017, April). Prediction of electricity consumption based on DT and RF: An application on USA country power consumption. In *2017 IEEE International Conference on Electrical, Instrumentation and Communication Engineering (ICEICE)* (pp. 1-7). IEEE.

Neumann, A. W., David, R., & Zuo, Y. (Eds.). (2010). *Applied surface thermodynamics*. CRC press.

Park, J. Y., Lim, J. S., Yoon, C. H., Lee, C. H., & Park, K. P. (2005). *Effect of a fluorinated sodium bis(2-ethylhexyl) sulfosuccinate (aerosol-OT, AOT) analogue surfactant on the interfacial tension of CO_2 + water and CO_2 + Ni-plating solution in near- and supercritical CO_2.* Journal of Chemical & Engineering Data, 50(2), 299–308. https://doi.org/10.1021/je0499667

Pereira, L. (2016). *Interfacial tension of reservoir fluids: an integrated experimental and modelling investigation* (Doctoral dissertation, Heriot-Watt University).

Pereira, L. M., Chapoy, A., Burgass, R., Oliveira, M. B., Coutinho, J. A., & Tohidi, B. (2016). Study of the impact of high temperatures and pressures on the equilibrium densities and interfacial tension of the carbon dioxide/water system. *The Journal of Chemical Thermodynamics*, *93*, 404-415.

Pereira, L. M., Chapoy, A., Burgass, R., & Tohidi, B. (2017). Interfacial tension of CO2+ brine systems: Experiments and predictive modelling. *Advances in Water Resources*, *103*, 64-75.

Qamar, R., & Zardari, B. A. (2023). Artificial neural networks: An overview. *Mesopotamian Journal of Computer Science*, *2023*, 124-133.

Ren, Q. Y., Chen, G. J., Yan, W., & Guo, T. M. (2000). Interfacial tension of (CO2+ CH4)+ water from 298 K to 373 K and pressures up to 30 MPa. *Journal of Chemical & Engineering Data*, *45*(4), 610-612.

Saraji, S., Piri, M., & Goual, L. (2014). The effects of SO2 contamination, brine salinity, pressure, and temperature on dynamic contact angles and interfacial tension of supercritical CO2/brine/quartz systems. *International Journal of Greenhouse Gas Control*, *28*, 147-155.

Sarmadivaleh, M., Al-Yaseri, A. Z., & Iglauer, S. (2015). Influence of temperature and pressure on quartz–water–CO2 contact angle and CO2–water interfacial tension. *Journal of colloid and interface science*, *441*, 59-64.

Schapire, R. E. (1990). The strength of weak learnability. *Machine learning*, *5*, 197-227.

Shah, V., Broseta, D., Mouronval, G., & Montel, F. (2008). Water/acid gas interfacial tensions and their impact on acid gas geological storage. *International Journal of Greenhouse Gas Control*, *2*(4), 594-604.

Smola, A. J., & Schölkopf, B. (2004). A tutorial on support vector regression. *Statistics and computing*, *14*, 199-222.

Suykens, J. A., & Vandewalle, J. (1999). Least squares support vector machine classifiers. *Neural processing letters*, *9*, 293-300.

Tavakolian, M., Najafi-Silab, R., Chen, N., & Kantzas, A. (2024). Modeling of methane and carbon dioxide sorption capacity in tight reservoirs using Machine learning techniques. *Fuel*, *360*, 130578.

Torabi, F., & Gandomkar, A. (2024). Experimental Evaluation of CO2-Soluble Nonionic Surfactants for Wettability Alteration to Intermediate CO2-Oil Wet during Immiscible Gas Injection. *Spe Journal*, *29*(09), 5071-5086.

Wang, Z., Li, S., Peng, D., Cheng, H., & Wei, Y. (2023). *The effect of interfacial tension on CO_2 oil-based foam stability under different temperatures and pressures.* Fuel, 341, 127755. https://doi.org/10.1016/j.fuel.2023.127755

Wu, Y. C., & Feng, J. W. (2018). Development and application of artificial neural network. *Wireless Personal Communications*, *102*, 1645-1656.

Xin, W., Lifeng, L., Zengmin, L., & Chengyuan, L. (2015). Determination of CO2/crude oil system interfacial tension and dynamic interfacial tension by ADSA method. *Izv. Khim. Bulg. Akad. Nauk.*, *47*, 945-948.

Yan, W., Zhao, G. Y., Chen, G. J., & Guo, T. M. (2001). Interfacial tension of (methane+ nitrogen)+ water and (carbon dioxide+ nitrogen)+ water systems. *Journal of Chemical & Engineering Data*, *46*(6), 1544-1548.

Yang, D., Tontiwachwuthikul, P., & Gu, Y. (2005). *Interfacial tensions of the crude oil+ reservoir brine+ CO_2 systems at pressures up to 31 MPa and temperatures of 27 C and 58 C.* Journal of Chemical & Engineering Data, 50(4), 1242-1249. https://doi.org/10.1021/je0500227

Yang, D., & Gu, Y. (2004, September). *Interfacial interactions of crude oil-brine-CO_2 systems under reservoir conditions.* In SPE Annual Technical Conference and Exhibition (pp. SPE-90198). SPE.

Zhang, C., & Wang, M. (2023). CO2/brine interfacial tension for geological CO2 storage: A systematic review. *Journal of Petroleum Science and Engineering*, *220*, 111154.

Zhang, H., Gong, H., He, X., Wu, J., Sun, H., Xu, L., & Dong, M. (2024). Simultaneous adjustment on the CO2/oil and CO2/water interface tensions using hydrophilic, lipophilic and CO2-philic surfactants during CO2 flooding to enhance shale oil recovery after hydraulic fracturing. *Chemical Engineering Journal*, *486*, 150244.

Zhang, J., Feng, Q., Zhang, X., Shu, C., Wang, S., & Wu, K. (2020). A supervised learning approach for accurate modeling of CO2–brine interfacial tension with application in identifying the optimum sequestration depth in saline aquifers. *Energy & Fuels*, *34*(6), 7353-7362.